Analysis of Synchronous Machine Turn-to-Turn Fault Currents

Presented in Partial Fulfillment of
the Requirements for the Degree of

Master of Science

with a Major in

Electrical Engineering

in the

College of Graduate Studies

University of Idaho

by

Matchyaraju Alla

Major Professor
Brian K. Johnson, Ph.D.

Committee
Herbert Hess, Ph.D.
Yacine Chakhchoukh, Ph.D.

Department Administrator
Mohsen Guizani, Ph.D.

May 2017

Authorization to Submit Thesis

This thesis of Matchyaraju Alla, submitted for the degree of Master of Science with a major in Electrical Engineering and titled "Analysis of Synchronous Machine Turn-to-Turn Fault Currents," has been reviewed in final form. Permission, as indicated by the signatures and dates below, is now granted to submit final copies to the College of Graduate Studies for approval.

Major Professor:	Brian K Johnson, Ph.D.	Date
Committee Members:	Herbert Hess, Ph.D.	Date
	Yacine Chakhchoukh, Ph.D.	Date
Department Administrator:	Mohsen Guizani, Ph.D.	Date

Abstract

In the event of internal faults in turbo generators large currents flow in the windings due to the unsymmetrical magnetic linkage between the stator windings of the lap-connected generators. This causes severe damage to the windings, shaft and coupling of the machine. Extensive study on these faults can help mitigate the damage caused by these faults by allowing design of protective schemes that detect faults more quickly. This thesis, backed by experimental results, proposes a method that depends on the negative sequence voltage, negative sequence current quantities and field currents to distinguish from internal or external faults as well as focusing on the analysis of internal faults in synchronous machines. The limitations of the existing protection practices in detecting the turn-to-turn faults were also researched. The main motivation for the work is to overcome the present limitations by using a new approach for modelling of generators for internal faults. Information on the magnitude of internal fault current can help validate the synchronous machine internal faults models based on a modified winding function theory approach and the multi-loop method. The work deals with development of a test setup for measuring the turn-to-turn fault currents of the salient pole synchronous generator in the lab. The process is initiated by calculating the approximated currents using the design aspects of the machine. These calculations are compared to the measured currents during various combinations of turn-to-turn faults. This thesis discusses the sensitivity of protection schemes applied for detecting turn-to-turn in the generator. The zero sequence voltage based approach, negative sequence differential protection and the proposed advanced rotor double frequency harmonic current based detection methods were each analyzed to determine their sensitivity for internal faults by varying from the number of shorted turns from 1 turn to 10 turns.

Acknowledgements

I would like to thank my major professor, Dr. Brian K.Johnson, for his advice and expertise on this research. I would also like to thank my committee, Dr. Herbert Hess and Dr. Yacine Chakhchoukh, whom I have worked closely with throughout this project.

I sincerely appreciate Dr. Normann Fischer from Schweitzer Engineering Laboratories for his continuous support through out my thesis. I am also thankful to my fellow student Sruthi Chilukuri of ECE department, Indian students association and my friends who have been part of my Masters's Degree Completion.

Finally, I am grateful and indebted for the support provided by my family who have been behind every life decision I have made. Without them, I would not be afforded the immense opportunities in life that I have been fortunate enough to have. This work is dedicated to my nephew for being my biggest role model.

Table of Contents

Authorization to Submit Dissertation . . . ii
Abstract . . . iii
Acknowledgements . . . iv
Table of Contents . . . v
List of Tables . . . vii
List of Figures . . . viii
Acronyms . . . xii

1 Introduction . . . 1
1.1 Turn-to-Turn Faults . . . 1
1.2 Causes of Turn-to-turn Faults . . . 2
1.3 Review of Existing Generator Protection Functions . . . 5
1.4 Proposed Solution . . . 8
1.5 Objectives of this Work . . . 9
1.6 Summary . . . 10

2 Machine Design and Modelling . . . 11
2.1 Review of Machine Design . . . 11
2.2 Winding Inductances . . . 13
2.3 Review of Electric Machine Models Suitable for Fault Analysis . . . 14
2.4 Inductance Calculation of the laboratory Synchronous Machine . . . 19
2.5 Inductance Field Measurements . . . 23
2.6 Approximate Turn-to-Turn Fault Current Calculation . . . 24
2.7 Summary . . . 34

3 Protection Elements for Turn-to-Turn Faults . . . 35
3.1 Percentage Differential Protection of Generator . . . 35
3.2 Negative Sequence Directional Element . . . 37
3.3 Rotor Field Measurements . . . 38
3.4 Summary . . . 39

4 Synchronous Machine Behavior During Internal Faults . . . 41
4.1 dq0 Representation of Stator and Rotor Circuits . . . 41
4.2 Synchronous Machine Behavior During Disturbances . . . 46
4.3 Summary on Field Currents Behavior for External and Internal Faults . . . 56

5 Experimental Results . . . 58
5.1 Test Setup . . . 58
5.2 Analysis on Turn-to-Turn Fault Current Magnitudes . . . 62

5.3 Experimental Results of Protection Elements Performance 67
5.4 Summary 80

6 Conclusions And Future Directions 82
6.1 Conclusions 82
6.2 Future Work 83

Bibliography 84

Appendices 86

A Turn-to-Turn Experimental Results 86

B Power Lab Machine Analysis 103

C Matlab Model 108

List of Tables

Table 2.1 Summary of the Measured Impedance of the Winding I 34
Table 2.2 Summary of the Measured Impedance of the Winding II 34

Table 5.1 Percentage Error of Voltages Across Turns 61
Table 5.2 Mapping to Represent Number of Turns as Percentage of Winding 63
Table 5.3 Experimental Fault Current Results When Testing Generator Under No-load Condition 64
Table 5.4 Results of Split Phase Protection During Fault Testing When Generator is synchronized to Grid 68
Table 5.5 Results of Negative Sequence Differential During Fault Testing When Generator is synchronized to Grid 69
Table 5.6 Measurements During Testing when Generator Under no-load Condition 76

List of Figures

Figure 1.1 Synchronous Generator Internal Failures 2
Figure 1.2 Equivalent Circuit for Turn-to-Turn Circulating Currents 4
Figure 1.3 Split Phase Protection Implementation Diagram 6
Figure 1.4 Residual Voltage Measurement Based Detection. 7

Figure 2.1 Winding Layout of One Parallel Branch of A phase 20
Figure 2.2 Representation of MMF Wave of Rotor Pole 21
Figure 2.3 Laboratory Synchronous Generator With Taps to Create Internal Faults. 23
Figure 2.4 Laboratory Machine Coil Representation with Connecting Taps for Internal Faults 24
Figure 2.5 Representation of Faulted Coils and Field Turns 25
Figure 2.6 Calculated One Turn Reactance for Various Relative Permeabilities of the Core 26
Figure 2.7 Calculated One Turn Current for Various Relative Permeabilities of the Core 26
Figure 2.8 Measured Impedances on Phase A When Field Winding and the B and C Phase Windings are Open 28
Figure 2.9 Measured Impedances on Phase A at Tap Points When the Field Winding is Shorted, B and C Phase Windings are Open 29
Figure 2.10 Measured Impedances of Phase A Winding When Field Winding is Open, B and C Phase Windings are Shorted 30
Figure 2.11 Measured Inductances of Phase A Winding When Field Winding, B and C Phase Windings are Shorted 31
Figure 2.12 IEEE 115 Standard Test Setup for Zero Sequence Impedance Measurement 33
Figure 2.13 Relay Measured Zero Sequence Impedance of the Phase A for the Laboratory Machine 33

Figure 3.1 Percentage Differential Protection Characteristic 36
Figure 3.2 Difference Between (a) Negative Sequence Current Differential Elements and (b) Phase Current Differential Elements [17] 37
Figure 3.3 Negative Sequence Directional Element [18] 38

Figure 4.1 Generator Windings in dqo Reference Frame 41
Figure 4.2 dqo Representation for Machine Analysis [9] 45
Figure 4.3 Short-circuit Oscillogram of Stator Currents [13] 46
Figure 4.4 Flux Patterns Under a) Synchronous, b) Transient, and c) Sub-transient Conditions in d and q-axes [19] 48
Figure 4.5 Equivalent d-axis Circuit for steady-state [8] 49
Figure 4.6 Equivalent d-axis Circuit for Transient State [8] 52

FIGURE 4.7 Equivalent d-axis Circuit for Sub-transient State [8] 54

FIGURE 5.1 Laboratory Machine Used for Experimental Results 59
FIGURE 5.2 Test setup for field measurements 60
FIGURE 5.3 Voltages Measured by the Relay: (a) Terminal Phase Voltage (V); (b) Voltage Across 10 Turns (V); (c) Voltage Across 1 Turn (V) . . . 61
FIGURE 5.4 Plot Between Fault Current at No-load and a Load Current of 18.7 at 0.82 pf Lagging versus Case Number 62
FIGURE 5.5 Open Circuit Terminal Voltage Versus Rotor mmf Per Pole 64
FIGURE 5.6 Turn-to-Turn Fault Current and Applied Voltage Versus Case Number When the Machine was Loaded to Carry 30 A with AVR Constant Voltage Mode 65
FIGURE 5.7 Turn-to-Turn Fault Current and Applied Voltage Versus Case Number When the Machine was Under No-load with AVR Constant Voltage Mode 66
FIGURE 5.8 Turn-to-Turn Fault Current and Applied Voltage Versus Case Number When the Machine was Loaded to Carry 15 A with AVR Constant Voltage Mode 66
FIGURE 5.9 Plot between Leakage Impedance and Percentage of Fault Location for Different Operating Conditions 67
FIGURE 5.10 Relay Measurements with 10 Turns Shorted, (a) Negative Sequence Differential Operate and Restraint Elements; (b) Magnitude of Fault Current (A); (c) Phase (IAX_A) and Neutral Currents (IAW_A) of the Machine (A); (d) Pre-fault Voltage Across 10 turns (V); (e) Magnitude of Negative Sequence Currents Measured at Phase and Neutral (A) 70
FIGURE 5.11 Measurements Including Rotor Field Current from Shunt for 10 Turns Shorted Under Loaded Condition of 15A & 0.86 lag pf, (a) Terminal Negative Sequence Current; (b) Terminal Voltages; (c) Terminal Phase Currents; (d) Field Double Frequency Current Measured Across 1 Ohm Shunt; (e) Terminal Negative Sequence Voltage . . . 71
FIGURE 5.12 Measurements Including Rotor Field Current from Shunt for 2 Turns Shorted Under Loaded Condition, (a) Terminal Negative Sequence Current; (b) Terminal Voltages; (c) Terminal Phase Currents; (d) Field Double Frequency Current Measured Across 1 Ohm Shunt; (e) Terminal Negative Sequence Voltage. 72
FIGURE 5.13 Negative Sequence Directional Element with 10 Turns Shorted, (a) Terminal Phase Currents; (b) Terminal Voltages; (c) Imaginary Component of Negative Sequence Impedance Measured at Terminal; (d) Real Component of Negative Sequence Impedance Measured at Terminal; (e) Magnitude of Negative Sequence Current Measured at Terminal; (f) Magnitude of Negative Sequence Voltage Measured at Terminal 73

FIGURE 5.14 Rotor Field Measurements During One Phase Breaker Open Condition External To the Generator Terminal CTs, (a) Magnitude of Negative Sequence Current Measured at Terminal; (b) Terminal Voltages; (c) Terminal Phase Currents; (d) Field Double Frequency Current Measured Across 1 Ohm Shunt 74
FIGURE 5.15 Negative Sequence Directional Element Operation During One Phase Breaker Open External To the Generator Terminal CTs, (a) Terminal Phase Currents; (b) Terminal Voltages; (c) Imaginary Component of Negative Sequence Impedance Measured at Terminal; (d) Real Component of Negative Sequence Impedance Measured at Terminal; (e) Magnitude of Negative Sequence Current Measured at Terminal; (f) Magnitude of Negative Sequence Voltage Measured at Terminal 75
FIGURE 5.16 Negative Sequence Over Voltage with 10 Turns Shorted When the Generator Is Energized but Disconnected From the Grid (a) Terminal Voltages; (b) Magnitude of Negative Sequence Voltage Measured at Terminal; (c) Magnitude of Zero Sequence Voltage Measured at Terminal; (d) Turn-to-turn Fault Current; (e) Circulating Current Between Branches 77
FIGURE 5.17 Negative Sequence Over Voltage with 2 Turns Shorted When the Generator Is Energized but Disconnected From the Grid (a) Terminal Voltages; (b) Magnitude of Negative Sequence Voltage Measured at Terminal; (c) Magnitude of Zero Sequence Voltage Measured at Terminal; (d) Turn-to-turn Fault Current; (e) Circulating Current Between Branches 78
FIGURE 5.18 Measurements Including Rotor Field Current from Shunt for 10 turns Shorting Under No-load Condition, (a) Turn-to-Turn Fault Current; (b) Terminal Voltage; (c) Field Double Frequency Current Measured Across 1 Ohm Shunt 79
FIGURE 5.19 Measurements Including Rotor Field Current from Shunt for 2 turns Shorting Under No-loaded Condition, (a) Turn-to-Turn fault current; (b) Terminal voltage; (c) Field Double Frequency Current Measured Across 1 Ohm Shunt 80

FIGURE A.1 10 Turns Short Circuit Under Loaded Condition 86
FIGURE A.2 7 Turns Short Circuit Under Loaded Condition 87
FIGURE A.3 5 Turns Short Circuit Under Loaded Condition 88
FIGURE A.4 3 Turns Short Circuit Under Loaded Condition 89
FIGURE A.5 2 Turns Short Circuit Under Loaded Condition 90
FIGURE A.6 1 Turn Short Circuit Under Loaded Condition 91
FIGURE A.7 7 Turns Short Circuit Connected to Grid or Disconnected with P = 0, Q = 0 92
FIGURE A.8 5 Turns Short Circuit Connected to Grid or Disconnected with P = 0, Q = 0 93
FIGURE A.9 3 Turns Short Circuit Connected to Grid or Disconnected with P = 0, Q = 0 94

Figure A.10 2 Turns Short Circuit Connected to Grid or Disconnected with P = 0, Q = 0 95
Figure A.11 1 Turn Short Circuit Connected to Grid or Disconnected with P = 0, Q = 0 96
Figure A.12 Measurements Including Rotor Field Current from Shunt for 5 Turn Short Circuit in Loaded Condition. 97
Figure A.13 Measurements Including Rotor Field Current from Shunt for 3 Turn Short Circuit in Loaded Condition. 98
Figure A.14 Measurements Including Rotor Field Current from Shunt for 2 Turn Short Circuit in Loaded Condition. 99
Figure A.15 Measurements Including Rotor Field Current from Shunt for 2 Turn Short Circuit Connected to Grid or Disconnected with P = 0, Q = 0 100
Figure A.16 Measurements Including Rotor Field Current from Shunt for 3 Turn Short Circuit Connected to Grid or Disconnected with P = 0, Q = 0 101
Figure A.17 Measurements Including Rotor Field Current from Shunt for 5 Turn Short Circuit Connected to Grid or Disconnected with P = 0, Q = 0 102

Acronyms

mmf - Magnetomotive force
RMF - Rotating Magnetic Field
EMF - Electromotive Force
AC - Alternating Current
RTDS - Real Time Digital Simulator
DC - Direct Current
K_d - Distribution Factor
K_p - Pitch Factor
K_w - Winding Factor
RMS - Root Mean Square
CT - Current Transformer
PT - Potential Transformer
MWFA - Modified Winding Function Approach
WFA - Winding Function Approach
FEM - Finite Element Method
AMPS - Analog Model Power system
AVR - Automatic Voltage Regulator
N_{ph} - Total number of turns in phase
g^{-1}- Inverse airgap function
$<>$- Average of turns function

CHAPTER 1

Introduction

Synchronous machines are widely-used elements in modern power systems for generating electric power. Generator failures can have a huge impact on the power supply and in turn cause a great financial loss for electric power generating station owners. This makes generator protection an important priority for power systems. Relay based protection is challenging, but also important for synchronous machines because relays are the fastest means to detect faults. Early fault detection avoids severe machine damage and, therefore, minimizes time and cost for repair. Traditionally, current differential relays are used to protect the synchronous generator against internal faults in the machine.

Winding construction is a key factor in the ability to detect faults. Multiturn coil windings are cost effective in small machines but in large machines it becomes difficult to insert each coil leg of a multiturn coil simultaneously into different slots. Roebel bar windings are manufactured in half-turn segments, making installation much easier on large machines. These single-turn designs can be cooled effectively. Today, multi-turn coils can be found on hydro machines with ratings of up to 150 MVA and 18 kV, with Roebel bar windings used for larger machines. Roebel bar windings are secured against turn-to-turn faults [1].

1.1 TURN-TO-TURN FAULTS

Turn-to-turn faults are the most common internal faults in synchronous machines. These faults challenge differential element sensitivity. Synchronous generator winding faults usually begin as high resistance turn-to-turn faults over a few turns, which cannot be detected by differential relays. As the faults evolve, the resistance decreases and the fault becomes detectable by differential relay. However, by this time, significant damage will have occurred to the coils. The time and cost to repair a synchronous generator after the evolution of these faults are much more significant than they would have been if the fault was detected earlier, when these faults involved only a few turns. A relay capable of detecting these faults early would avoid damage such as shown in Fig. 1.1. Due to higher fault currents, sometimes the core laminations would damaged leading to much longer outages.

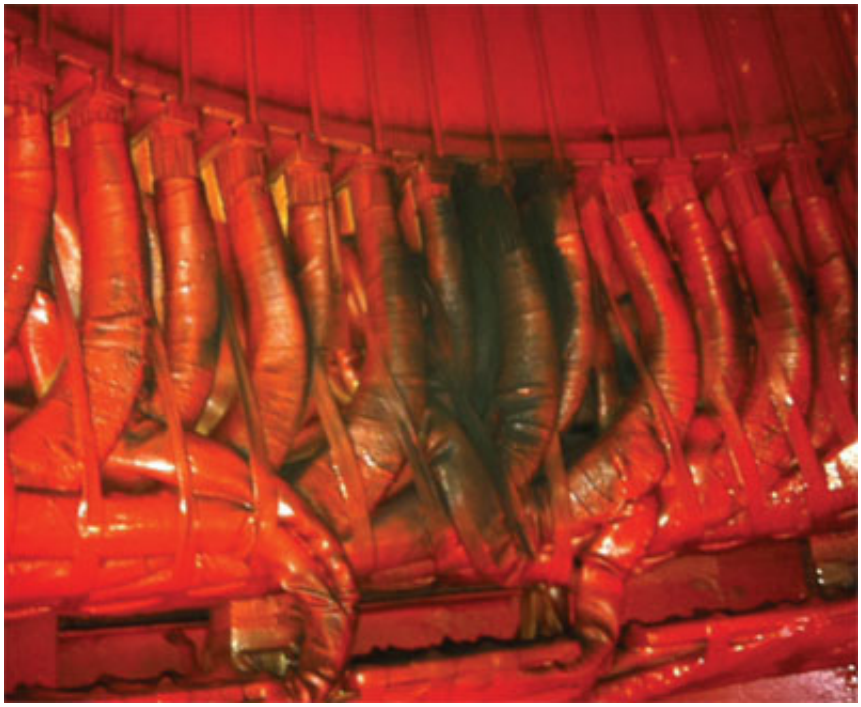

FIGURE 1.1: Synchronous Generator Internal Failures

The commonly applied differential relay element is not capable of detecting high-resistance ground faults close to the generator neutral or high-resistance turn-to-turn faults that involve few turns.

In hydroelectric generators, the probability of turn-to-turn faults is greater than other machine designs. Hydroelectric generators are often wound with multi-layer and multi-turn windings. Under normal operation, there is very little difference in the current in each parallel branch. However, during an internal fault, currents will circulate between the parallel branches of winding within one phase. In hydro machines, a significant percentage of stator faults begin as turn-to-turn faults. Due to the very high effective turns ratio between the windings and the shorted turn, inter-turn faults cause extremely high currents in the faulted loop, quickly leading to progressive damage. If these faults can be detected before they evolve into phase-to-phase or ground faults, then the damage to the machine and associated down time can be greatly reduced.

1.2 CAUSES OF TURN-TO-TURN FAULTS

Turn-to-turn faults are often caused by movement between the coils. Two-turn coils are more vulnerable as the insulation in these conductors is not strong enough to hold

against friction due to movement. However the single turn coils are designed such that the single turn Roebel bar windings are separated not only by their winding insulation material but also by a tough bakelite insulation material. This extra insulation saves the winding from wear and tear reducing the probability of faults.

Voltage surges are another important factor causing turn to turn faults. At power system frequencies, voltage is distributed linearly throughout the winding. However, during a fast front voltage surge, a much greater percentage of the surge appears across the first few turns, this may lead to faults. When single-turn bar windings are used in a hydro electric generator, turn-to-turn faults are not a concern. For other designs, however, turn-to-turn faults must be considered as realistic failure modes when protecting the machine.

1.2.1 *Flow of Current Due to Turn-to-turn Faults*

The shorted turn current circulation, as shown in Fig. 1.2, is primarily dependent on two factors. First, the shorted turn reduces the voltage in the branch by an amount proportional to the line-to-neutral voltage divided by the total number of turns in the branch. This voltage difference drives a current, which circulates through the parallel branches. The net magnetomotive force (MMF) adds to zero around the circuit, and consequently, the associated flux does not cross the air gap. Fault current is limited only by leakage reactance. Another important factor for circulating current is added flux produced by the current flowing in the shorted turn. If rated current is flowing at the generator terminals and one thinks about the shorted winding behavior as an auto transformer, then the current in the shorted turn can be estimated as the product of the rated current and the total number of turns making up the circuit in order to maintain ampere-turn balance [2]. The large current couples strongly with another coil in the same slot. Depending on the configuration of the winding, this coil may be part of the same phase or a different phase. If it is a part of the same phase, then the induced current acts to reduce the current produced by the voltage difference.

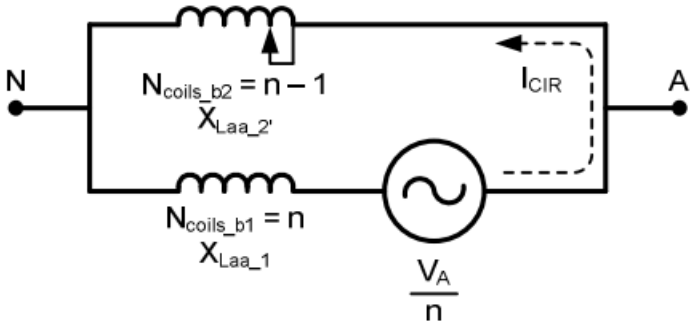

FIGURE 1.2: Equivalent Circuit for Turn-to-Turn Circulating Currents

$$I_{CIR} = \frac{k\frac{V_A}{n}}{X_{Laa1} + X_{Laa2'}} \tag{1.1}$$

where:
$\frac{V_A}{n}$ is the voltage per turn
I_{CIR} is the circulating current between the branches
n is the number of turns in the branch
k is the number of shorted turns
X_{Laa1} is the leakage reactance of branch1
$X_{Laa2'}$ is the leakage reactance of branch2

For windings with two parallel branches, the leakage reactance for the unfaulty branch (X_{Laa1}) will be twice the leakage inductance value provided in the machine data sheet. However, determining the leakage reactance of the faulted winding ($X_{Laa2'}$) may be difficult. While it is adequate to consider Fig. 1.2 and the associated equation (1.1)for the understanding of the circulating current, there are difficulties in applying equation (1.1) in practical situations and limits to its accuracy. An IEEE tutorial on the protection of synchronous generators [3] lists a typical value for the circulating current due to a shorted turn as approximately four percent of the generator full-load current. However, the generator manufacturer should be consulted for an accurate value. Circulating current is determined by the number of turns that are short-circuited and the volts-per-turn value of the machine. Because neither of these factors changes during a turn-to-turn fault, the circulating current does not depend on the machine loading.

1.3 REVIEW OF EXISTING GENERATOR PROTECTION FUNCTIONS

Currently, two methods are commonly used for detecting the inter-turn faults in synchronous generators. Split phase differential protection can be used if there are parallel circuits of each phase and suitable CTs connections are available. Otherwise, zero-sequence voltage based detection is used for detection. In addition to the two methods, there are few places where negative sequence differential is also used for detection.

1.3.1 *Split Phase Differential Element*

Split phase protection is also called transverse protection of generator winding [2]. It may be applied to detect inter-turn faults in generators wound with two sets of three phase windings. Each winding is separately brought out of the machine and connected in parallel. When currents in the two windings are compared, and any difference in current would indicate an inter-turn fault. The split phase element allows a separate pickup setting to be applied for each phase. Additionally, the pickup can be biased by the load current using a slope characteristic. Ideally, the split-phase element should be sensitive enough to detect a single shorted turn. Even though the current in this turn can be six to seven times the machine nominal current, the current seen by the split-phase protection can be quite small, on the order of one-twentieth of the generator full-load current [4]. In addition, a spurious split-phase current can be measured due to current transformer (CT) errors or CT saturation during external faults. Therefore, primary consideration in the application of split-phase protection is the method of measuring the difference in the currents between the parallel branches and the proper selection of the CTs used for this purpose.

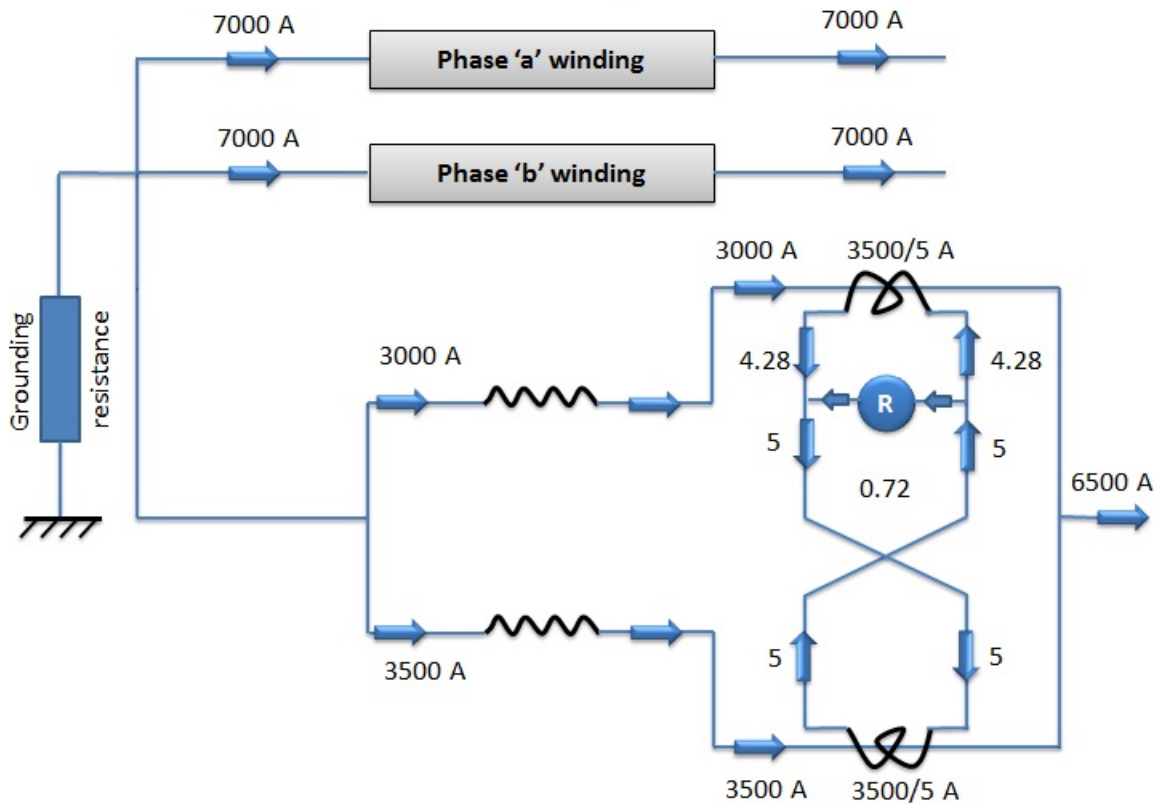

FIGURE 1.3: Split Phase Protection Implementation Diagram

The Fig. 1.3 shows the implementation of split phase protection for detecting turn-to- turn faults. During normal conditions, there will be negligible circulating current between the branches. During any turn-to-turn short circuits, the flow of circulating current between the branches is significantly higher as shown in Fig. 1.3 and can be used for detection.

1.3.2 *Limitations for Sensitivity of Split Phase Protection*

Fig. 1.3 has an underlying assumption that the winding branches are identical and that they have the same inductance. In practice, however, this is not quite the case due to manufacturing tolerances, such as differences in the construction of each of the branches and variations in the air gap. These differences between the parallel branches result in a natural (standing) circulating current occurring between the branches without any turn-to-turn faults. These differences also result in a transient circulating current during external fault conditions.

1.3.3 *Stator turn-to-turn fault based on residual voltage measurement*

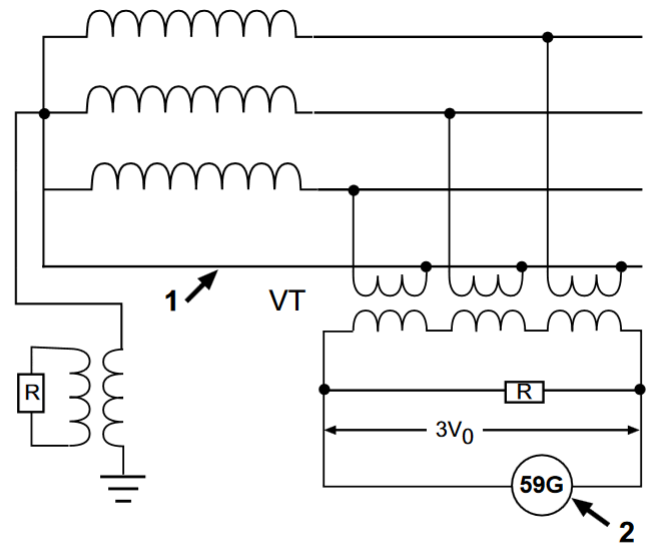

FIGURE 1.4: Residual Voltage Measurement Based Detection

Turn-to-turn faults, which are normally difficult to detect, quickly develop into ground faults which are tripped by the stator ground-fault protection. Common practice in most countries is to ground the generator neutral through a resistor, which limits the maximum ground-fault current at the terminal to 5-10 A primary. In this case the transient voltages in the stator system during intermittent phase to ground faults are kept within acceptable limits. And hence, ground-faults, which are tripped within one second from fault inception, only cause negligible damage to the laminations of the stator core.

For generators where the stator winding configuration does not allow the application of split-phase differential protection, a neutral voltage method may be used to detect turn-to-turn stator winding faults. Three VTs are connected in wye, and the primary ground lead is tied to the generator neutral. The secondary is connected in a broken delta with an overvoltage relay connected across its open delta to measure unbalance voltage [5].

By connecting the primary ground lead to the generator neutral, the 59N relay is made insensitive to stator ground faults, as shown in Fig. 1.4. The relay will, however, operate for turn-to-turn faults, which increase the unbalance voltage above the low normal levels. The installation requires that the cable from the neutral of the VT which goes to the generator neutral should be insulated for the system line-to-ground

voltage. The 59N relay is tuned to fundamental frequency (60/50 Hz) voltage since some third harmonic voltages will be present across the broken-delta VT input [6]. One of the drawbacks of this scheme is that if the line to neutral insulated cable that connects the VT neutral to the generator neutral points sustains a ground fault, it will solidly ground the generator. For this reason, periodic testing of the cable is typically recommended.

Though negative sequence differential protection detects the turn-to-turn faults, it has issues with sensitivity. The use of negative sequence differential protection for turn-to-turn fault detection will be shown in Chapter4.

1.4 PROPOSED SOLUTION

Internal faults in a machine can have dangerous consequences if allowed to remain on the machine. Accurate representation of the behavior of the machine during a turn-to-turn fault condition is a significant step for protective system design. Even one shorted turn can cause 3 to 4 pu rated current to flow in that faulted turn, causing localized heating in the core. As mentioned earlier, significant faults in the machine start as turn-to-turn faults and then evolve to phase to ground or phase-to-phase faults. A phase quantity based percentage differential element cannot see any difference in the phase quantities for a turn-to-turn fault, as will be shown in Chapter 3. Split phase protection works effectively but the principles cannot cannot be applied for the machines where the windings are not accessible for placement of current transformers. Zero sequence overvoltage protection can detect internal faults of the machine but there are issues with the grounding cable insulation that runs between the dedicated PT that is used for the turn-to-turn protection and the neutral of the generator. In-addition, sensitivity limits the coverage of winding. Negative sequence differential protection can detect turn-to-turn faults and can also detect internal faults involving high resistance. Though it offers greater sensitivity than previous methods, it still has issues with sensitivity.

This thesis proposes two methods for improved secure detection of stator turn-to-turn faults and validates their sensitivity with experimental results from a synchronous machine test setup that is capable of generating turn-to-turn faults up to 11% of the winding. The proposed method works with the machine online and offline.

1.4.1 *Turn-to-turn Fault Detection Technique When Generator is Connected to the System*

Turn-to-turn fault currents cause negative sequence currents to be seen by the terminal CTs of the generator. These negative sequence currents will induce double frequency currents in the field winding. Therefore, measurement of double frequency currents in the field winding, supervised by a negative sequence directional element to block on power system fault, will detect faults involving up to 2 turns of the winding.

1.4.2 *Turn-to-turn Fault Detection Technique When Generator is Disconnected from the System and Field is Excited*

The negative rotating mmf caused by the turn-to-turn faults induces double frequency currents to flow in the field winding even when the stator terminal currents are zero. Hence, the negative sequence voltage measured at the terminal of the stator and the double frequency currents measured in the field winding can detect faults involving up to 2% of the stator winding when the generator is disconnected but the field is energized or the machine is about to be synchronized to the grid.
In most of the cases, turn-to-turn faults are cleared by the phase differential or 100 % stator ground protection when they evolve to more severe faults in the winding. The proposed method catches these faults before that happens.

1.5 OBJECTIVES OF THIS WORK

The primary goal of this thesis is to propose, develop and test a method to detect internal faults in synchronous machines and validate the proposed methods. Other important objectives include:

1. Calculating the approximate machine turn-to-turn fault currents using only the available physical data of the machine
2. Predicting the approximate turn-to-turn fault current magnitudes and verifying them with the results from a laboratory test setup for faults involving up to 11 percentage of the winding
3. Measuring the circulating currents in parallel windings for the turn-to-turn faults to determine the sensitivity of split phase overcurrent protection
4. Measuring the negative sequence current quantities at the neutral and the terminals of the generator for determining the sensitivity of negative sequence differential scheme

5. Measuring the double ac fundamental frequency currents induced in the rotor field winding to validate the proposed methods

6. Determining and verifying the sensitivity of the negative sequence differential, directional elements and zero sequence overvoltage elements for the turn-to-turn fault detection.

1.6 SUMMARY

This chapter highlights the need to analyze the effect of turn-to- turn fault currents in order to develop an effective protective scheme.The chapter included overview on the causes for turn-to-turn faults and the existing protection approaches for detection. The machine protection review focused on the existing split phase differential scheme and the zero sequence overvoltage protection using a special dedicated potential transformer. This chapter also introduced proposed methods using a combination of negative sequence differential quantities on the stator and the double frequency currents in the field winding to improve the sensitivity for detection of turn-to-turn faults.

CHAPTER 2

Machine Design and Modelling

The following sections provide the basic mathematical equations describing synchronous machine behavior required for calculating the impedance of the stator coils to approximately calculate turn-to-turn fault currents.

2.1 REVIEW OF MACHINE DESIGN

The root-mean-square (rms) value of the sinusoidally varying speed voltage component can be expressed [7] as (2.1).

$$E_{rms} = 4.44 f \phi K_w N_{ph} \tag{2.1}$$

Where f is frequency, ϕ is the average flux per pole and N_{ph} is total number of series turns per phase.
In ac machines, especially those of higher ratings, a phase winding is formed by interconnecting identical coils whose coil sides are positioned in two or more adjacent slots. These distributed windings may also have coils that are short pitched, that is, coils which span less than 180 degrees of the flux wave [8]. The effects of both distribution and short pitching of the coils can be separately accounted for by distribution and pitch factors, K_d and K_p respectively. The combined effect of both distribution and short pitching on the induced voltage is usually represented by the winding factor, K_w. Thus K_w can be expressed as in (2.2).

$$K_w = K_p K_d \tag{2.2}$$

1. Distribution Factor(K_d)
   The phase windings of an ac machine may consist of series and/or parallel combinations of more than one coil under a different pole-pair. Within each pole-pair region, the coils of a distributed winding are distributed over many pairs of slots. This will help in reducing the higher order harmonics in the MMF waveform [8].

2. Pitch Factor(K_p)
   Short-pitching, or chording, refers to using coils with width less than one pole-

pitch. Chording is often used in machines with fractional-slot windings (non-integral number of slots per pole or slots per pole per phase) in a double-layer winding arrangement. Chording may also be used to reduce or suppress certain harmonics in the phase emfs. Chording results in shorter end connections, but the resultant fundamental phase emf is reduced with chording. As such, coil span is rarely made less than 2/3 pole-pitch because the additional turns necessary will offset whatever savings gained in the end connections [8].

In general, the fundamental mmf of a distributed winding with a winding factor of K_w, and a total of N_{pole} turns over a two-pole region may be expressed as

$$F_{a1} = \frac{4n_{pole}K_w i cos\theta_e}{2\pi} \tag{2.3}$$

Where i_s is the stator current flowing in the winding and θ_e is spatial angle. Assuming that a total N_{ph} phase turns in the P-pole machine are divided equally among P/2 pole-pair regions, the number of turns per pole-pair is

$$n_{pole} = \frac{N_{ph}}{(P/2)} \tag{2.4}$$

In terms of N_{ph}, the fundamental frequency mmf is

$$F_{a1} = \frac{4N_{ph}K_w i_s cos\theta_e}{\pi P} \tag{2.5}$$

By comparing (2.5) with (2.3), which gives the fundamental mmf component produced by a concentric winding, it can be deduced that the same fundamental mmf component can be produced by a winding with N_{eff} turns of full-pitch concentric coils per pole-pair [7] can be obtained as shown in (2.6).

$$N_{eff} = \frac{2N_{ph}K_w}{P} \tag{2.6}$$

For analytical purposes, the same fundamental mmf can be produced by an equivalent continuous current sheet, that is produced by the same current i_s flowing in a hypothetical winding of sinusoidally varying turn density,

$$n(\theta_e) = \frac{N_{ph}sin_{\theta_e}}{2} \tag{2.7}$$

Such a current sheet has a total number of turns per pole pair of N_s. It produces a sinusoidally distributed spatial mmf that is given by

$$F_a = \frac{1}{2}\int_{\theta_e}^{\theta_e+\pi} n(\theta_e) i d\theta_e \tag{2.8}$$

By comparing the mmf expression (2.8) with that of (2.7), the following relationships between the different number of turns mentioned so far is

$$\frac{N_{sine}}{2} = \frac{4N_{eff}}{2\pi} \tag{2.9}$$

The expression of the fundamental flux density, assuming a uniform airgap of g, is (2.10)

$$B_{a1} = \frac{\mu_0 F_{a1}}{g} = \frac{4\mu_0 N_{Ph} K_w i cos\theta_e}{Pg} \tag{2.10}$$

The expression for the flux per pole due to the fundamental flux density component is (2.11)

$$\phi_{pole} = L\int B_{a1} R d\theta_m = LR\int_{-\pi/2}^{\pi/2} B_{a1}(\theta_e) d\theta_e \frac{2}{p} \tag{2.11}$$

Equation (2.11) can be further expressed as

$$\phi_{pole} = \frac{4\mu_0 LR(2N_{ph}K_w i/P)2}{\pi Pg} = \frac{4\mu_o LR}{\pi g(2/P)N_{eff} i} \tag{2.12}$$

Where R is the effective radius of air-gap and L is the active length of the stator core.

2.2 WINDING INDUCTANCES

In this section, the basic expressions of the self and mutual winding inductances for an elementary machine will be derived. The self-inductance of winding s, on the stator of machine with N_{eff} turns per pole pair and P poles, not including leakage fluxes, is given by (2.13)

$$L_{ss} = \frac{P}{2} N_{effs} \phi_{pole}/i = \frac{4\mu_0 N_{effs}^2 LR}{\pi g P} \tag{2.13}$$

The flux linked by the rotor winding r of N_{effr} effective turns, due to the field onto the stator windings with N_{eff}, effective turns, is (2.14)

$$\lambda_{rs} = \frac{P}{2} N_{effr} L \int_{-\pi+2/\alpha}^{\pi+2/\alpha} \frac{4\mu_0 N_{eff} i_s cos(\theta) R d\theta_e(\frac{2}{P})}{2\pi g} \quad (2.14)$$

The rotor inductance L_{rs} linking λ_{rs} and i_s is shown in (2.15)

$$L_{rs} = \lambda_{rs}/i_s = 4\mu_0 N_{effr} N_{effs} LR cos(\alpha) \quad (2.15)$$

It can be readily shown through symmetry that $L_{rs} = L_{sr}$. The self- inductance of the rotor winding can also be expressed in the same way as

$$L_{rr} = \lambda_{rr}/i_r = 4\mu_0 N_{effr}^2 LR \quad (2.16)$$

Where i_r is rotor field current.

2.3 REVIEW OF ELECTRIC MACHINE MODELS SUITABLE FOR FAULT ANALYSIS

Extensive studies have performed in the past to develop the machine models that can be used to simulate dynamic performance of the machine. A review starts with the basic two axis dqo model of the machine and goes into the limitations of the dqo based models. Phase domain models produce more accurate results than dqo models but they have limitations as will be discussed later. This section will end with the multi-loop method which should have better accuracy compared the phase domain models.

2.3.1 *Parks Transformation Based Models*

In the late 1920's, R. H. Park [9] formulated a change in reference frame which effectively replaced the variables for machine analysis affiliated with the stator windings of a synchronous machine with variables associated with a fictitious windings rotating in synchronism with the rotor field flux. By transforming the stator variables to a frame of reference fixed to the rotor, he eliminated the dependence of synchronous machine inductance matrix on rotor position. A transformation matrix transforms the inductances of a synchronous machine from the stator frame of reference to the rotor frame of reference.

2.3.2 *Drawbacks for Internal Fault Analysis*

However, the dqo models have some shortcomings. It is not feasible to model internal faults directly in dqo frame. Although some internal fault models may have used the dqo theory to calculate the approximate values of faulted inductances, the actual solutions of the differential equations are performed in the phase-domain [10]. Furthermore, using dqo, the error in the calculation of faulted winding inductances becomes larger as the fault point approaches the end of the winding. Most existing models of synchronous machines in electromagnetic transients programs use a dqo model to express the physical behavior of the machine in terms of mathematical equations and model the response to external transients. These equations are usually implemented in electromagnetic transients programs using an interface-based approach by solving machine equations in dqo frame and injecting machine currents into the network as current sources.

The main assumption in the dqo theory is that the eigenvalues of the inductance matrix of a machine are unvarying as the rotor position changes [11]. These models are widely used since the algorithm is numerically fast; also electric utilities use validated generator dqo models for the stability analysis tools. These models, however, are not capable of correctly predicting the transient performance of the synchronous machines in irregular conditions such as during the presence of internal faults or rotor eccentricity. Furthermore, these models cannot account for the effects of non-sinusoidal distribution of the windings and permeance in synchronous machines. This is due to the fact that some of the fundamental assumptions of the dqo model may not apply in these situations.

The generator model in the Real Time Digital Simulator (RTDS) [12] implements a numerically stable synchronous machine model for electromagnetic transient analysis which accounts for fine details of machine physical characteristics such as the winding distribution, rotor geometry and operating-point dependent saturation. The model is capable of properly representing winding- and permeance-related time harmonics, and predicting the transient behavior of synchronous machines in conditions such as internal fault.

The behavior of synchronous machines under internal faults has not been thoroughly studied and few machine models exist. Due to inability of the traditional dqo model to represent internal faults synchronous machine fault models are generally derived in the phase domain (abc domain), where the voltage and flux linkage equations are directly developed in a fixed phase reference without coordinate transformation. In the abc models, the stator is assumed to have three windings, i.e., one winding per

phase. Therefore, this model is convenient to simulate internal faults in machines with one winding per phase.

2.3.3 *Phase Domain Models*

The term phase domain means that the values of machine inductances change with the change in rotor position and level of saturation [10]. The phase domain feature of this model makes it capable of simulating synchronous machines internal faults. To be able to simulate synchronous machine internal faults, the self and mutual inductances of machine windings including faulted windings must be computed as functions of rotor position and saturation.

2.3.4 *Modified Winding Function Approach for Obtaining the Inductances of Electric Machines*

Unlike the dqo theory, the Modified Winding Function Approach (MWFA) is capable of taking into account non-sinusoidally distributed windings [11]. Also, this method is computationally more efficient than the finite element method. In this approach, a suitable integration loop is used to determine, using Ampere's law, the resultant air-gap flux density at any given angle. A winding distribution function is used to calculate the Ampere-turns over the integration loop. A great motivation for the application of the winding function approach is the capacity to consider the actual distribution of windings turns rather than idealized sinusoidal distributions.

2.3.5 *Winding Function Approach (WFA)*

The winding function approach (WFA) was introduced as a new method for modeling induction machines based on a coupled electric circuit approach [10]. Winding function theory was developed by Schmitz and Novotny [11] as an important tool for the calculation of AC machine inductances. This approach was initially used to model the air-gap dynamic eccentricity in induction machines. In the reference [11], the winding function approach was modified by taking into account Gauss's law in addition to Ampere's law to calculate the flux density created by each winding. The accuracy of the model for simulation of internal faults in synchronous machines depends on the accuracy of the calculation of the inductance of the faulted windings; i.e., the asymmetry developed due to the fault must be considered in the modeling of the machines. Lipo [13] presented the turns and modified winding function theory as a versatile tool for the calculation of inductances for salient pole or round rotor

synchronous machines. Since this theory has the capability to take any winding distribution on the stator or any gap distribution around the rotor into account, it can be used for modeling and analyzing fault conditions. The space harmonics produced by a machine winding can be determined by its winding function, which depicts the MMF distribution in the air gap in terms of space distribution. As in the case with most inductance calculations, it is assumed that

1. The iron of the rotor and stator has infinite permeability and saturation is not considered.

2. The stator surface is considered smooth and the effects of slots are corrected by the carter coefficient.

According to winding function theory, the mutual inductance between any two windings i and j in any electric machine can be computed by the equation(2.17):

$$L_{ij}(\theta_{rm}) = \mu_0 r \int_0^{2\pi} g^{-1}\theta_{rm} N_i(\theta_{rm}, \phi) N_j(\theta_{rm}, \phi) d\phi \tag{2.17}$$

Equation (2.17) can be used to calculate the mutual inductance between two windings x and y, whose turns functions are n_x and n_y is shown in (2.18).

$$\begin{aligned} L_{xy} = 2\mu_0 rl < g^{-1}(\Psi,\theta) n_y(\Psi,\theta) n_x(\Psi,\theta) > \\ -2\mu_0 rl \frac{< g^{-1}(\Psi,\theta) n_y(\Psi,\theta) >< g^{-1}(\Psi,\theta) n_x(\Psi,\theta) >}{g^{-1}(\Psi,\theta)} \end{aligned} \tag{2.18}$$

The term g^{-1} is termed the inverse gap function, which becomes a constant for the uniform airgap machine and is a constant in the d-axis under the pole face and approximately zero in the q-axis for a salient-pole machine. The term $<>$ represents the average of the turns function. The angle θ defines a particular angular position along the stator inner surface while Ψ is the angular position of the rotor with respect to a stator reference. But this theory is less applicable in the analysis of synchronous machines due to the approximations for a non-uniform air-gap and complicated windings configuration.

2.3.6 *Modified Winding Function Approach (MWFA)*

In this approach, the actual distribution of air-gap length, the effects of slots, and MMF drop in the iron are incorporated into an approach to calculate the inductances of an experimental synchronous machine [11]. Comparison with the inductance

values calculated using FEM shows that considering these aspects of the machine significantly improves the accuracy of calculated inductances. One way of compensating for these factors is to define an effective permeance function based on the physical air-gap function and utilizing experimental values. The minimum data required to use this model is the number of poles, number of stator slots, actual distribution of the windings, and the geometry of rotor poles. In contrast to the dqo based approach, this method correctly represents the phase belt harmonics, and the inductances of small portions of a winding can be represented more accurately.

2.3.7 *Multi-loop Method*

The multi-loop theory was developed to analyze the behavior of currents and fluxes in the internal branches of the generators with multiple branches. The complexity of the inductance calculation and the large number state variables required for simulation equations make this model difficult to apply in practical large generators. The multi-loop model and parameters described in [14] is more convenient than the classical phase domain method for the analysis of internal faults. According to the model, an AC machine is considered as an electric circuit linked with a ferromagnetic circuit. The difference between ac machines and general static circuits is the existence of relative movement between the stator and the rotor. Hence, some loop inductances of ac machines vary relative with the rotor position, that is, these inductances are time-variant and space-variant coefficients. The single coil is taken as the fundamental unit in order to study and discuss the electromagnetic relation of ac machines. The difference between the calculated values and experimental data is bigger when only the fundamental of air-gap magnetic field is modeled in the simpler phase domain models. However, when accounting for the higher harmonics by the multi-loop method, the calculated values are close to the experimental data [14].

2.3.8 *Application of the Finite Element Method (FEM) in Obtaining the Inductances of Electric Machines*

The FEM is a very detailed and accurate method that can be used for analyzing electric machines. In a FEM analysis, the exact geometry of machine parts such as dimensions of stator, rotor and their slots, precise distribution of the windings and air-gap length are taken into account. The electromagnetic properties of the material used in the machine are considered in a FEM analysis. Although finite element analysis is a very accurate and detailed method of analyzing electric machines, it is also a very

time consuming process. In FEM based studies, the inductances of machines must be calculated for each rotor position, and various loading conditions and field excitations. Such analysis, although performed only once, is extremely time-consuming. FEM solutions had been developed to simulate internal faults and winding-and permeance-based time harmonics. FEM considers details of machine materials, geometry, saturation level, etc., and also has the capability of providing extremely detailed plots of the functional variation of inductances with rotor position through repeat solutions. FEM can be used to obtain the inductances of an experimental machine, and to verify the inductance values calculated by the modified winding function approach (MWFA) and the multi-loop method. The FEM can be used as a alternative method to validate and fine tune the MWFA approach and multi-loop method.

2.4 INDUCTANCE CALCULATION OF THE LABORATORY SYNCHRONOUS MACHINE

A 4 pole salient pole synchronous machine consisting of 54 slots is studied in this thesis. It has two parallel branches per phase and it is a double layer wound machine. The machine has 9 stator coils in series per phase and each coil has total 10 turns. It has a total of 90 turns in one parallel branch for one phase. The total number of turns in the machine are 540. The rotor has 6 poles and each pole has 536 turns per pole. The machine winding layout of one parallel branch of A phase is shown in Fig. 2.1.

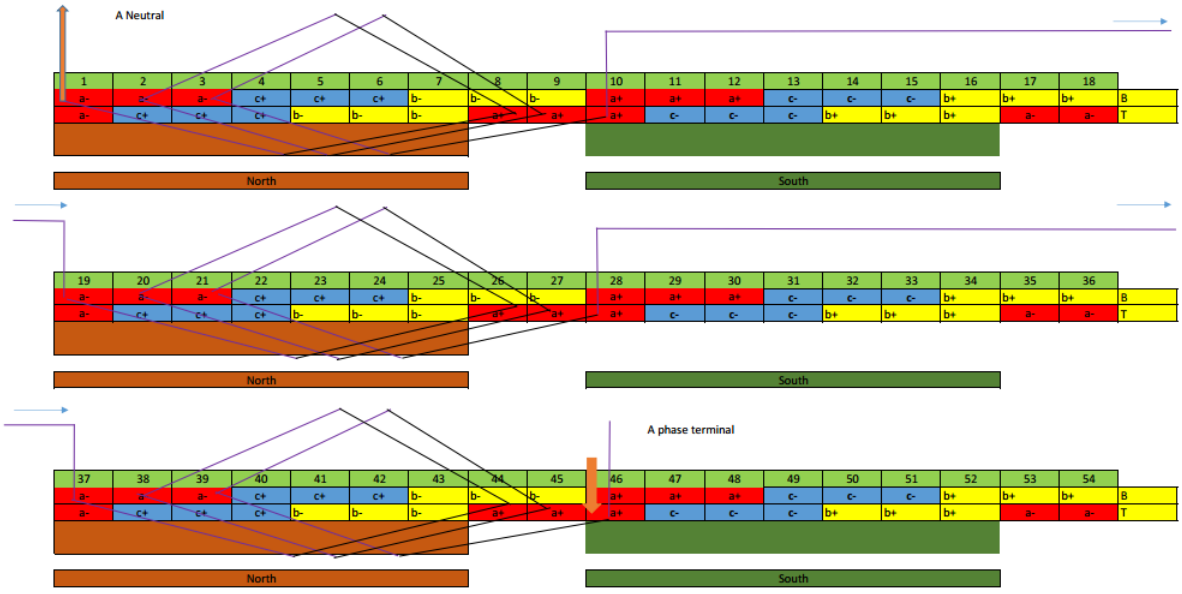

FIGURE 2.1: Winding Layout of One Parallel Branch of A phase

A simplified magnetic model will be developed inductance calculation in Appendix B. The mmf per pole is equal to the number of turns on the field pole and multiplied by the field current. The field mmf generates a rectangular wave around the pole with the fundamental flux density (Bmax) shown in Fig. 2.2.

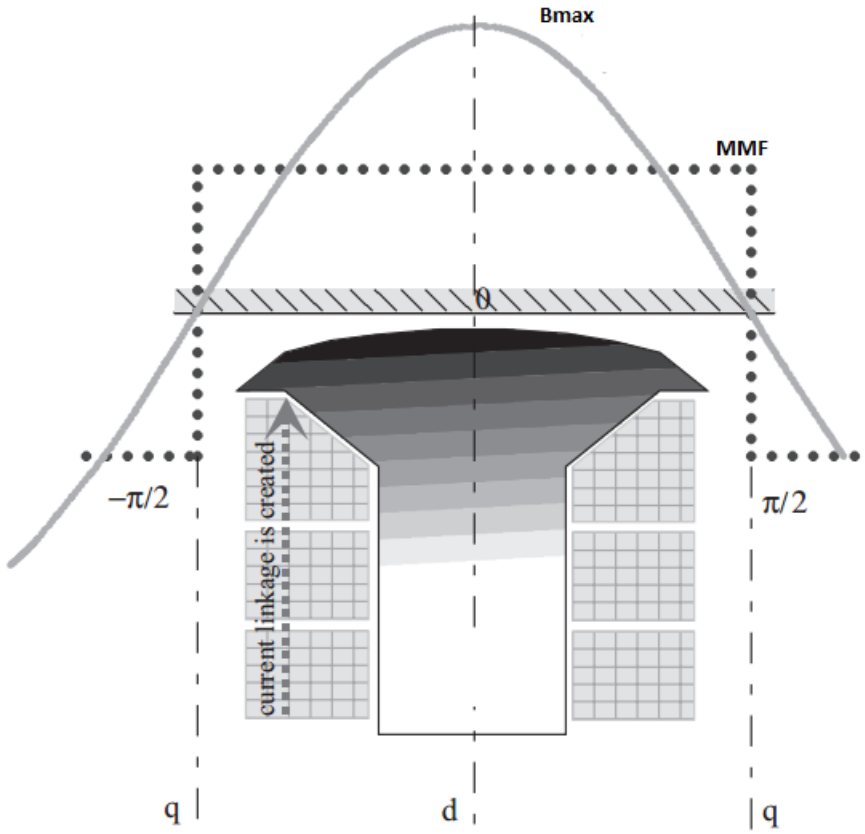

FIGURE 2.2: Representation of MMF Wave of Rotor Pole

In an actual machine, the MMF wave produced by each winding consists of a fundamental component and odd space harmonics. Each winding is made of a limited number of coils. Flow of current in each coil creates a square wave MMF and the combination of coils create a MMF wave which is close to a sinusoidal waveform, but also it contains odd space harmonics. Space harmonics can be minimized by using the fractional pitch windings. In addition, the rotor pole arc is not exactly circular but has different curvatures along the pole faces [15]. This design feature makes the flux density more sinusoidally distributed and minimizes the effects of space harmonics further. The effects of slot harmonics can also be minimized by skewing the rotor in small machines and by the application of fractional slot windings in larger machines. Thus, in electromagentic transient program models for electric machines, it is assumed that the machine windings produce a sinusoidal MMF, i.e. space harmonics and slot harmonics are ignored. This assumption is generally accepted in electric machine models for power system studies. Saturation is modeled by adjusting the magnetizing inductance as a function of total d-axis magnetizing current. This treatment is done

for both salient pole and round rotor machines. Saturation on q-axis and effects of cross coupling saturation are ignored. Saturation in the leakage paths is ignored [12].

2.4.1 *Stator inductances*

In a two pole synchronous machine, over the course of each complete rotation of the rotor, each of the stator inductances assumes the same values twice. Therefore, stator inductances show a space variation of period equal to π and hence consist of a constant value and even space harmonics. Similarly, the values of mutual inductances between stator and rotor repeat once in every complete rotation of the rotor. These inductance functions have the period of 2π and consist of odd space harmonics. In the dqo analysis, the space harmonics higher than the second space harmonic are ignored, and the functions that follow are used to represent the inductances of a synchronous machine (for an equivalent two pole machine). This is tantamount to the assumption of windings with a perfectly sinusoidal distribution. Machine inductances also vary with saturation. Stator inductances show a space variation of frequency equal to twice the fundamental frequency and hence, predominantly consist of a constant value and a second space harmonic. The following equations from (2.19) to (2.25) provide the self and mutual inducatances of the a, b and c phases of the stator.

$$L_{aa}(\theta_r) = L_s + L_m cos[2(\theta_r)] \tag{2.19}$$

$$L_{bb}(\theta_r) = L_s + L_m cos[2(\theta_r - 2\pi/3)] \tag{2.20}$$

$$L_{cc}(\theta_r) = L_s + L_m cos[2(\theta_r - 4\pi/3)] \tag{2.21}$$

$$L_{ab}(\theta_r) = -M_s - L_m cos[2(\theta_r + \pi/6)] \tag{2.22}$$

$$L_{bc}(\theta_r) = -M_s - L_m cos[2(\theta_r + 3\pi/6)] \tag{2.23}$$

$$L_{ca}(\theta_r) = -M_s - L_m cos[2(\theta_r + 5\pi/6)] \tag{2.24}$$

Where both L_s and L_m are constants and $L_s > L_m > 0$.
All of the above equations are in the phase domain and are dependent on the rotor

position because of the pole structure in a salient pole synchronous machine. In round rotor machines, inductances will not vary with the rotor position. The rotor and damped bar self inducatances are constant with respect to the rotor position but the rotor to stator mutual inductances will vary with respect to the rotor position. Those will be explained in detail in Chapter 4.

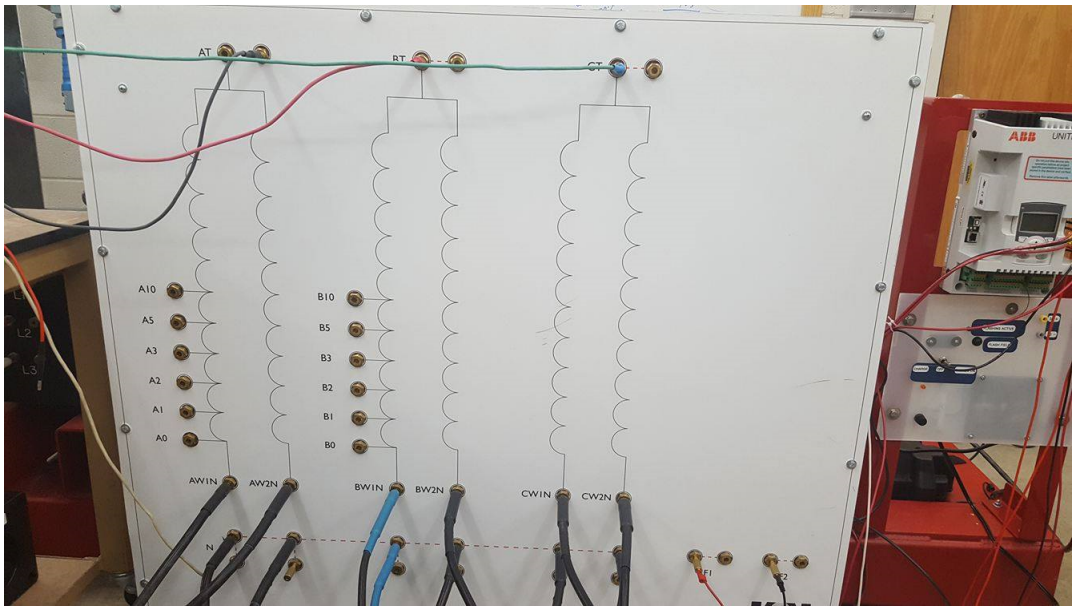

FIGURE 2.3: Laboratory Synchronous Generator With Taps to Create Internal Faults

2.5 INDUCTANCE FIELD MEASUREMENTS

The laboratory synchronous machine shown in Fig. 2.3 has the taps available for creating turn-to-turn faults. The taps can facilitate shorting of 10 turns, 7 turns, 5 turns, 3 turns 2 turns and 1 turn; and can be used to create turn-to-turn and turn-to-ground faults. As explained earlier, the laboratory synchronous machine has 9 coils in series for each parallel branch of a phase. Each coil has 10 turns and that can be represented as shown in Fig. 2.4. The taps from Fig. 2.3 are also delineated in Fig. 2.4.

FIGURE 2.4: Laboratory Machine Coil Representation with Connecting Taps for Internal Faults

2.6 APPROXIMATE TURN-TO-TURN FAULT CURRENT CALCULATION

Appendix B shows the calculation for determining approximate turn-to-turn fault currents. These approximate values which are obtained from the basic parameters of the machine can be used to predict the behavior of the flux linkages with the rotor field winding.

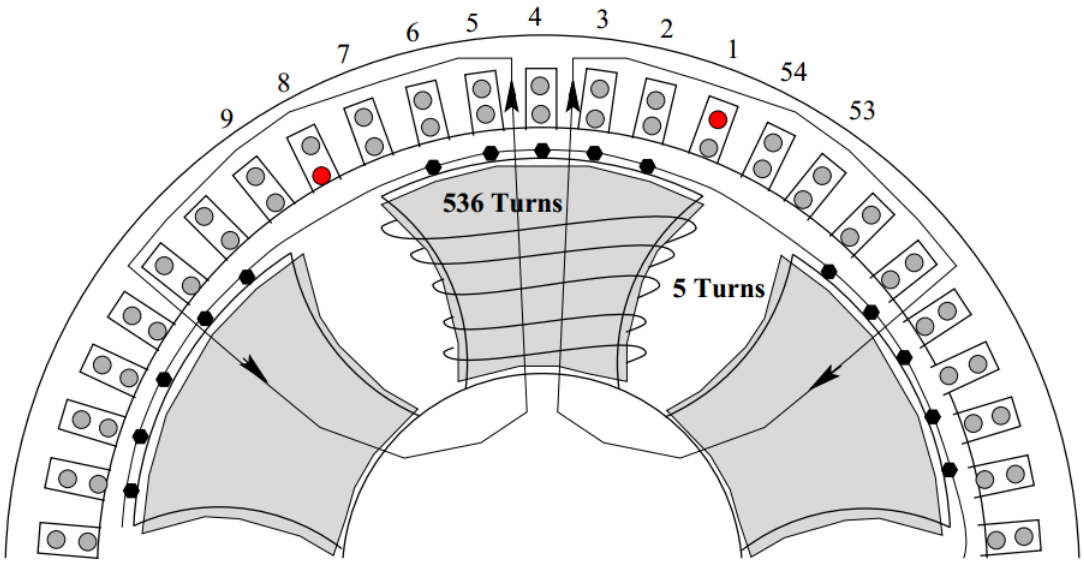

FIGURE 2.5: Representation of Faulted Coils and Field Turns

Fig. 2.5 shows the visual representation that can be used as a basis to understand the simplified model of the synchronous machine for the calculation of inductance of turns. The inductance calculation first calculated the flux per pole linking the turn using (2.1). The assumption used in the approach is 10% of the inductance calculated using the flux per pole, is leakage inductance. This leakage inductance can be used to calculate the approximate magnitude of turn-to-turn fault currents. The Appendix B also uses zero sequence reactance to approximately estimate the magnitude of turn-to-turn fault currents.

Fig. 2.6 shows the approximate calculation of the reactance of the short circuit current for one turn as relative permeability is varied. Fig. 2.7 shows the approximate current in a single shorted turn as relative permeability is varied. The reactance values can be compared with the values in Table 2.1.

The calculated impedances and currents can also be compared with the experimental results in the Chapter 5.

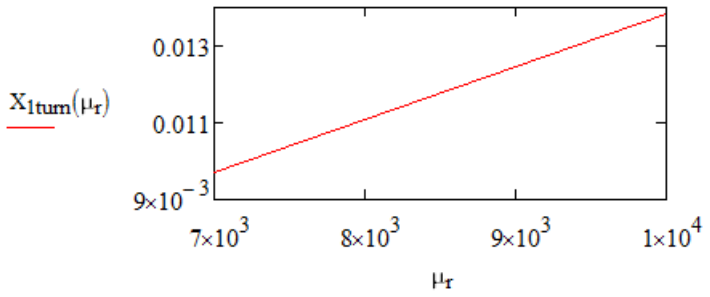

FIGURE 2.6: Calculated One Turn Reactance for Various Relative Permeabilities of the Core

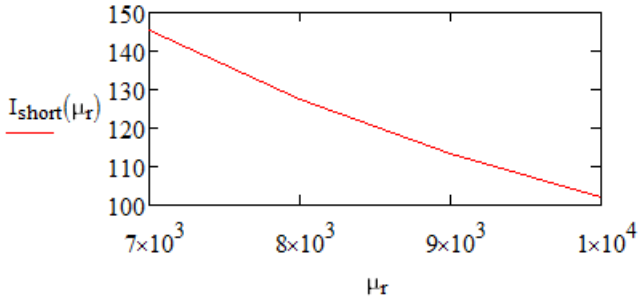

FIGURE 2.7: Calculated One Turn Current for Various Relative Permeabilities of the Core

2.6.1 *Experimental Measurements of Impedances*

The current and voltage signals recorded using a SEL relay are post processed in MATLAB. The follow cases were tested

1. Field circuit is open, B and C phases are open, excite A phase with voltage using an auto transformer, rotate the rotor manually
2. Field circuit is shorted, B and C phases are open, excite A phase with auto transformer, rotate the rotor manually
3. Field circuit is open, B and C phases are shorted, excite A phase with auto transformer, rotate the rotor manually
4. Field circuit, B and C phases are shorted, excite A phase with auto transformer, rotate the rotor manually.

Equation (2.25) is used for calculating the impedance associated with the winding from the relay measurements.

$$Z_{measured} = \frac{V_{measured}}{I_{measured}} \tag{2.25}$$

Fig 2.8 shows the effective impedance of one phase A winding branch when phases B and C are open and the field is open. The impedance of the full phase leg, a 10 turn coil, 5 turns and one turn are plotted. The equations and MATLAB code used to generate these plots are shown in Appendix C. In this measurement, the impedance of the winding varies with the rotor position. It is shown that the impedance value goes high when the rotor axis is aligned with the winding axis where the flux will be maximum. Similarly, the impedance value goes lower when the rotor axis is in quadrature with the winding axis where the flux is minimum. An effect due to damper bars is also present because the relative speed between the stator field and rotor is present between them.

In Fig. 2.8, Fig. 2.9, Fig. 2.10 and Fig. 2.11, the impedance per branch, per 10 turns and per 5 turns and for one turn each are plotted. Note that the effective impedance decreases as the number of turns decreases.

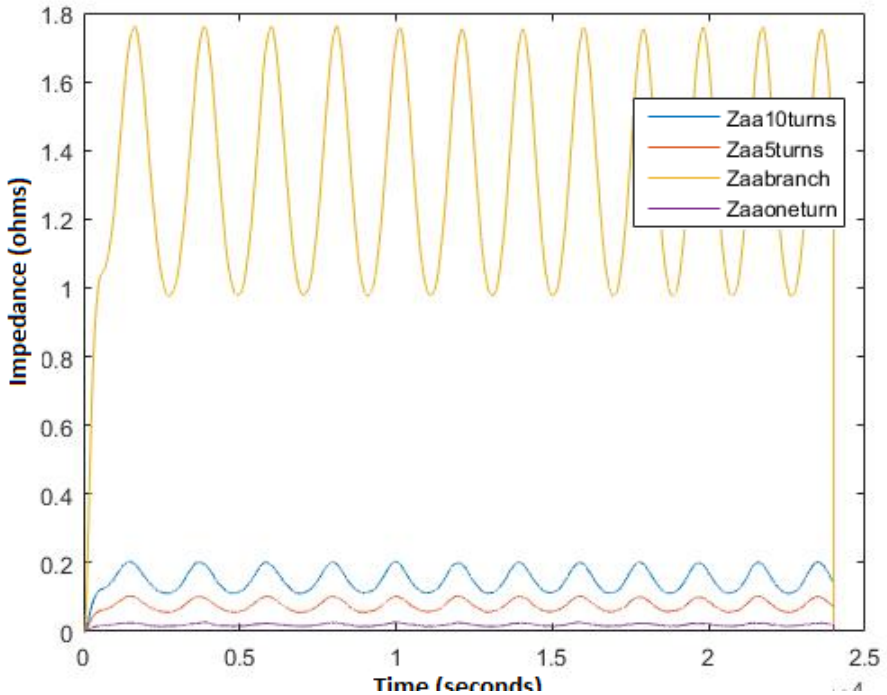

FIGURE 2.8: Measured Impedances on Phase A When Field Winding and the B and C Phase Windings are Open

Fig. 2.9 shows the impedance of one phase A branch when phases B and C are open and but now the field is closed. Since the field winding is closed, the current flowing in the field winding reduces the impedances compared to the case in Fig 2.8.

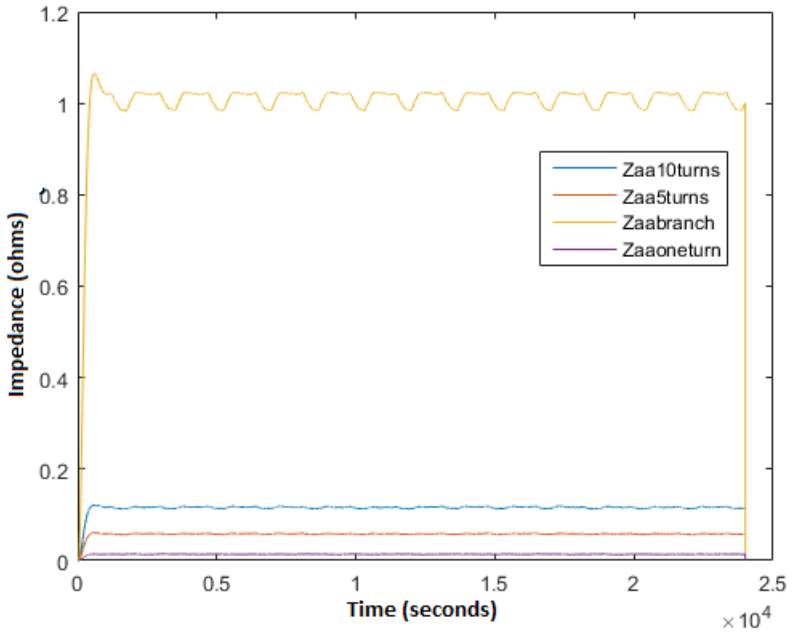

FIGURE 2.9: Measured Impedances on Phase A at Tap Points When the Field Winding is Shorted, B and C Phase Windings are Open

The impedance seen for different points on one phase A branch when the phase B and C windings are shorted and the field winding is open are shown in Fig. 2.10. Since the field winding is open, there will not be any opposing flux induced from the field winding, hence the impedance varies with the rotor position but the magnitude is less than in the case 1 or case 2 due to the mutual action of the phase windings B and C.

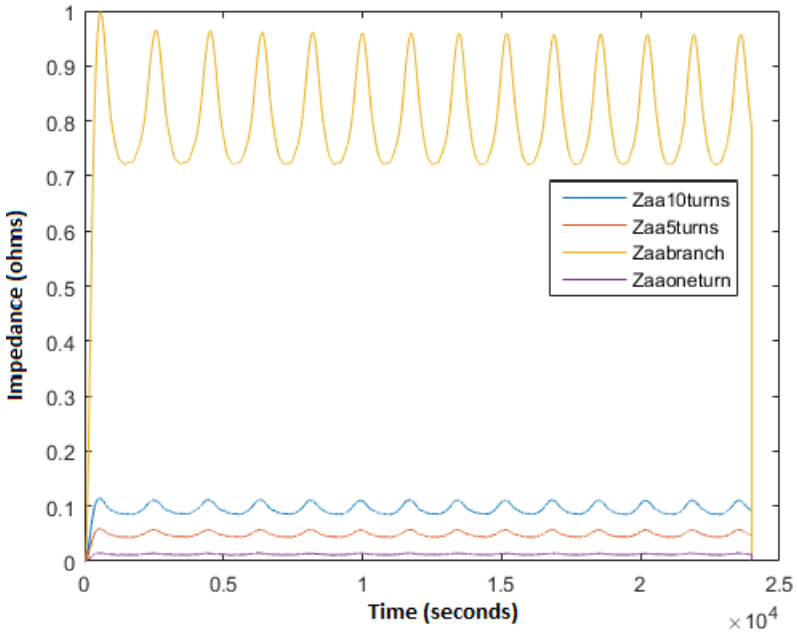

FIGURE 2.10: Measured Impedances of Phase A Winding When Field Winding is Open, B and C Phase Windings are Shorted

The impedance different points on one branch of phase A when phases B and C are shorted and field winding is shorted are shown in Fig. 2.11. This case includes the mutual effect of the current flowing in the other phase windings and field winding. As a result the effective impedance are lower.

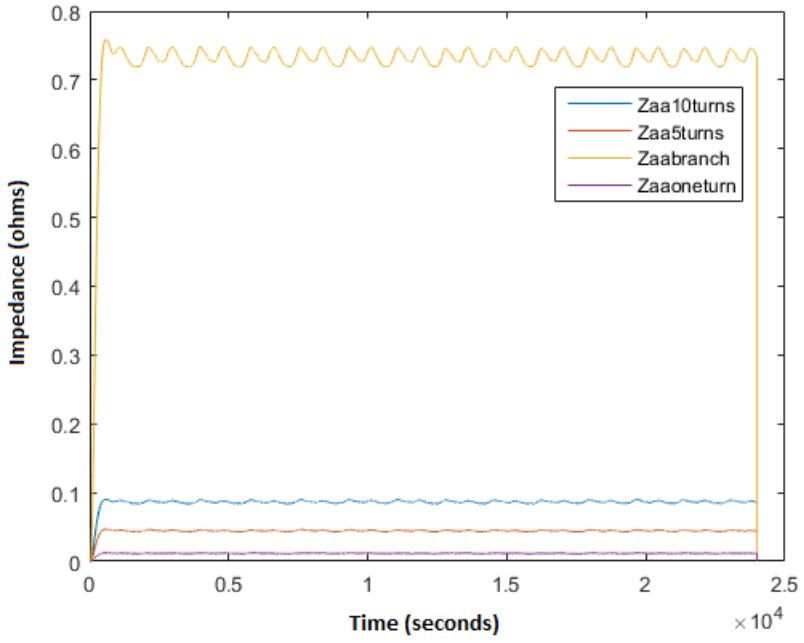

FIGURE 2.11: Measured Inductances of Phase A Winding When Field Winding, B and C Phase Windings are Shorted

2.6.2 *Leakage Reactance of the Machine*

In rotating electrical machines, the total flux does not participate in electromagnetic energy conversion as a whole: the proportion of the flux that participates in energy conversion is called the main flux (air-gap flux), ϕ_m, of the machine, and the flux components not acting in this process are defined as the leakage flux ϕ_l. The main flux crosses the air gap of rotating machines. An important function of the main flux therefore being to link electromagnetically both the stator and the rotor. In this sense, an air-gap flux, ϕ_m, creates an air-gap flux linkage, Ψ_m, to the investigated winding, and consequently links different parts of the machine. The leakage fluxes of the stator and rotor do not generally cross the air gap. They contribute to the generation of the total flux linkage of the winding by producing a leakage flux linkage Ψ_l component to only that winding. Flux leakage occurs in both the stator and the rotor windings. The corresponding leakage flux linkages are the flux leakage Ψ_{sl} of the stator and the flux leakage Ψ_{fl} of the rotor. A leakage flux also occurs in the permanent magnet materials of the machine. Because of the flux leakage, more magnetic material, and correspondingly more magnetizing current, are required than in the case without flux leakage. Flux leakage is often considered a negative phenomenon. However, flux leakage in some cases has a positive role also. For instance, the transient inductance

$L_d^{'}$ of a synchronous machine shown in (2.26) is dominated by the sum of the stator and rotor flux leakage i.e. $L_d^{'} = L_{sl} + L_{fl}$. Where L_m is the magnetizing inductance of the machine [15] and is larger than L_{sl} and L_{fl}.

$$L_d^{'} = L_{sl} + \frac{L_{fl}L_m}{L_{fl} + L_m} \tag{2.26}$$

The calculation of leakage inductances from the structural dimensions of the machine is a rather demanding task. Some of the leakage inductances are real ones created by a real leakage flux. Imaginary leakage inductances are employed to correct inaccuracies resulting from simplifications made in the calculation [15]. The flux components that do not cross the air gap self-evidently belong to the leakage flux.
Among these components we have:

1. Slot leakage flux
2. Tooth tip leakage flux
3. End winding leakage flux
4. Pole leakage flux

Since, it is difficult to measure the leakage inductance of the machine, it can be approximated by the zero sequence reactance of the machine. IEEE Standard 115-1995 [3] describes the test procedure for determining the zero sequence reactance of the machine. With the neutral terminals of the windings connected together as for a normal operation, the three-line terminals are also connected together so that the three phases are in parallel. A single-phase alternating voltage is applied between the line terminals and the neutral terminals. It is preferable that the machine be driven at normal speed, with the field short-circuited and with normal cooling. However, nearly the same values will be obtained with the rotor at standstill, and the test may, therefore, be conducted under this condition if the heating during the test is not excessive. To conduct this test the machine windings are connected as shown in the Fig. 2.12 and test readings were taken when the field circuit is shorted.
The zero-sequence impedance is obtained using (2.27)

$$Z_{0stator} = \frac{3.V_{applied}}{I_{measured}} \tag{2.27}$$

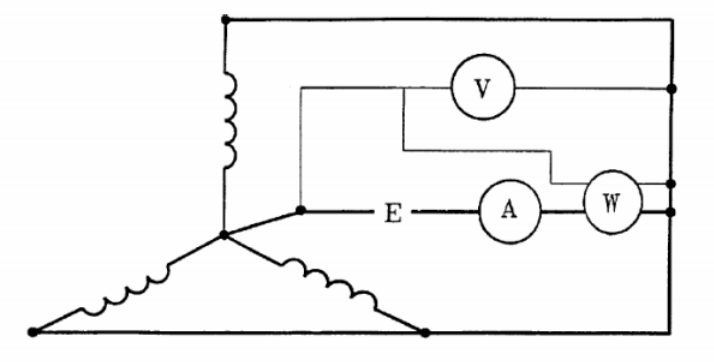

FIGURE 2.12: IEEE 115 Standard Test Setup for Zero Sequence Impedance Measurement

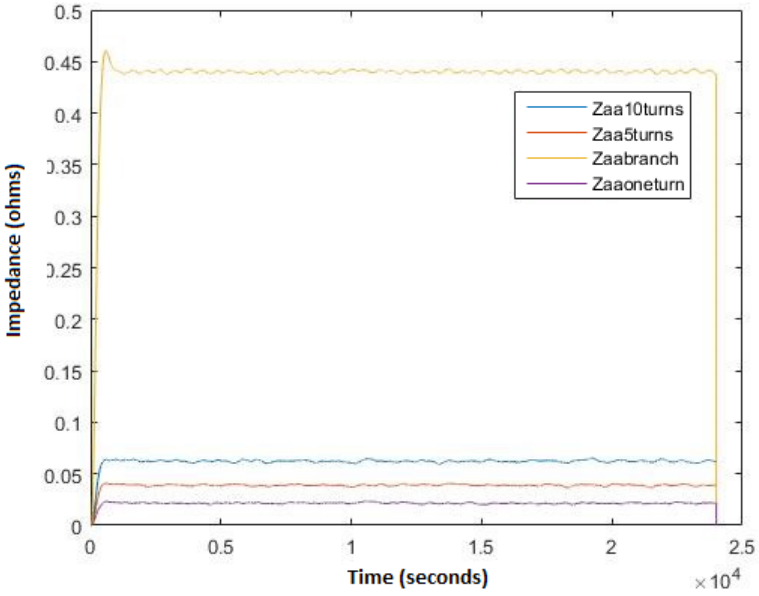

FIGURE 2.13: Relay Measured Zero Sequence Impedance of the Phase A for the Laboratory Machine

The calculated zero sequences impedance for the total branch, 10 turn, 5 turns and 1 turn versus rotor position are shown in Fig. 2.13. Tables 2.1 and 2.2 summarizes the impedances measured by the relay for all the above cases and those can be compared with the approximate impedance calculations in Appendix B which were calculated using the method described earlier in this chapter. The approximate calculations will be used to estimate fault currents for setting up a protection scheme.

TABLE 2.1: Summary of the Measured Impedance of the Winding I

	Field winding, B & C phases are open			Field winding is open, B & C phases are shorted		
	Min	Max	Avg	Min	Max	Avg
Impedance per branch (ohms)	0.9779	1.761	1.361	0.7234	0.9916	0.8334
Impedance per 10 turns (ohms)	0.1117	0.2034	0.1575	0.0859	0.1136	0.09969
Impedance per 5 turns (ohms)	0.05665	0.1025	0.07783	0.04379	0.0536	0.05043
Impedance per 1 turn (ohms)	0.01505	0.0252	0.02011	0.01165	0.01413	0.01271

TABLE 2.2: Summary of the Measured Impedance of the Winding II

	Field Winding is Shorted, B & C Phases are Open	Field Winding, B & C Phases are Shorted	Leakage Impedance When Field Winding is Shorted
Impedance per branch (ohms)	1.019	0.7291	0.1456
Impedance per 10 turns (ohms)	0.1139	0.08598	0.02008
Impedance per 5 turns (ohms)	0.05925	0.4436	0.0130
Impedance per 1 turn (ohms)	0.012	0.0116	0.0068

2.7 SUMMARY

This chapter summarized the basic machine details that are needed to calculate the approximate impedance per turn of a synchronous machine. This result can be used to analyze the severity of turn-to-turn faults in a synchronous machine. This chapter also reviewed the literature related electrical machine modelling with a focus towards internal fault calculation. The machine modeling review focused on magnetic circuit models, a modified winding function approach and multi-loop method of machine behavior during faults among others. This chapter also showed impedances measured on the laboratory generator by the relay for different internal fault conditions.

CHAPTER 3

Protection Elements for Turn-to-Turn Faults

Synchronous machine damage due to turn-to-turn faults can be minimized if those faults are detected quickly. This chapter reviews the theory behind several detection methods that are commonly used for identifying the internal faults in the machine and introduces concepts that will be used in the proposed method.

3.1 PERCENTAGE DIFFERENTIAL PROTECTION OF GENERATOR

Short circuits between the phases of the stator windings to normally cause very large fault currents. The short circuit increases risk of damage to insulation, windings and the stator core. The large short circuit currents cause large forces, which can damage other components in the power plant, such as the turbine and the generator-turbine shaft. The short circuit can also cause an explosion or a fire. The extent damage caused by the short circuit current depends on the fault duration. Immediate detection and fault clearance can reduce the extent of damage and in turn the repair cost and time. Immediate fault clearance of this fault of type is therefore of paramount importance to limit damage and thus economic loss. Both the fault current contributions from the external power system (via the generator transformer and/or the block circuit breaker) and from the generator itself must be disconnected as fast as possible. Fast reduction of the mechanical power from the turbine is of great importance. Instantaneous fault clearance is essential if the generator is connected to the power system close to other generators, if not the transient stability of the non-faulted generators will be in stake. Normally, the short circuit fault current for this type of fault is very large, it is significantly larger than the generator rated current. But sometimes, a short circuit can occur between phases close to the neutral point of the generator causing relatively small fault current. The fault current fed from the generator itself can also be limited due to low excitation of the generator. This can be possible at the start up of the generator, before synchronization to the network. Therefore, it is desirable to be able to have sensitive detection of generator phase-to-phase short circuits so it is able to detect small fault currents. This protection is normally implemented using differential elements.

Differential protection works on the kirchhoff's current law and can detect faults involving high currents. It compares the currents of both terminal and neutral CTs on

each phase and calculates the operating quantity by the phase difference of the two currents. In addition, a restraining quantity is calculated as the sum of the magnitudes of two currents. The percentage differential protection characteristic has a minimum operating point and typically has two slopes to avoid operation due to CT errors or due to CT saturation during external faults. Fig. 3.1 illustrates a relay percentage differential characteristic.

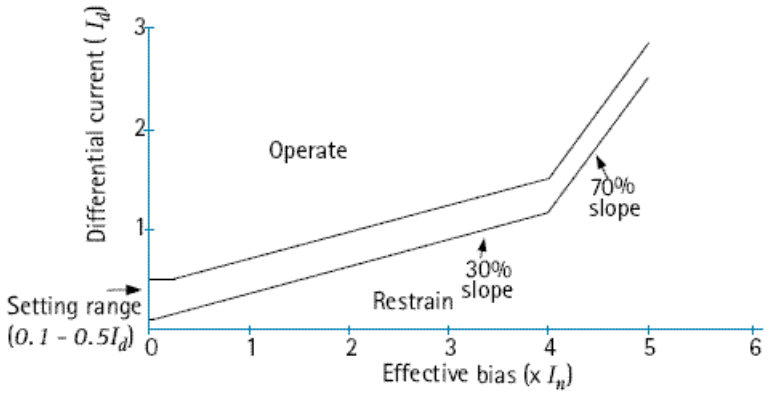

FIGURE 3.1: Percentage Differential Protection Characteristic

Though this protection sounds efficient there is a setback, this protection suffers from the sensitive issues for the faults involving high resistance. If the faults are close to the neutral of the winding, the differential protection may not detect them because of lower operating currents.In addition, this method has limited about to detect shorted turns on the same phase.

3.1.1 *Negative Sequence Differential Protection*

Usually, a negative-sequence differential element is used to detect turn-to-turn faults within the transformer windings [16]. Negative sequence differential protection works on the same principle of phase current differential protection but it considers the calculated negative sequence terminal current and neutral end current quantities [17].

Fig. 3.2 shows the difference between the phase current differential quantities and negative sequence differential quantities based on the measurements at the terminal and neutral currents of the generator. Ideally when CT errors are neglected, the phase differential operate current resides on the restraining axis before the fault occurs whereas the negative sequence differential locus starts from the origin. These negative sequence quantities are very sensitive for detecting high resistance faults and other internal faults where the chances for the phase differential to fail are high.

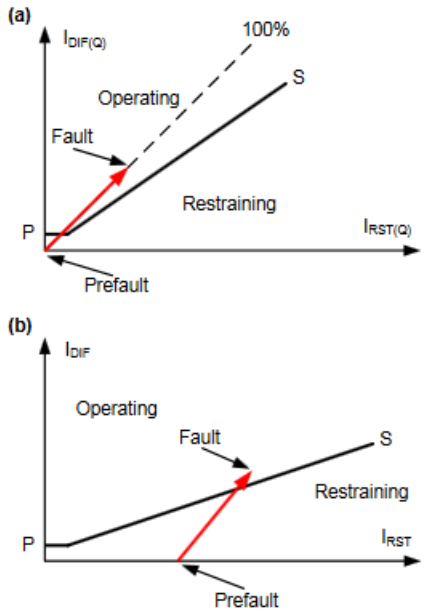

FIGURE 3.2: Difference Between (a) Negative Sequence Current Differential Elements and (b) Phase Current Differential Elements [17]

The 87Q restraining signal alone is not able to properly secure the element under CT saturation. As explained previously, phase currents are responsible for CT errors. Under nearly balanced external faults, the phase currents can be high while the negative-sequence currents (and therefore the 87Q restraining signal) can be very small or even zero. However, CT saturation can also happen because of a long lasting dc offset component in the current, even though the current magnitude is not very high. This is often the case for generator protection relays during the inrush of a nearby transformer or for remote system faults (due to the very large X/R ratio near generators).

3.2 NEGATIVE SEQUENCE DIRECTIONAL ELEMENT

During system unbalances (including short circuits and open-phase conditions), the negative sequence source is on the system side of the apparatus CTs. This source creates a current flow that closes back through the impedance of the stator, reactor, or capacitor bank, creating a proportional negative sequence voltage drop measured by the relay. As a result, the apparent negative-sequence impedance measured at the terminals of the protected apparatus during system unbalances is negative [18].
During unbalanced conditions in the protected apparatus, a negative-sequence source is on the apparatus side of the CTs. This source drives the negative-sequence current

that closes through the negative-sequence system impedance, creating a proportional negative-sequence voltage drop measured by the relay. Since there are no negative sequence voltage sources in the system, the apparent negative sequence impedance is measured at the terminals during unbalances or internal faults in the protected apparatus is positive. The functionality of the negative sequence directional element is shown in Fig. 3.3.

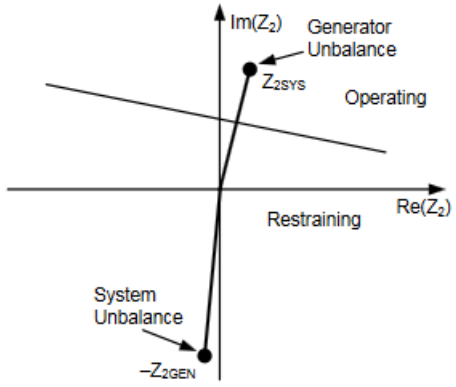

FIGURE 3.3: Negative Sequence Directional Element [18]

Normally, to use this apparent negative-sequence impedance polarity for tripping it is necessary to compare the fault direction at both terminals of the protected apparatus to make sure the fault is not beyond the opposite terminal of the protected apparatus. Still whether or not the total percentage of the winding is covered for protection is a concern.

3.3 ROTOR FIELD MEASUREMENTS

Negative-sequence currents flowing in the stator create a rotating magnetic field in the direction opposite to the rotor spin. As a result, the negative-sequence current induces double frequency currents in the field winding and other parts of the rotor, including the damper windings (if any) and the rotor core surface. Due to skin effect, the double frequency currents will complete their path through the rotor surface and produce rotor heating that can eventually cause rotor damage. In steady state, the flux linking the rotor is constant and hence the opposition to the field current is only due to the resistance of the field winding. But during any disturbance, the flux linking the rotor and stator changes and that will cause currents to be induced in the rotor field winding and damper bars. Since the current through the damper bars cannot

be available to measure, the effect of damper bars current can be ignored from a protection point of view. The mmf of a single-phase winding can be resolved into two rotating mmf waves, each with an amplitude of one-half the maximum amplitude of F_{ag1}, with one, F^{+}_{ag1}, traveling in the + θ_{ae} direction and the other, F^{-}_{ag1}, traveling in the -θ_{ae} direction. Both have an electrical angular velocity θ_{ae} (equal to a mechanical angular velocity of 2ωe/poles):

$$F^{+}_{ag1} = \frac{1}{2} F_{Max} cos(\theta_{ae} - \omega_e t) \tag{3.1}$$

$$F^{-}_{ag1} = \frac{1}{2} F_{Max} cos(\theta_{ae} + \omega_e t) \tag{3.2}$$

Equation (3.1) represents the positive travelling flux wave that produces the useful torque. While the negative traveling flux wave produces a negative and pulsating torque as well as losses. This negative travelling wave causes the double frequency currents to be induced in the field winding. This will be used for detecting turn-to-turn faults under grid disconnected condition in Chapter 5.

$$F^{+}(\theta_{ae}, t) = F^{+}_{a1} + F^{+}_{b1} + F^{+}_{c1} = \frac{3}{2} F_{Max} cos(\theta_{ae} - \omega_e t) \tag{3.3}$$

In general, a rotating field of constant amplitude will be produced by a 3 phase winding excited by balanced 3 phase currents of frequency f_e when the respective phases are offset by 120 deg in space. Equation (3.3) represents the positive rotating magnetic field for 3 balanced currents in 3 phase machine. Any unbalance whether external or internal can cause double frequency currents to be induced in the rotor field winding and that mmf relation can be used to detect turn-to-turn faults when the generator is connected to the grid. This will be discussed in a later chapter.

3.4 SUMMARY

This chapter discussed the protection elements commonly used for the detection of internal faults in a generator. Although the phase current differential element fails to identify the turn-to-turn faults in the generator, a negative sequence differential protection may seem to offer greater sensitivity for the detection. Negative sequence directional elements can also be used to discriminate between internal and external faults in the generator and also can supervise an element or make a trip decision. However, the two elements can only work if the generator is on-line. If the generator

is offline, an alternate scheme is necessary. This chapter proposed using disturbances created in the field current for stator faults for the detection of stator turn-to-turn faults.

CHAPTER 4

Synchronous Machine Behavior During Internal Faults

This chapter provides a detailed discussion of the synchronous machine behavior for internal and external faults using a mathematical model described in Chapter2.

4.1 dqo representation of stator and rotor circuits

The dqo model limitations for modeling internal faults were discussed in Section 2.3.2. However, because of the convenient representation of the synchronous machine in rotating reference frame, the approximate behavior of the synchronous machine during faults can be explained using the dqo model. Using the Park's transformation [9], the 3 phase stator winding equations can be transformed to the dqo reference frame as shown in Fig. 4.1 in which the inductances are constant irrespective of the rotor position. The Park's transformation, also known as the dqo transformation, are also applied to reflect the phase quantities (V, I, ϕ) onto the d and q-axis and can be inverted also for the reverse transformation.

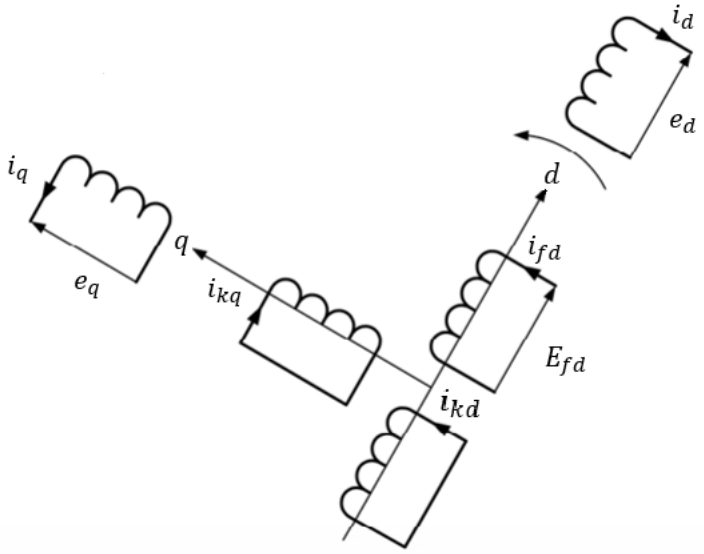

Figure 4.1: Generator Windings in dqo Reference Frame

The following nomenclature will be used in this chapter

f_d = field winding

K_d = d-axis amortisseur winding

K_q = q-axis amortisseur winding

$$\Psi_a = -L_{aa}i_a - L_{ab}i_b - L_{ac}i_c + L_{afd}i_{fd} + L_{akd}i_{kd} + L_{akq}i_{kq} \tag{4.1}$$

where

i_a, i_b, i_c = instantaneous stator currents in Phases a, b, c

L_{aa},L_{bb},L_{cc} = self-inductances of the stator windings

i_{fd}, i_{kd}, i_{kq} = field and amortisseur circuit currents

L_{ab}, L_{bc}, L_{ca} = mutual inductances between the stator windings

L_{afd},L_{akd},L_{akq} = mutual inductances between stator and rotor windings

L_{ffd}, L_{kkd}, L_{kkq} = self-inductances of rotor circuits

The following equations represent the phase voltages in terms of phase flux linkages and currents.

$E_a = -R_a i_a + d\Psi_a/dt$

E_a = Instantaneous stator phase-to-neutral voltage

R_a = Armature resistance

Ψ_a,Ψ_b,Ψ_c = Instantaneous value of the flux linkage

t = time

Similar equations can be expressed for other remaining phases.

$$\Psi_a(t)/i_a(t) = \Psi_b(t)/i_b(t) = \Psi_c(t)/i_c(t) \tag{4.2}$$

$$P(\theta_r) = \sqrt{\frac{2}{3}} \begin{bmatrix} cos\theta_r & cos[\theta_r - 2\pi/3] & cos[\theta_r - 4\pi/3] \\ sin\theta_r & sin[\theta_r - 2\pi/3] & sin[\theta_r - 4\pi/3] \\ 1/\sqrt{2} & 1/\sqrt{2} & 1/\sqrt{2} \end{bmatrix} \tag{4.3}$$

The phase domain above flux linkage equation (4.1) can be transformed to rotating reference frame using park's transformation matrix shown in (4.3). Where θ_r represents speed of the rotating reference frame. The transformed d and q-axes flux linkages are shown in (4.4) and (4.5).

$$\Psi_q = L_q i_q + L_{mq}i'_g + L_{mq}i'_{kq} \tag{4.4}$$

$$\Psi_d = L_d i_d + L_{md}i'_f + L_{md}i'_{kd} \tag{4.5}$$

Where stator inductances L_d and L_q are represented in (4.6) and (4.7), and these are constant inductances in steady-state. The prime quantities in (4.4) and (4.5) indicate that all the rotor quantities were referred to stator turns base.

$$L_d = L_s + M_s + \frac{3}{2}L_m \tag{4.6}$$

$$L_q = L_s + M_s - \frac{3}{2}L_m \tag{4.7}$$

$$\Psi_0 = L_{0s}i_0 \tag{4.8}$$

where L_{0s} represents the stator zero-sequence reactance.
Equation(4.7)represents the zero- sequence flux linkages. The field winding flux linkages and amortisseur winding flux linkages are shown in equations (4.9) to (4.12) in which all the rotor quantities are referred to stator turns base. The four equations indicate that there are two effective damper windings on the q-axis. These two damper windings will show two different time constants in the dynamic response.

$$\Psi_f^{'} = L_{md}i_d + L_{md}i_{kd}^{'} + L_{ff}^{'}if^{'} \tag{4.9}$$

$$\Psi_{kd}^{'} = L_{md}i_d + L_{md}i_f^{'} + L_{ff}^{'}i_f^{'} \tag{4.10}$$

$$\Psi_g^{'} = L_{mq}i_q + L_{gg}^{'}i_g^{'} + L_{mq}i_{kq}^{'} \tag{4.11}$$

$$\Psi_{kq}^{'} = L_{mq}i_q + L_{mq}i_g^{'} + L_{kqkq}^{'}i_{kq}^{'} \tag{4.12}$$

The abc voltage equations are transformed into d-axis and q-axis resulting in (4.13) and (4.14). Equation (4.15) shows the zero sequence term.

$$E_d = p\Psi_d - \Psi_q p\theta - R_a i_d \tag{4.13}$$

$$E_q = p\Psi_q + \Psi_d p\theta - R_a i_q \tag{4.14}$$

$$E_0 = p\Psi_0 - R_a i_0 \tag{4.15}$$

where P represents derrivative with respect to time and $\Psi_q p\theta$ and $\Psi_d p\theta$ are speed voltages (voltages induced due to flux change in space).
The speed voltages are the dominant components of the stator voltage during normal operation. The $p\Psi_d$ and $p\Psi_q$ terms in (4.13) and (4.14) are transformer effect voltages (due to flux change with respect to time).
Under steady-state conditions, $p\Psi_d$ = $p\Psi_q = 0$. The instantaneous phase-to-neutral voltages E_a, E_b, and E_c are replaced with equivalent instantaneous voltages mapped onto the rotating d and q-axis E_d and E_q, respectively. The instantaneous phase currents i_a, i_b, and i_c are replaced with equivalent instantaneous currents mapped on the d and q-axes, i_d and i_q, respectively.
In general, the behavior of the generator impedances can be summarized as follows:In the synchronous reference frame under steady state conditions dc currents flow in the stator i_d and I_q and field windings and the damper currents are zero. The flux linkages between all windings are constant. The inductance looking into the stator is therefore the series combination of the mutual and leakage inductances $(L_{1s} + L_{ad})$ and $(L_{1s} + L_{aq})$ as shown in Fig. 4.2a. Where $(L_{1s}$ is the stator leakage reactance).

Next, consider the response of d-axis terms when the generator is subjected to an external fault. Neglecting the damper windings, it is evident from the previous figure that a current is induced in the field winding due to the fault. As a result, the inductance looking into the d-axis becomes the parallel combination of the mutual inductance (L_{ad}) or (L_{md})) and field inductance over a period determined by the time constant of the field circuit, typically about 1 second. In addition, most synchronous generators will either have a damper winding or will have electrical paths through the rotor iron that mimic the effects of the damper winding. When the damper circuits are considered, the inductance of the d-axis becomes the parallel combination of the 3 branches of the equivalent circuit in Fig. 4.2. This is effective over the period determined by the time constant of the damper winding circuits [19]. The period during which the damper circuit governs the stator impedance is called the sub-transient and typically lasts for 2 to 4 cycles. Subsequently, the damper current decays to zero and the impedance is then governed by the field inductance and is effective for a period on the order of 1 second as discussed earlier. This is also known as the

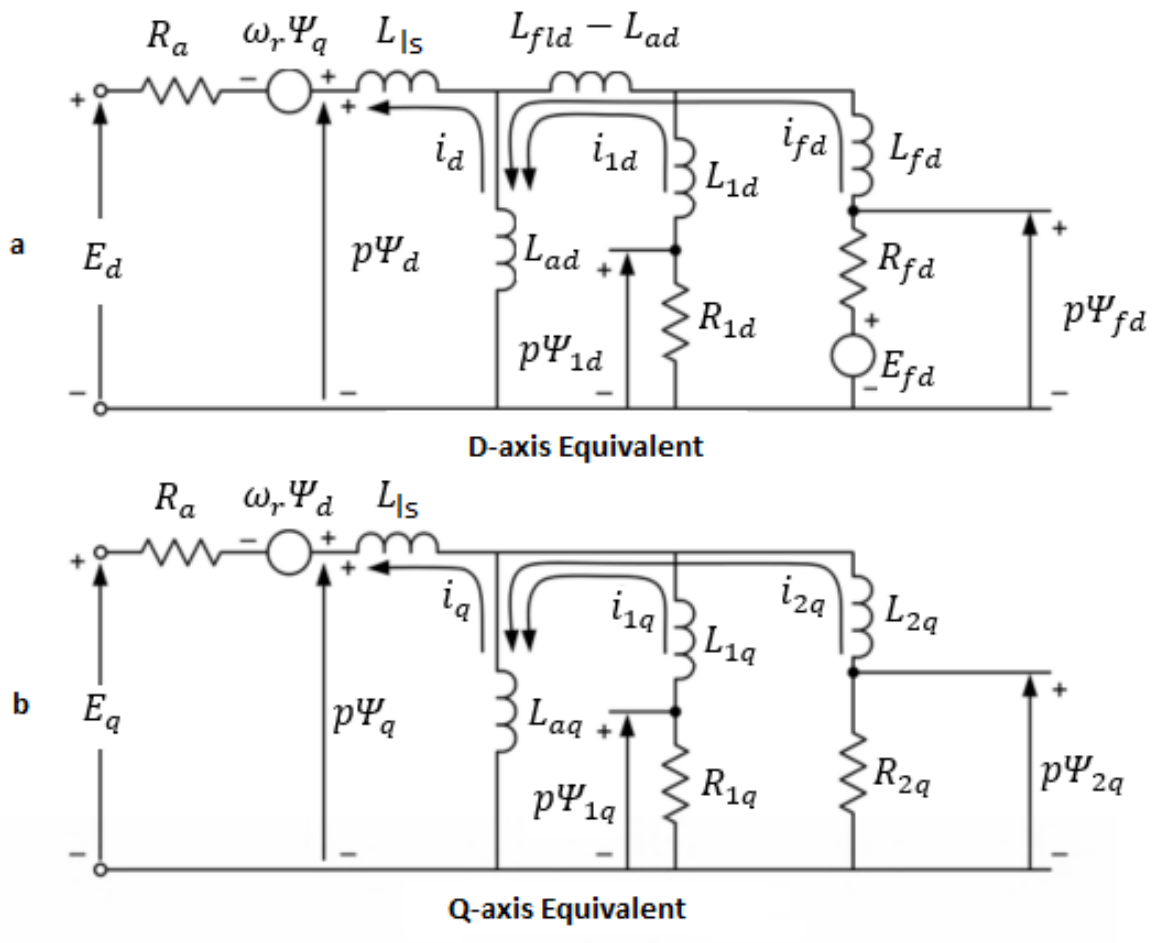

FIGURE 4.2: dqo Representation for Machine Analysis [9]

transient period. The q-axis has no field circuit. However, the overall effects during a fault are similarly defined by time constants the two q-axis damper circuits.

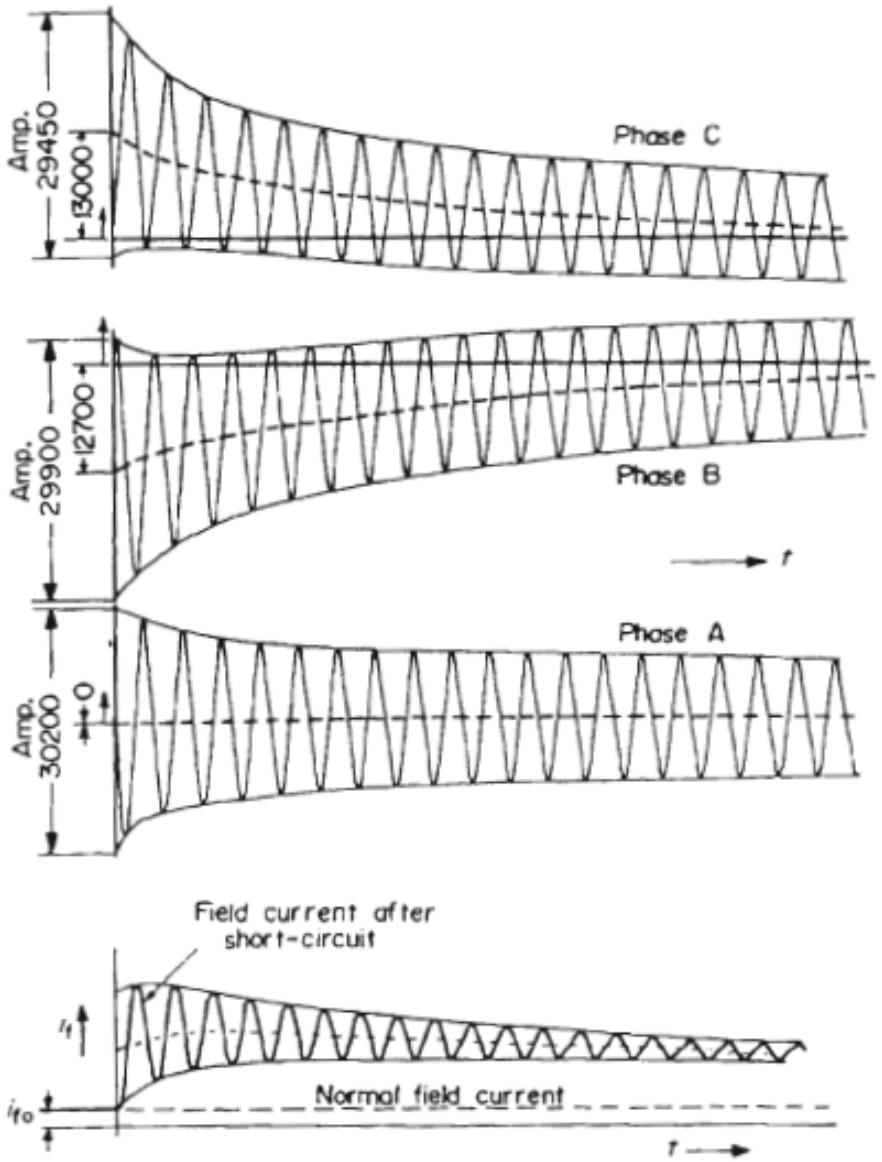

FIGURE 4.3: Short-circuit Oscillogram of Stator Currents [13]

4.2 SYNCHRONOUS MACHINE BEHAVIOR DURING DISTURBANCES

Overall, the short-circuit oscillogram of the stator currents when a 3-phase short circuit is applied to the machine whose stator is initially open circuited and its field excitation held constant, as shown in Fig. 4.3 is commonly used to demonstrate the transient response phenomena shown in Fig. 4.4. Two distinctly different decay periods are exhibited by the symmetrical portion of the short circuit current, which are

generally referred to as the sub-transient and transient periods. The first few cycles of the short-circuit when the rate of current decay is very rapid are attributable mainly to the changes in the currents of the damper windings and referred to as sub-transient period as discussed in section 4.1. The rate of current decay in the transient period is slower and is attributed mainly to changes in the currents of the rotor field windings. In addition there will be a decaying dc offset due to point of fault on the voltage wave. The initial values of the transient fluxes in inductively coupled circuits can be determined by using the theorem of constant flux linkage. For an inductive circuit with finite resistance and emf, it's flux linkage cannot change instantly and if there is no resistance or emf in the circuit its flux linkage would remain constant [8]. Based on this, the constant flux theorem can be used to determine the currents immediately after a change in system operation in terms of the currents before the change. The typical flux distributions of a synchronous machine during the sub-transient, transient and steady-state periods after a stator side disturbance can be explained by using the constant flux linkage theorem as shown in Fig. 4.4. In the sub-transient period which immediately follows the disturbance, the stator-induced flux is limited by the changes in currents in the outer damping windings from penetrating the rotor as shown in Fig. 4.4 (c). The machine enters the transient period as the damper winding currents decay, and the current changes in the field windings react more slowly as shown in Fig. 4.4 (b). The field and damper windings of the rotor are both penetrated by the stator-induced flux in the steady-state Fig. 4.4 (a). The constraint conditions that will be used next in the derivation of the effective inductances of the machine for the sub-transient, transient and steady-state periods can be better understood with the help of Fig. 4.4 [19].

4.2.1 *Steady-state Behavior of Synchronous Machine*

Fig. 4.4 (a) shows the magnetic flux paths one would obtain from measuring the positive-sequence reactance of the machine in steady-state conditions. Typically, one would apply a positive-sequence source to the equipment, and the relationship between the phase voltages and currents would produce a desirable operating condition. When a synchronous generator is operating at synchronous speed with its field circuit open (windings not shown) and with a 3-phase set of positive-sequence currents applied to the armature windings, the currents produce a magnetic field. The resulting mmf will excite the magnetic circuit in the rotor. Fig 4.4 (a) shows the magnetic flux path associated with the armature winding magnetic field and the fundamental sine

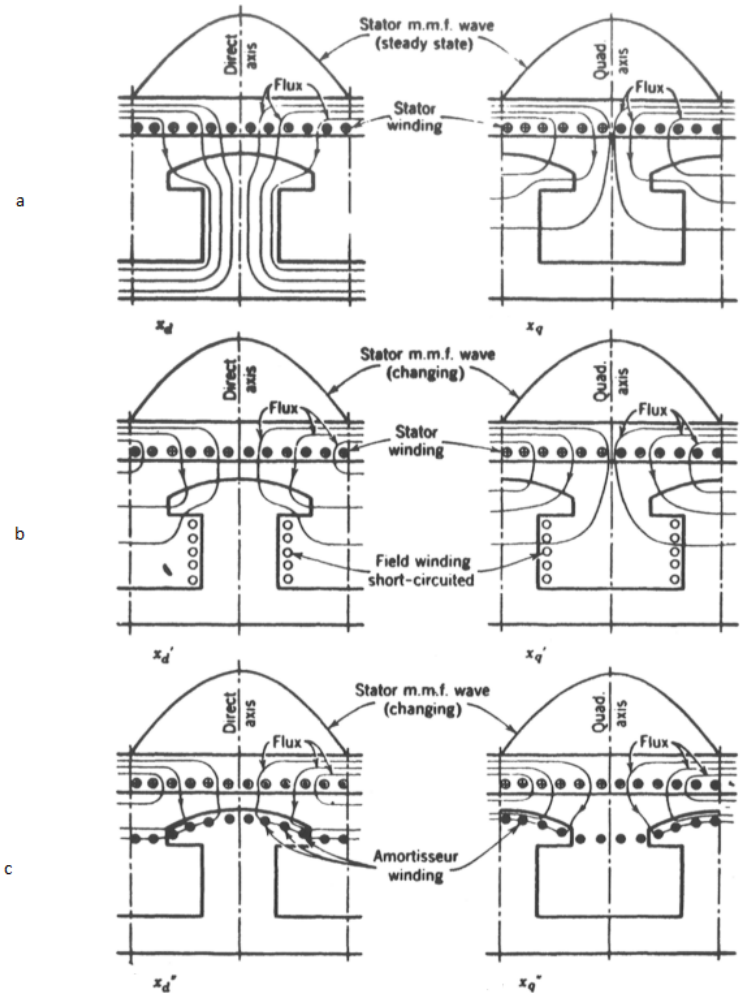

FIGURE 4.4: Flux Patterns Under a) Synchronous, b) Transient, and c) Sub-transient Conditions in d and q-axes [19]

wave that represents the mmf produced by the same steady-state stator currents. Fig. 4.4 (a) shows the magnetic flux path for two operating conditions:

(a) The rotor is positioned so that its direct axis coincides with the maximum value of the mmf. In this case, the reluctance is at a minimum, because the flux path is mainly through the iron core of the rotor. Therefore, the flux is at a maximum. The inductance measured in the stator will be maximum. This provides the necessary d-axis steady-state reactance.

(b) The rotor is positioned so that its quadrature axis coincides with the maximum value of the mmf. In this case, the reluctance is at a maximum because only a part of the flux path goes through the rotor iron core. Therefore, the flux is at

a minimum. The inductance measured in the stator will be minimum. This is referred to as the q-axis steady-state reactance.

In general, $X_d > X_q$, because inductance is proportional to the inverse of the reluctance. For round rotor machines, $X_d = X_q$, because there is little difference in the reluctance of the flux paths for different rotor positions. In general, inductance is defined as the ratio of the flux linked to current. As explained earlier, when the peak of the rotating mmf is aligned with the d-axis, the ratio of the stator flux linkage to stator current is referred to as the d-axis synchronous inductance, L_d. Likewise, when the peak of the rotating mmf is aligned with the q-axis, the ratio of the stator flux linkage to stator current is the q-axis synchronous inductance, L_q. A change in Ψ_d or Ψ_q in synchronous operation where all rotor winding currents are unchanged must be accompanied by a corresponding change in i_d or i_q, as shown in (4.16) and (4.17).

$$\Delta\Psi_d = L_d \Delta i_d \tag{4.16}$$

$$\Delta\Psi_q = L_q \Delta i_q \tag{4.17}$$

In other words, the effective inductances relating Ψ_d and Ψ_q to i_d and i_q are L_d and L_q, respectively. Fig. 4.5 shows the d- axis equivalent circuit for the steady-state condition. From this, it can be seen that during steady-state the opposition to the d-axis current is only L_d.

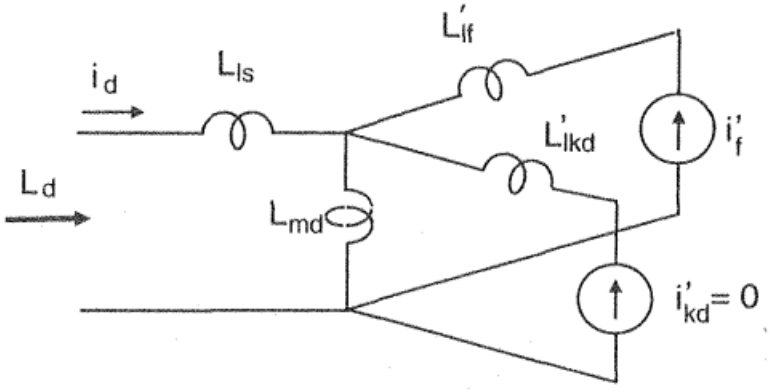

FIGURE 4.5: Equivalent d-axis Circuit for steady-state [8]

For such a change in stator currents, the flux linkages on both the d- and q-axes may be viewed as consisting of two components: that which remains unchanged

when stator currents vary and that which changes along with the stator current. That is,

$$\Psi_d = \Psi_d^{st} + \Delta\Psi_d \quad \textit{and} \quad \Psi_q = \Psi_q^{st} + \Delta\Psi_q \tag{4.18}$$

where Ψ_d^{st} and Ψ_q^{st} are the components which remain unchanged or stationary through the change in stator currents, and Ψ_d and Ψ_q are the corresponding components which change with stator currents. Since the damper winding currents, $i_{kd}^{'}$ and $i_{kq}^{'}$, are zero in steady-state, the unchanged components may be expressed as (4.19) and (4.20).

$$\Psi_d^{st} = \Psi_d - \Delta\Psi_q = \Psi_d - L_d i_d = L_{md} i_f^{'} \tag{4.19}$$

$$\Psi_q^{st} = \Psi_q - \Delta\Psi_q = \Psi_q - L_q i_q = L_{md} i_g^{'} \tag{4.20}$$

In steady-state, the rotor speed, ω_r, is equal to ω_e, thus E_f and E_g in (4.23) are the field excitation voltages induced to the stator referred to the d-axis and q-axis, respectively. These two speed voltage terms that correspond to the two stationary flux linkage components determines the voltage behind steady-state reactances.

$$E_f - jE_g = j\omega_r(\Psi_q^s t - \Psi_d^{st}) = (\omega_r L_{md} i_f{}' - \omega_r L_{mq} i_g^{'}) \tag{4.21}$$

4.2.2 *Transient Time Period Behavior of Synchronous Machine*

The transient reactances, $X_d^{'}$ and $X_q^{'}$, are important in stability studies and short-circuit studies lasting more than several cycles after the initial disturbance. Suppose that the synchronous machine is operated at synchronous speed with a short-circuited field circuit when a positive-sequence source is applied suddenly to the armature windings. It is possible to disregard the effect of the damper windings, because their effect decays after the first during the first two to four cycles. Two scenarios are presented:

(a) The d-axis coincides with the mmf maximum. The resulting inductance presented during the first several cycles (t > 2 cycles) is $L_d^{'} = X_d^{'}/\omega$

(b) The q-axis coincides with the mmf maximum. The resulting inductance presented during the first several cycles (t > 2 cycles) is $L_q^{'} = X_q^{'}/\omega$

As seen in Fig. 4.4 (b), the flux follows paths through the air and the iron. Therefore, $X_d^{'}$ and $X_q^{'}$ have similar magnitudes even for salient-pole machines. However, it is evident from the figure that $X_d \gg X_d^{'}$ due to the low reluctance for the flux to flow

in steady-state condition than transient condition. During the transient period, the induced currents in the field windings are still changing to oppose the change in flux linkage caused by the changing stator currents. The sudden establishment of flux across the air gap is opposed by establishing a current in the field winding, tending to hold Ψ_F at zero.
First consider the changes in flux linkages of the windings on the d-axis. With

$$\Delta\Psi_f = L_{md}\Delta i_d + L_{ff}^{'}\Delta i_f^{'} = 0 \tag{4.22}$$

$$\Delta\Psi_d = L_d\Delta i_d + L_{md}^{'}\Delta i_f^{'} \tag{4.23}$$

Eliminating the change in field current to express $\Delta\Psi_d$ in terms of Δi_d only, results in

$$\Delta\Psi_d = [L_d - L_{md}^2/L_{ff}^{'}]\Delta i_d \tag{4.24}$$

The ratio of $\Delta\Psi_d$ to Δi_d in this situation is referred to as the d-axis transient inductance, that is

$$L_d^{'} \cong \Delta\Psi_d/\Delta i_d = L_d - L_{md}^2/L_{ff}^{'} \tag{4.25}$$

Where $L_{ff}^{'}$ is self inductance of the field winding. Likewise, by considering the changes in flux linkages of the windings on the q-axis, one can show that the q-axis transient inductance is given by

$$L_q^{'} \cong \Delta\Psi_q/\Delta i_q = L_q - L_{mq}^2/L_{gg}^{'} \tag{4.26}$$

Where $L_{gg}^{'}$ is the q-axis damper winding self inductance.

Fig. 4.6 shows the equivalent d- axis representation during transient period. The damper bar currents died away and the change in field current is opposing the change in flux linkage due to short circuits. Hence the leakage reactances of field and and stator winding together offer the impedance to the currents in transient state.

4.2.2.1 *Transient Flux Linkages and Voltages Behind the Transient Inductances*

Equation (4.25) gives the change in Ψ_d to a change in i_d when both i_d and i_f are free to change. Likewise, one can derive a similar relationship between $\Delta\Psi_q$ and Δi_q when both i_q and i_g are free to change. Again, the components in Ψ_d and Ψ_q which will

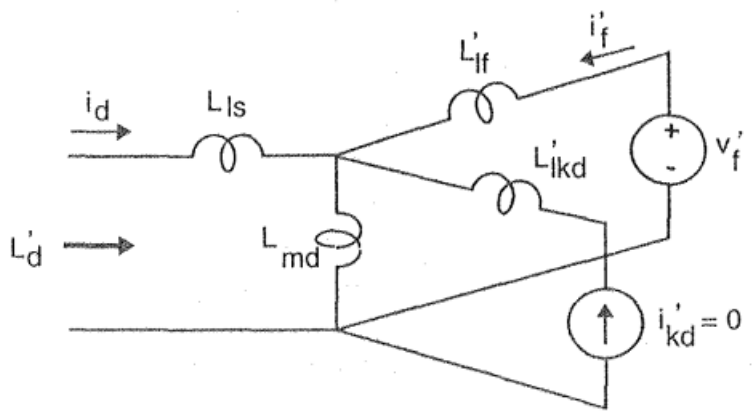

FIGURE 4.6: Equivalent d-axis Circuit for Transient State [8]

remain unchanged by transient stator currents under the transient condition where both Ψ_f and Ψ_g are being held constant by changes in $i_f^{'}$ and $i_g^{'}$,can be identified. They are given by (4.27) and (4.28).

$$\Psi_d^{'} = \Psi_d - \Delta\Psi_d = \Psi_d - L_d^{'} i_d \tag{4.27}$$

$$\Psi_q^{'} = \Psi_q - \Delta\Psi_q = \Psi_q - L_q^{'} i_q \tag{4.28}$$

The definitions of the alternate forms of the effective speed voltage terms associated with the transient flux linkages, $\Psi_q^{'}$ and $\Psi_d^{'}$, are

$$E_q^{'} \doteq \omega_r \Psi_d^{'} = \omega_r L_{md} \Psi_f^{'} / L_{ff}^{'} \tag{4.29}$$

$$E_d^{'} \doteq -\omega_r \Psi_q^{'} = \omega_r L_{mq} \Psi_g^{'} / L_{gg}^{'} \tag{4.30}$$

$E_q^{'}$ and $E_d^{'}$ are the voltages behind the transient inductances in the q and d-axes, respectively. These voltages will determine the currents flowing in turns during the turn-to-turn short circuits.

4.2.3 *Sub-transient Behavior of Synchronous Machine*

The sub-transient reactances $X_d^{''}$ and $X_q^{''}$ are important in short-circuit studies during the first two cycles after the initial disturbance. Again, suppose that the synchronous

machine is rotated at synchronous speed with a short-circuited field circuit, and this time a positive-sequence source is applied to the armature windings. Consider now the effect of the damper windings shown in the Fig. 4.2, because their effect is important during the first two cycles.
Two scenarios are given:

a) The d-axis coincides with the mmf maximum. The resulting effective inductance presented during the first two cycles (t < 2 cycles) is $L_d^{''} = X_d^{''}/\omega$.

b) The q-axis coincides with the mmf maximum. The resulting effective inductance presented during the first two cycles (t < 2 cycles) is $L_q^{''} = X_q^{''}/\omega$.
As seen in Fig. 4.4 (c), the flux follows paths through the air and the iron, and the effect of the dampers is such that the reluctance of the flux path for the d-axis test is smaller. Therefore $X_q^{''} > X_d^{''}$. However, it is evident that $X_d >> X_d^{'} > X_d^{''}$.
It is to be noted that, the reactances associated with the rotor q-axis are used in steady-state only for salient-pole machines and not for round rotor machines. However, in transient studies, they are also considered for round rotor machines if there is significant differences in the magnitudes. The output power of a salient-pole rotor synchronous generator has a different expression than the formula used for the round rotor machine. As a general rule, for round rotor machines, the following is true:

$$X_d \cong X_q >> X_q^{'} \cong X_d^{'} > X_q^{''} \cong X_q^{''} \tag{4.31}$$

The following applies for salient-pole machines:

$$X_q = X_q^{'} > X_q^{''} > X_d^{''} \tag{4.32}$$

For the sub-transient period, changing currents induced in the rotor windings will keep the flux linkage of every rotor circuit initially constant. Since all rotor currents are zero at t = 0-, the flux linkages are also zero and by the law of constant flux linkages must remain zero at t = 0+. With the d-axis rotor flux linkages held constant, that is

$$\Delta\Psi_f^{'} = \Delta\Psi_{kd}^{'} = 0 \tag{4.33}$$

results in

$$\Delta\Psi_f^{'} = L_{md}\Delta i_d + L_{ff}^{'}\Delta i_f^{'} + L_{md}\Delta i_{kd}^{'} = 0 \tag{4.34}$$

$$\Delta\Psi_{kd}^{'} = L_{md}\Delta i_d + L_{md}\Delta i_f^{'} + L_{kdkd}^{'}\Delta i_{kd}^{'} = 0 \tag{4.35}$$

The corresponding change in the d-axis stator flux linkage is given by

$$\Delta\Psi_d = L_d\Delta i_d + L_{md}\Delta i_f^{'} + L_{md}\Delta i_{kd}^{'} \tag{4.36}$$

Substituting (4.18) into (4.35) and defining the ratio of $\Delta\Psi_d$ to Ψi_d in this situation as the d-axis sub-transient inductance $L_d^{''}$, results in the d-axis sub-transient inductance $L_d^{''}$ as shown in (4.34).

$$L_d^{''} = L_{1s} + \frac{L_{md}(\frac{L_{lkd}^{'}L_{lf}^{'}}{L_{lkd}^{'}+L_{lf}^{'}})}{L_{md} + (\frac{L_{lkd}^{'}L_{lf}^{'}}{L_{lkd}^{'}+L_{lf}^{'}})} \tag{4.37}$$

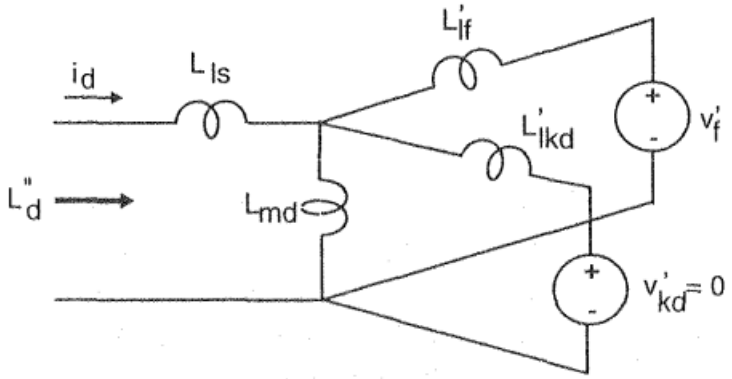

FIGURE 4.7: Equivalent d-axis Circuit for Sub-transient State [8]

The d-axis sub-transient inductance is the Thevenin equivalent inductance of the d-axis stator circuit as viewed from the stator d-axis terminals shown in Fig. 4.7. Note that V_{kd}' is 0, but damper currents are no longer 0. It is the combined inductance of L_{ls} in series with the parallel combination of L_{md}, $L_{lf}^{'}$ and $L_{lkd}^{'}$ as shown Fig. 4.7. Similar derivations and conclusions can be derived for the q-axis. Very little flux is established initially in the field winding and the sub-transient inductance is due largely to the damper windings.

4.2.3.1 *Sub-transient Flux Linkages and Voltages Behind the Sub-transient Inductances*

As in steady-state and transient conditions, one can identify the components in Ψ_d and Ψ_q which will remain unchanged by transient stator currents under the sub-transient condition when the flux linkages of the rotor field and damper windings are constant.

$$\Psi_d^{''} = \Psi_d - \Delta\Psi_d = \Psi_d - L_d^{''} i_d \tag{4.38}$$

$$\Psi_q^{''} = \Psi_q - \Delta\Psi_q = \Psi_q - L_q^{''} i_q \tag{4.39}$$

Likewise, one can also define the speed voltage components associated with $\Psi_d^{''}$ and $\Psi_q^{''}$ as (4.40) and (4.41).

$$E_q^{''} \doteq \omega_r \Psi_d^{''} = \omega_r L_{md} {i_f}' \tag{4.40}$$

$$E_d^{''} \doteq -\omega_r \Psi_q^{''} = \omega_r L_{mq} i_g^{'} \tag{4.41}$$

$E_q^{''}$ and $E_d^{''}$ are the voltages behind the sub-transient inductances in the q- and d-axis, respectively. During external or internal faults these voltage sources will cause the current to flow.

$$\Delta\Psi_f^{'} = L_{md}\Delta i_d + L_{ff}^{'}\Delta i_f^{'} + L_{md}\Delta i_{kd}^{'} = 0 \tag{4.42}$$

Equation (4.42) represents the change in flux linkage of the rotor field winding due to change in stator currents, field current and damper bar current. This is a cumulative effect in which, the field winding current will see this disturbance.
The negative-sequence reactance is calculated as the average between the sub-transient direct-axis reactance $X_d^{''}$, and the sub-transient quadrature axis reactance $X_q^{''}$ as shown in (4.43). Because the impedance of the armature winding is always changing, the average is used to calculate the negative-sequence reactance.

$$X_2 = \frac{X_d^{''} + X_q^{''}}{2} \tag{4.43}$$

The zero-sequence reactance is calculated using (4.44).

$$X_0 = X_{self,AVG} - 2X_{Mutual,AVG} \tag{4.44}$$

where

$X_{self,AVG} = \omega L_{sa}$

$X_{Mutual,AVG} = \omega L_{ma}$

L_{sa} = average self-inductance of the armature winding in Henrys per phase

L_{ma} = average mutual inductance of the armature winding in Henrys per phase.

Since leakage reactance is not easy to calculate, sometimes it is approximated as zero-sequence reactance. Reference [12] claims that the inequality (4.44) among all the the parameter holds good for salient pole synchronous machine.

$$X_d > X_d^{'} > X_d^{''} > X_{leakage} < X_{zerosequence} \tag{4.45}$$

Equations (4.42) and (4.43) determines the quantities that can be used for identifying turn-to-turn faults. The sub-transient parameters determine the negative sequence reactance and hence the negative sequence currents that can circulate during turn-to-turn faults. Equation (4.42) represents the changes in field current due to changes in stator currents and damper bar currents.

4.3 SUMMARY ON FIELD CURRENTS BEHAVIOR FOR EXTERNAL AND INTERNAL FAULTS

Based on the analysis presented in this chapter the following conclusions can be drawn.

1. In steady-state, due to 3 phase balanced sinusoidal currents in the abc phases, the rotating magnetic field (RMF) generated by the positive sequence currents will rotate with rotor in the same direction and there will not be any induced currents in the damper bars and rotor windings. The field current is DC and is being limited by the field winding resistance.

2. For any external unbalance in the system, the flow of negative sequence currents will generate a rotating magnetic field (RMF) and that rotates in the opposite direction to the physical rotation causing double frequency currents to be induced in the field winding and damper bars.

3. Internal faults inside the machines, will cause the flow of negative sequence currents which will produce double frequency currents in the field winding and damper bars. This suggests that measuring the double frequency currents in the field winding can increase the sensitivity of turn-to-turn fault detection. Chapter 5 will explore this further.

4. If the machine is disconnected from the external system, large magnitude turn-to-turn fault currents will still flow which can create the standing mmf wave and that will cause the currents to flow in the damper bars and field windings. Since the axes of field winding and d-axis damper bars are the same, the effect of damper bar current can cause the field current to change. Once the sub-transient period is over, the damper bar currents will die off quickly and the field winding current will change due to the change in flux linkage by the turn-to-turn fault currents. If these disturbances are detected quickly, the turn-to-turn sensitivity can be enhanced and in turn the damage to the machine can be reduced. This suggests that, the negative sequence voltage coupled coupled with the double frequency currents in the field winding can increase the sensitivity of detection of turn-to-turn faults under unloaded open circuit conditions. Chapter 5 will explore this as an option for enhancing protection.

CHAPTER 5

Experimental Results

This chapter will examine the sensitivity of existing generator protection elements and also examine proposed elements using experimental results. The experimental results will also be used to validate the method proposed in Chapter 2 for calculating turn-to-turn fault currents.

5.1 TEST SETUP

The laboratory machine shown in Fig. 5.1 was configured for performing turn-to-turn faults at different winding locations. The dashed portion in Fig. 5.2 represents the two parallel branches of the phase A winding to which the taps are available to carry out turn-to-turn faults. The numerical relay shown in the Fig. 5.2 has current inputs connected from CTs at the winding terminals and winding neutrals. The voltage inputs directly from the terminals of the synchronous generator. The synchronous generator in the figure can be synchronized to the grid through the Analog Model Power System (AMPS). Since the relay shown in the figure cannot directly measure the DC field currents, the double frequency component of the field current was measured by measuring the voltage across a 1 ohm current shunt resistor added in the filed circuit. The double frequency currents can be indirectly calculated from that measured voltage.

Overall, the objective of the test setup shown in Fig. 5.2 was to measure

1. The turn-to-turn fault currents
2. The phase CT currents
3. The neutral CT currents
4. Field current
5. Terminal voltages
6. Turn-to-turn pre-fault voltages.

The measured data were used to calculate

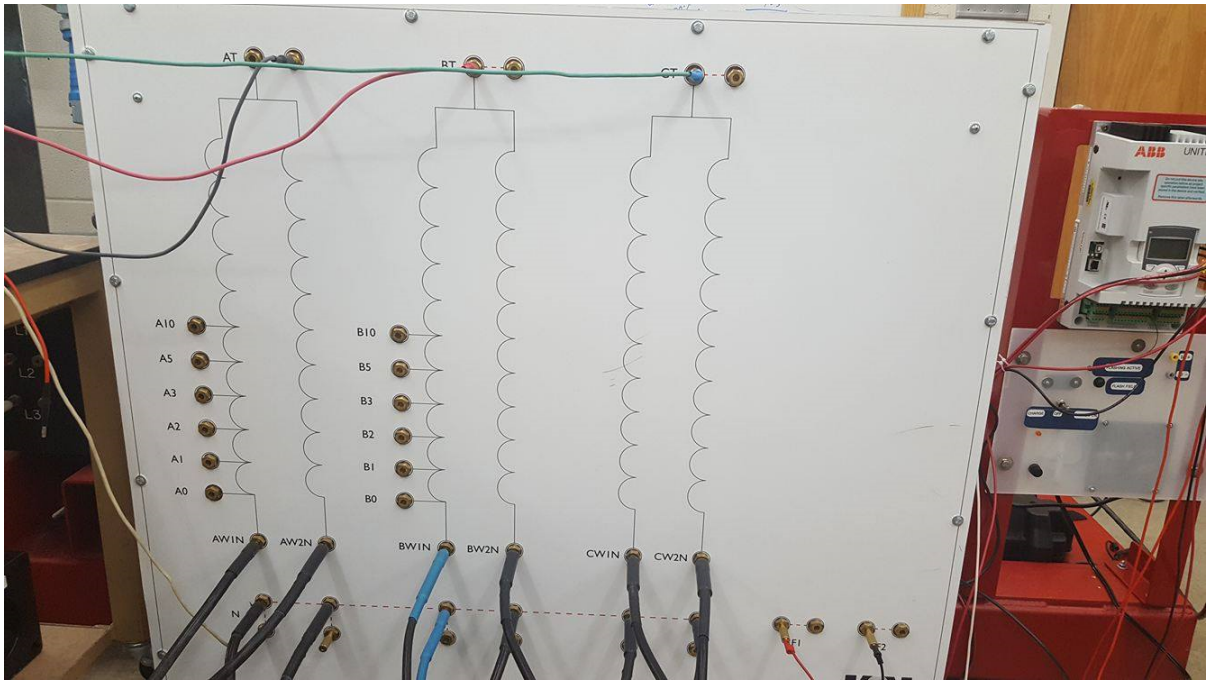

FIGURE 5.1: Laboratory Machine Used for Experimental Results

1. The negative sequence currents at the neural
2. The negative sequence currents at the terminal
3. Zero sequence voltage at the terminal
4. Double frequency currents on the field winding
5. Impedance of the shorted turns

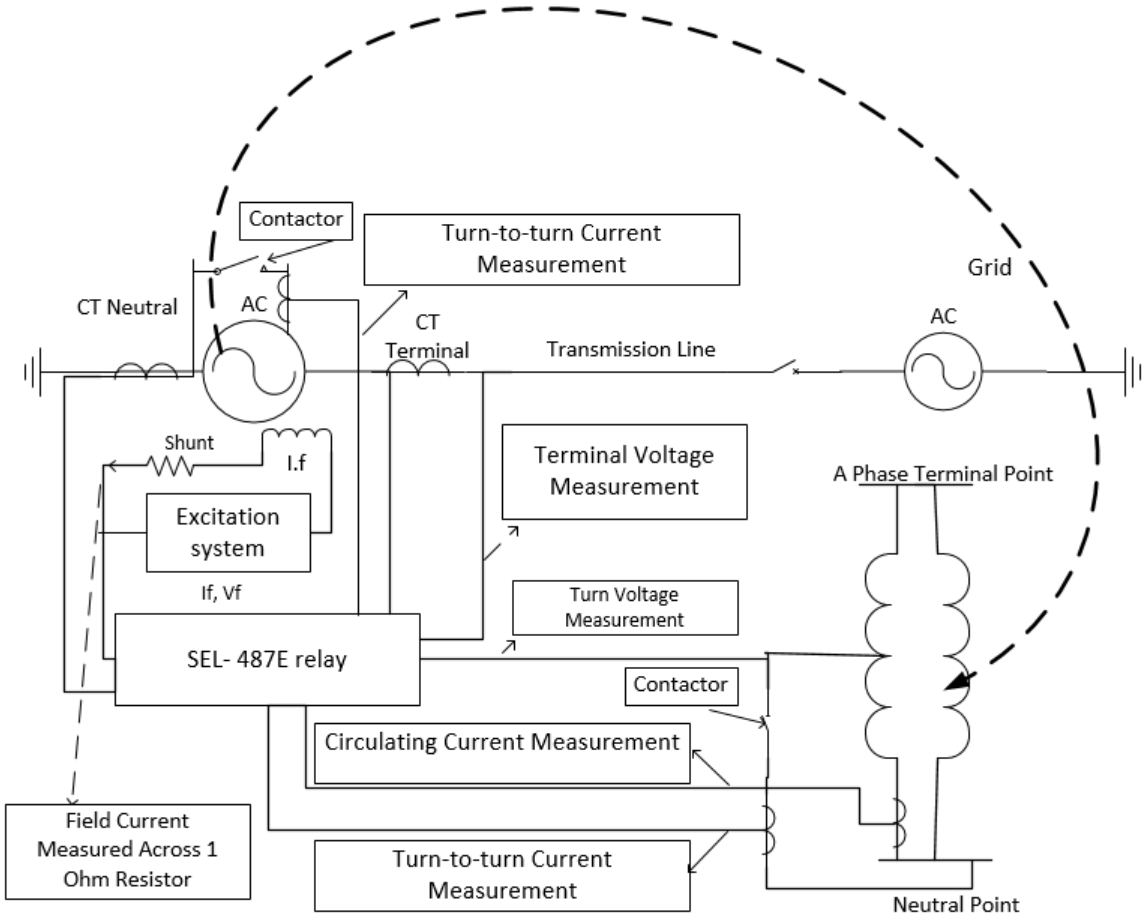

FIGURE 5.2: Test setup for field measurements

The Fig. 5.3 shows the measured phase A voltage at the terminal, the voltage across 10 turns and the voltage across one turn up from the neutral of the machine. The numerical relay used in the test setup can sample the analog signals at 8 kHz. Fig. 5.3 (a) shows that, the terminal voltage of the machine contains higher order slot harmonics. As explained in the previous chapters, the dqo model considers only the fundamental component of the waveform for dynamic analysis of the machine, an increase in harmonic content in the voltage waveform can produce significant errors. It can also be seen that the harmonic content in the voltage waveform increases as the measurement points move to taps that are close to the neutral of the winding. Since the one and 10 turn points examined are physical wound across one pole with a short pitch winding, they will not possess any symmetry and hence the induced voltage across them contains significant harmonic content as shown in Fig. 5.3 (b) and (c). In these cases, analysis using fundamental voltage quantity only will produce significant

errors. Hence, using the dqo model for internal faults analysis can produce significant errors.

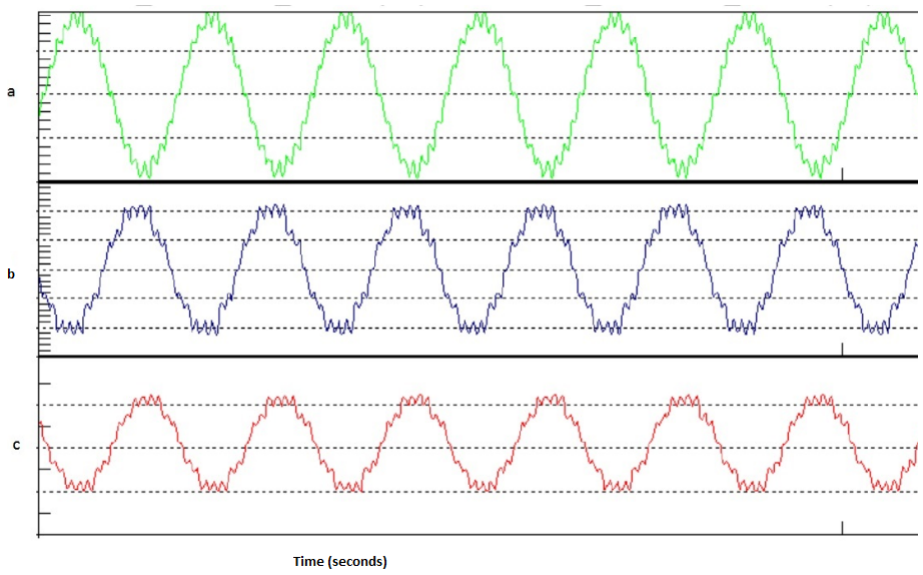

FIGURE 5.3: Voltages Measured by the Relay: (a) Terminal Phase Voltage (V); (b) Voltage Across 10 Turns (V); (c) Voltage Across 1 Turn (V)

TABLE 5.1: Percentage Error of Voltages Across Turns

Tap Position	**Terminal Voltage in Test (V)**	**Measured Turn Voltage (V)**	**Calculated Value (V)**	**Error (%)**
10 turns	127.4	14.91	14.155	5.33
7 turns	127.4	10.7	9.98	7.21
5 turns	127.4	7.6	7.078	7.37
3 turns	127.4	4.4	4.25	3.52
2 turns	127.4	3.1	2.83	9.54
1 turn	127.4	1.49	1.416	5.22

Table 5.1 shows the percentage error of the voltages across the turns compared to the calculated voltages. The voltages considered here are the relay measured fundamental component voltages. The symmetry of the winding and the harmonic content causes the increase in percentage error of the voltage magnitude.

The synchronous machine was used for internal shorted turn faults using the setup shown in Fig. 5.2. It was tested in different cases with 10, 7, 5, 3, 2 or 1

turns shorted. The results were used to determine the sensitivity of negative sequence differential, negative sequence directional and split-phase protection elements by post processing the COMTRADE files using Real Time Digital Simulator (RTDS). The proposed detection techniques were also tested to determine their sensitivity. Before going into the protection elements performance, the next section will describe the analysis conducted to determine the magnitude of turn-to-turn fault currents.

5.2 ANALYSIS ON TURN-TO-TURN FAULT CURRENT MAGNITUDES

Fig. 5.4 shows that the magnitudes of fault currents do not vary much from no-load condition to the loaded condition, hence analyzing the fault currents during no-load condition is preferred for simplicity. In no-load condition there will not be any effect of mutual coupling from the other phase currents.

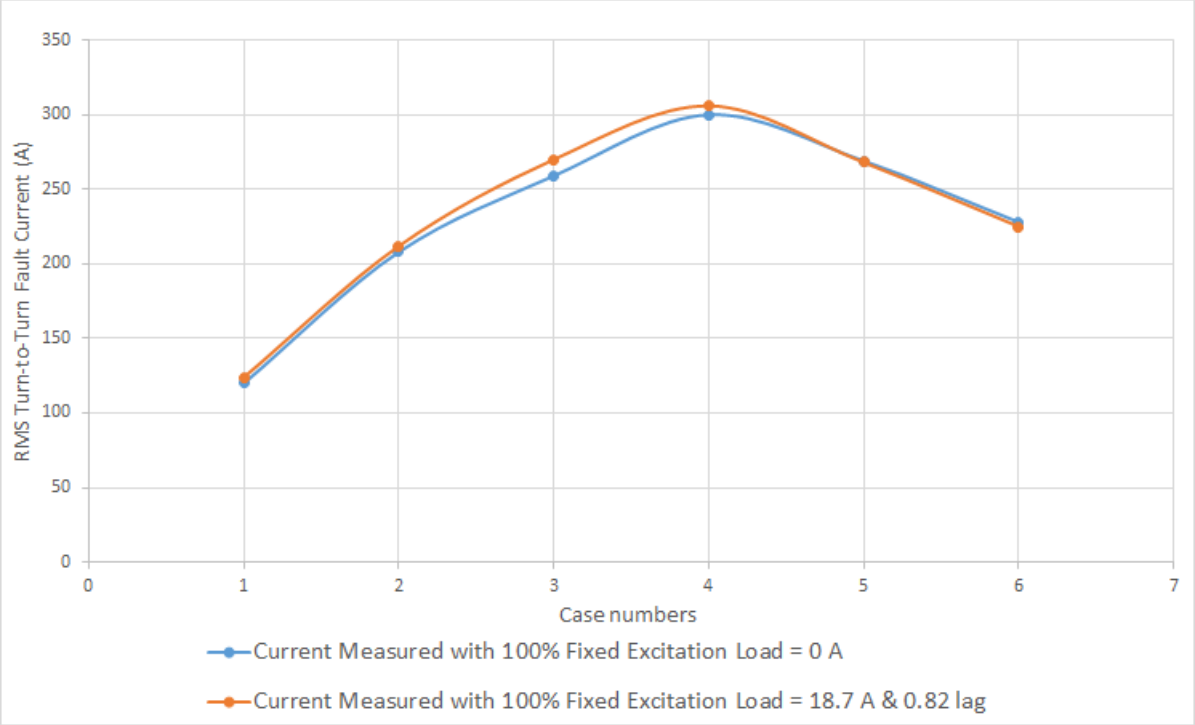

FIGURE 5.4: Plot Between Fault Current at No-load and a Load Current of 18.7 at 0.82 pf Lagging versus Case Number

The case number in Fig. 5.4 relates to the percentage of winding shorted as mapped in Table. 5.2.

TABLE 5.2: Mapping to Represent Number of Turns as Percentage of Winding

Case Number	Turns Under Fault	Percentage of Turns
1	1	1.111
2	2	2.222
3	3	3·333
4	5	5·555
5	7	7·777
6	10	11.111

Under no-load condition, the field current required to produce rated terminal voltage of the machine is I_f= 3.13 A. The rotor pole has a concentrated winding of number of turns per pole are (N_{rotor}) = 536. Therefore, the mmf generated by the field pole under no-load condition with the field current of 3.13 A is

$$Field_{MMFpeak} = 2136 \text{ AT}$$

Using equation (5.1), the peak flux density can be calculated as

$$B_{ag1peak} = (F_{ag1peak})\mu_0 / Airgap_g \tag{5.1}$$

$$B_{ag1peak}=0.765T$$

The fundamental component of mmf generated by the fault current in the stator winding can be calculated as shown in (5.2). Here, K_w represents the effects of distributed and short pitched stator winding and the value of K_w is 0.9019.

$$F_{stator} = 4K_w N_s I_s / \pi \tag{5.2}$$

Where,
N_s is the number of stator turns involved in the fault
I_s is the fault current through the winding.

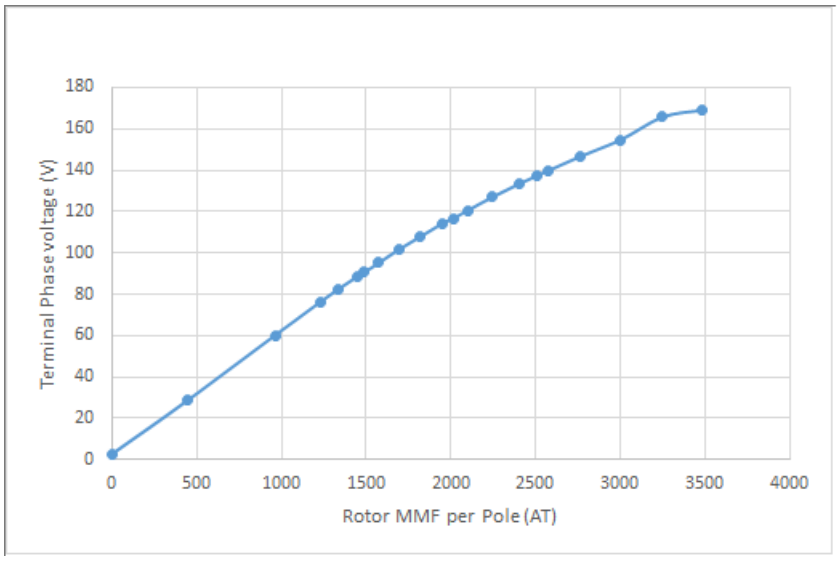

FIGURE 5.5: Open Circuit Terminal Voltage Versus Rotor mmf Per Pole

TABLE 5.3: Experimental Fault Current Results When Testing Generator Under No-load Condition

Case Number	Number of Turns Shorted	Fault Current RMS (A)	Stator MMF Peak (AT)	Rotor MMF Peak (AT)	Stator MMF /Rotor MMF
1	10 Turns	218	3710.3	2136	173
2	7 Turns	277	3300.1	2136	154
3	5 Turns	313	2663.6	2136	124
4	3 Turns	289	1475.6	2136	69
5	2 Turns	233	793.1	2136	37
6	1 Turn	141	239.9	2136	11.23

The open circuit characteristics (OCC) shown in Fig. 5.5 is used to represent the saturation behavior of the machine. From the OCC, it can be seen that when the mmf goes beyond 2200 AT per pole, a portion of the core starts to saturate. Usually at the rated voltage of the machine, the stator core teeth go into slight saturation causing the induced voltage to be reduced to below the theoretical value. An increase in rotor mmf at the no-load condition drives the core to saturated phase as shown in Fig. 5.5, causing the fundamental voltage to be lower and the harmonic content to be higher. When the rotor mmf exceeds beyond 3000 AT peak, the core goes into deep saturation and most of the flux goes through the air causing the leakage reactance to be higher.

As mentioned, this saturation also limits the induced voltage in the faulted turns. From the Table 5.3, it is to be noted that beyond 5 turns shorted, the decrease in short circuit current relative to the cases with fewer turns shorted is due to the increase in core saturation.

Fig. 5.6, Fig. 5.7, and Fig. 5.8 represent the fault current RMS magnitude versus the percentage of winding shorted for various load conditions under different excitation system modes of operation for the Automatic Voltage Regulator (AVR). As mentioned earlier, the case numbers in these figures relates to the percentage of winding as shown in Table. 5.2. The testing conditions are:

1. The machine was under no-load with AVR constant voltage mode Fig. 5.4.
2. The machine was under no-load with manual excitation Fig. 5.4.
3. The machine was loaded to carry 15 A (UPF) with AVR constant voltage mode Fig. 5.8.
4. The machine was loaded to carry 30 A (UPF) with AVR constant voltage mode Fig. 5.6.
5. The machine was loaded to carry 18.7 A (0.82 pf lag) with manual excitation Fig. 5.4.

These figures also indicate that there are slight variations in the magnitudes of turn-to-turn fault current magnitudes because of changes in saturating conditions of the synchronous generator.

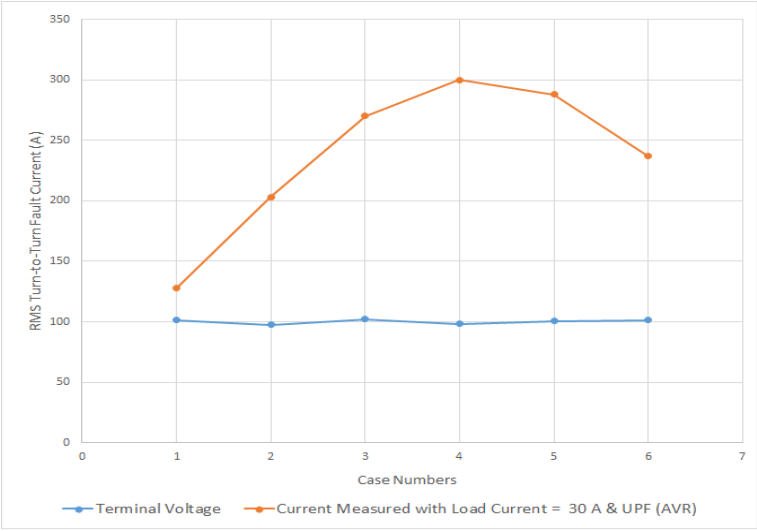

FIGURE 5.6: Turn-to-Turn Fault Current and Applied Voltage Versus Case Number When the Machine was Loaded to Carry 30 A with AVR Constant Voltage Mode

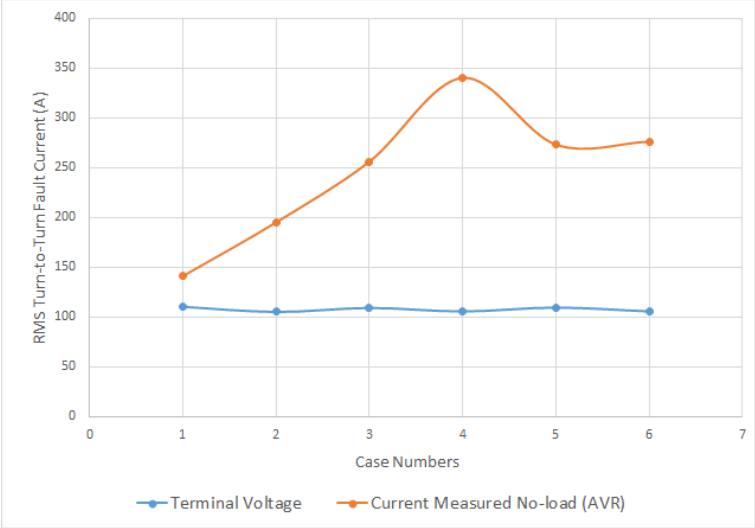

FIGURE 5.7: Turn-to-Turn Fault Current and Applied Voltage Versus Case Number When the Machine was Under No-load with AVR Constant Voltage Mode

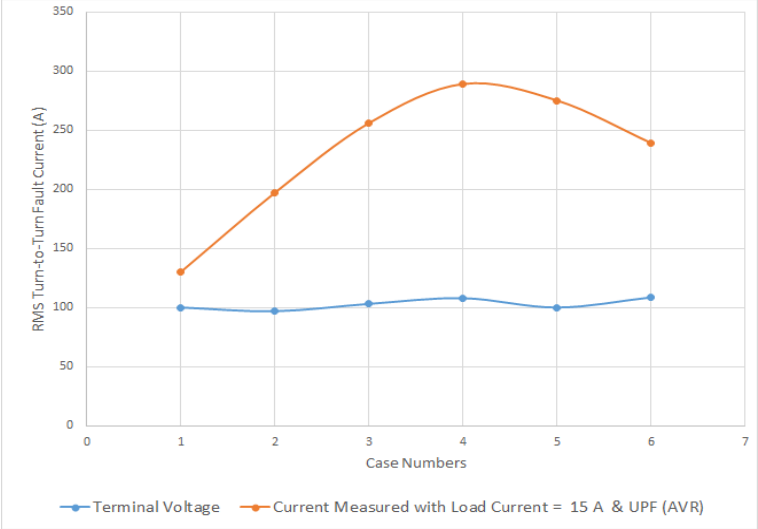

FIGURE 5.8: Turn-to-Turn Fault Current and Applied Voltage Versus Case Number When the Machine was Loaded to Carry 15 A with AVR Constant Voltage Mode

As described earlier, only the partial leakage inductances and winding resistances are in opposition to the fault current during a turn-to-turn short-circuit. The leakage impedances of the winding calculated from the measurements during faults under the different conditions are plotted in Fig. 5.9. The leakage impedance is calculated from the pre-fault voltage and the fault current during turn-to-turn faults. The impedance increases beyond 5 turns shorted is due to the increase in core saturation.

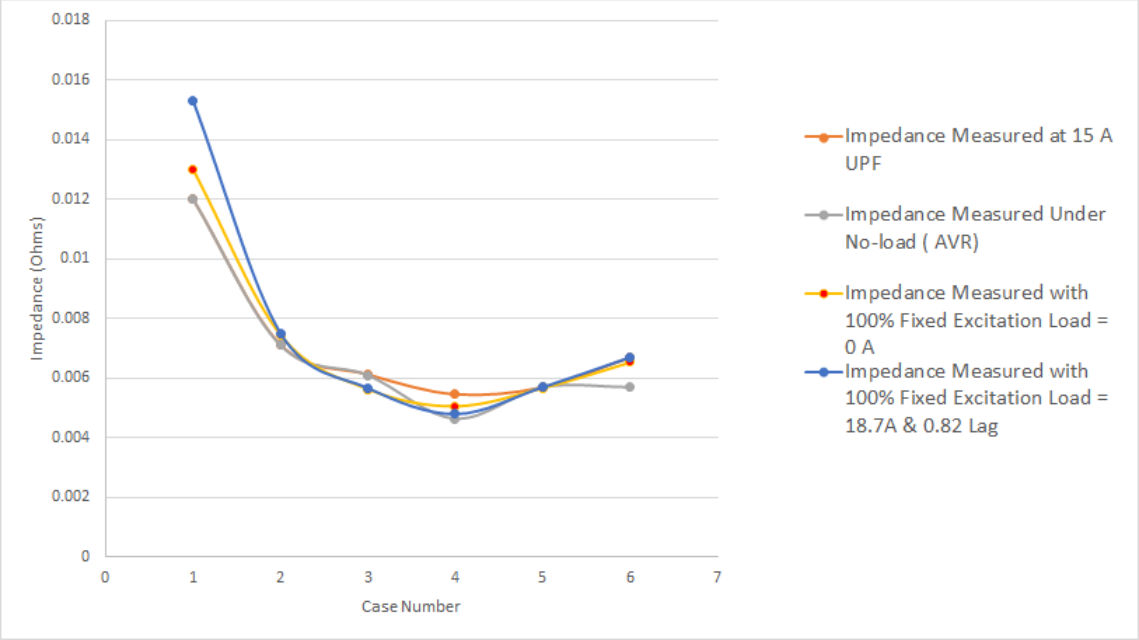

FIGURE 5.9: Plot between Leakage Impedance and Percentage of Fault Location for Different Operating Conditions

5.3 EXPERIMENTAL RESULTS OF PROTECTION ELEMENTS PERFORMANCE

As described in Chapter 4, there are two commonly used techniques for detecting turn-to-turn faults using protective relays. The sensitivity of these two methods will be examined in this section.

5.3.1 *Protection Elements Performance When Generator is Synchronized to the Grid*

A summary of the turn-to-turn fault currents for different fault conditions when generator is synchronized to the grid are listed in Tables 5.4 and 5.5

The results in Table. 5.4 column 5 show that split phase protection described in Chapter 1, is able to measure sufficient circulating current between the branches to selectively detect the faults shorting down to two turns, if the circulating current set point is set above 2A. Note also that split phase protection can only be used to detect internal faults in generators with parallel branches are available to take current measurements.

Figure 5.10 (a) shows the operating and restraining quantities based on the negative sequence currents of the terminal and phase quantities that are described in Chapter 3. If the negative sequence differential element slope is set above 15%, the element can detect faults down to 5 turns shorted. Fig. 5.10 (b) shows the magnitude of the

TABLE 5.4: Results of Split Phase Protection During Fault Testing When Generator is synchronized to Grid

Case Number	Number of Turns Shorted	Pre-fault Voltage Across Turns (V	Theoretical Pre-fault Voltage (V)	Circulating Current (A)	Impedance of Shorted Turns (ohm)
1	10 Turns	15.65	14.11	13	0.0657
2	7 Turns	10.91	9.87	11.04	0.03
3	5 Turns	7.84	7.05	7.28	0.0240
4	3 Turns	4.670	4.23	3	0.0150
5	2 Turns	3.13	2.82	2.828	0.0128
6	1 Turn	1.55	1.41	0	0.0110

fault current generated when 10 turns were short circuited. Fig. 5.10 (c) displays the phase A currents measured at the terminal and neutral ends of the windings. Since the measured quantities appear to be similar after post processing, it can be confirmed that the phase differential is not likely to pickup due to a difference between them. Fig. 5.10 (d) shows the pre-fault voltage across the 10 turns and Fig. 5.10 (e) displays the magnitude of negative sequence currents calculated at the terminals and the neutral ends of the windings. Prior to the fault, the negative sequence quantities are below the I_{2min} setting. The negative sequence differential element performance is shown in Table. 5.5 column 6. The element can securely detect faults shorting of 5 or more 5 turns on the machine, including generators whose branches are not available for split phase protection. Reducing the setting slope may cause the relay to respond for external faults with terminal CT saturation.

TABLE 5.5: Results of Negative Sequence Differential During Fault Testing When Generator is synchronized to Grid

Case Number	**Number of Turns Shorted**	**Fault current (A)**	**Terminal I2 (A)**	**Neutral I2 (A)**	**Maximum slope (I_2OP / I_2RT) %**
1	10 Turns	245.7	1.30	0.97	16.08
2	7 Turns	290.7	1.23	1.21	16.9
3	5 Turns	326.2	0.96	0.90	18.77
4	3 Turns	309.8	0.53	0.45	NA
5	2 Turns	244.0	0.40	0.34	NA
6	1 Turn	140.7	0.17	0.17	NA

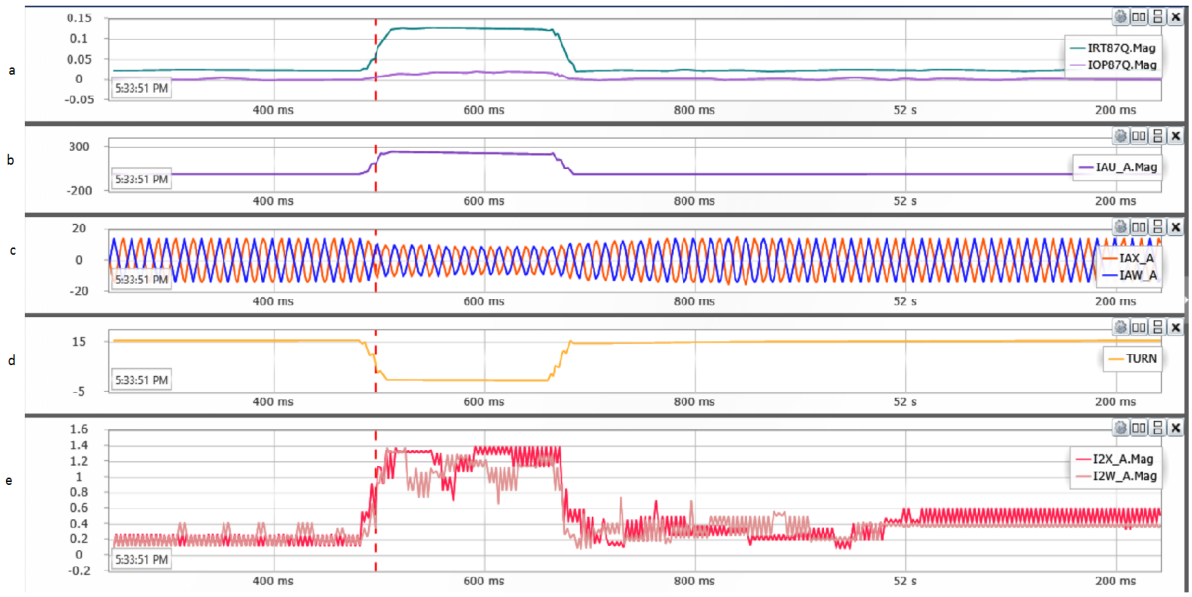

FIGURE 5.10: Relay Measurements with 10 Turns Shorted, (a) Negative Sequence Differential Operate and Restraint Elements; (b) Magnitude of Fault Current (A); (c) Phase (IAX_A) and Neutral Currents (IAW_A) of the Machine (A); (d) Pre-fault Voltage Across 10 turns (V); (e) Magnitude of Negative Sequence Currents Measured at Phase and Neutral (A)

5.3.1.1 *Measurements for Proposed Detection Method*

To increase the sensitivity of the turn-to-turn fault detection, this thesis proposes a new method using a negative sequence directional element at the stator terminals combined with double frequency current in rotor. In addition to the stator quantities from the previous case, the voltage produced by field current across 1 ohm current shunt resistor was captured. Fig. 5.11 (a) shows the increase in negative sequence currents measured at the terminal. Fig. 5.11 (b) shows terminal voltage during for the case shorting 10 turns. Fig. 5.11 (c) shows the phase currents measured at the terminal. Fig. 5.11 (d) shows voltage across a 1 ohm shunt in the field winding. Note the 120 Hz (double frequency) behavior while the fault is applied. Fig. 5.11 (e) shows the negative sequence voltage calculated from the terminal measurements. From these results, it can be concluded that the negative sequence currents flowing in the phases do cause double frequency currents to flow in the field winding. During the whole testing process, the AVR was in manual mode so the set-point of the terminal voltage can only be controlled manually and there was no AVR response to impact the results.

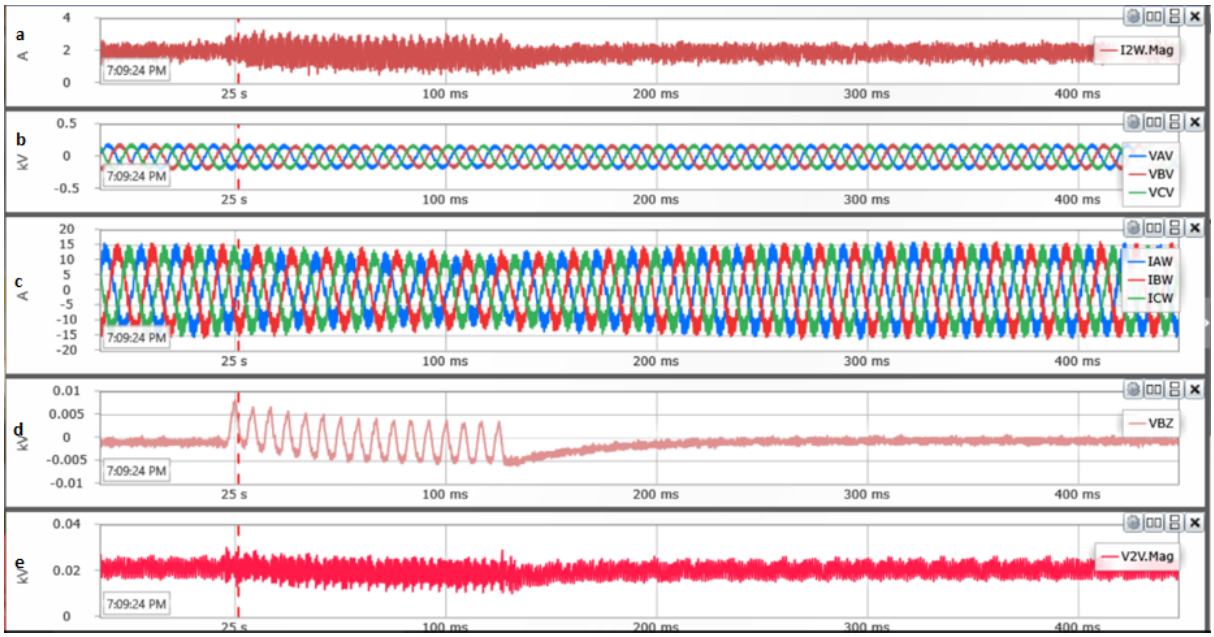

FIGURE 5.11: Measurements Including Rotor Field Current from Shunt for 10 Turns Shorted Under Loaded Condition of 15A & 0.86 lag pf, (a) Terminal Negative Sequence Current; (b) Terminal Voltages; (c) Terminal Phase Currents; (d) Field Double Frequency Current Measured Across 1 Ohm Shunt; (e) Terminal Negative Sequence Voltage

To verify the sensitivity of this method, stator quantities and field double frequency currents were captured during 2 turns shorted under a loaded condition

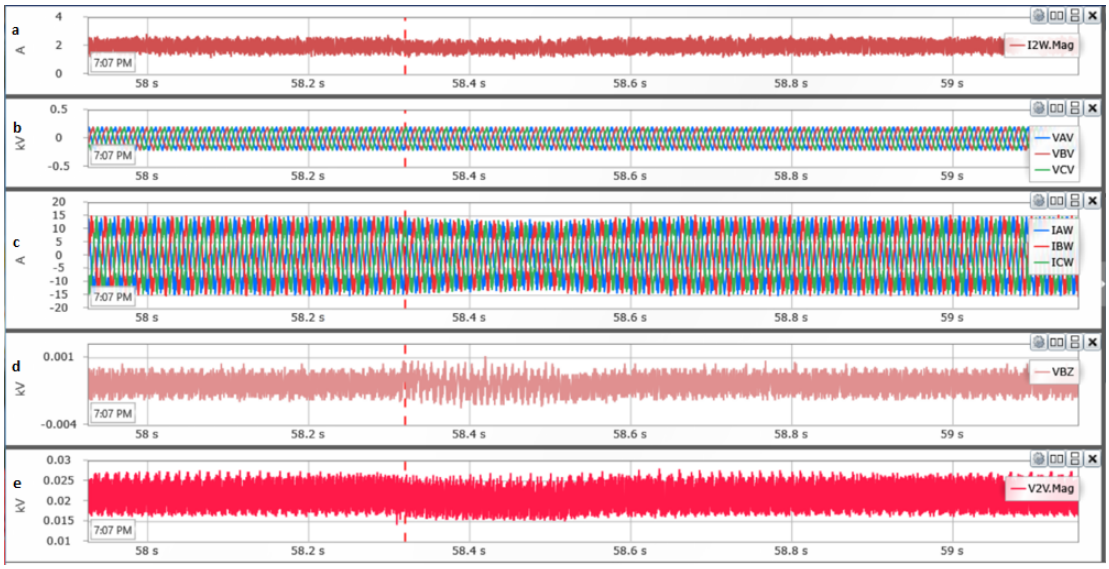

FIGURE 5.12: Measurements Including Rotor Field Current from Shunt for 2 Turns Shorted Under Loaded Condition, (a) Terminal Negative Sequence Current; (b) Terminal Voltages; (c) Terminal Phase Currents; (d) Field Double Frequency Current Measured Across 1 Ohm Shunt; (e) Terminal Negative Sequence Voltage

of 15 A at 0.86 pf lag and they are shown in Fig. 5.12. Fig. 5.12 (a) shows the increase in negative sequence currents measured at the terminal. Fig. 5.12 (b) shows terminal voltage during for the case shorting 10 turns. Fig. 5.11 (c) shows the phase currents measured at the terminal. Fig. 5.12 (d) shows voltage across 1 ohm shunt in the field winding. Note the 120 Hz (double frequency) behavior while the fault is applied. Fig. 5.12 (e) shows the negative sequence voltage calculated from the terminal measurements. Fig. 5.12 (d) shows that the double frequency currents can be measured even for the faults involving 2 turns of the winding. Figures A.12 to A.14 in Appendix A shows the rotor field measurements for additional turn-to-turn faults in section (d) of every figure. These figures also demonstrate the flow of negative sequence currents in the stator windings in section (a) of every figure.

Fig. 5.13 shows the demonstration of negative sequence directional element with 10 Turns shorted under loaded condition of 15 A at 0.86 pf lag. Fig. 5.13 (a) shows the phase currents measured at the terminal. Fig. 5.13 (b) shows the terminal voltages of the machine. Fig. 5.13(c) shows the calculated imaginary component of negative sequence impedance measured at the terminal. Fig. 5.13 (d) shows the calculated real component of negative sequence impedance measured at the terminal. As the measured negative sequence impedance at the terminal is positive, the directional element determines the direction as reverse because of terminal CT polarity. Fig. 5.13

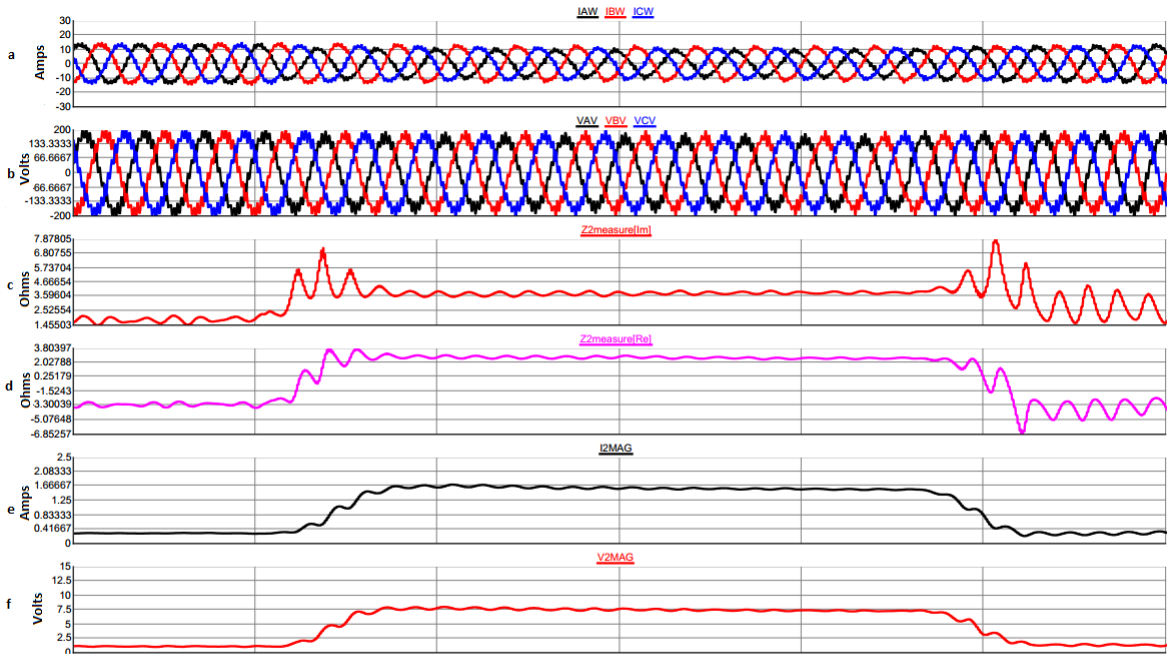

FIGURE 5.13: Negative Sequence Directional Element with 10 Turns Shorted, (a) Terminal Phase Currents; (b) Terminal Voltages; (c) Imaginary Component of Negative Sequence Impedance Measured at Terminal; (d) Real Component of Negative Sequence Impedance Measured at Terminal; (e) Magnitude of Negative Sequence Current Measured at Terminal; (f) Magnitude of Negative Sequence Voltage Measured at Terminal

(e) shows the magnitude of negative sequence current measured at terminal. Fig. 5.13 (f) shows the magnitude of negative sequence voltage measured at terminal. Based on the results here, negative sequence impedance can potentially be used to supervise the rotor double frequency elements. This is next tested with an external fault condition.

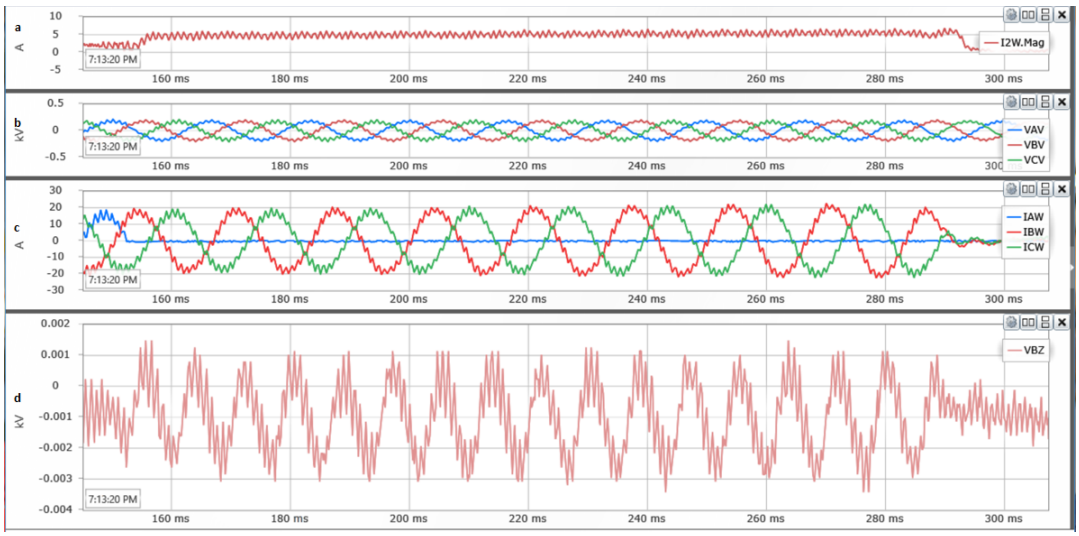

FIGURE 5.14: Rotor Field Measurements During One Phase Breaker Open Condition External To the Generator Terminal CTs, (a) Magnitude of Negative Sequence Current Measured at Terminal; (b) Terminal Voltages; (c) Terminal Phase Currents; (d) Field Double Frequency Current Measured Across 1 Ohm Shunt

Fig. 5.14 shows that the negative sequence currents flowing in the stator windings for the phase open external to the terminal CT also cause double frequency currents to flow in the field winding. But security against such conditions can be provided by supervising using a negative sequence directional element. To verify the negative sequence directional element, the breaker on one phase external to the generator is open and the negative sequence impedance measured by using terminal negative sequence current and terminal negative sequence voltage for that corresponding fault is negative. Usually the negative sequence impedance of the generator is small, the sensitivity of the element depends on the sensitivity of negative sequence voltage. Fig. 5.15 shows the operation of negative sequence directional element for the open phase condition external to the terminal CTs. Fig. 5.15 (a) shows the phase currents measured at the terminal. Fig. 5.15 (b) shows the terminal voltages of the machine. Fig. 5.15(c) shows the calculated imaginary component of negative sequence impedance measured at the terminal. Fig. 5.15 (d) shows the calculated real component of negative sequence impedance measured at the terminal. Since the measured negative sequence impedance is negative because of Terminal CTs polarity, the negative sequence directional element confirms the direction as a forward fault away from the generator. As mentioned earlier, negative sequence impedance measured by the relay for the generator faults is positive indicating in reverse direction relative to the CT polarity. Fig. 5.13 (e) shows the magnitude of negative sequence

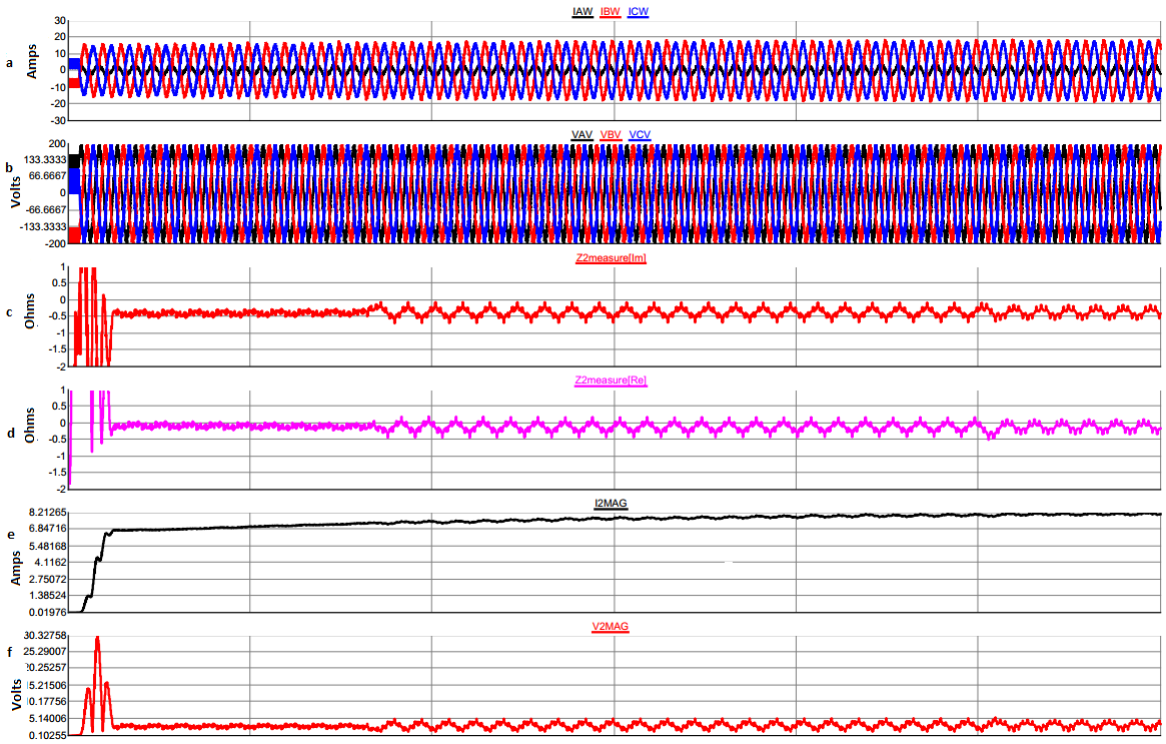

FIGURE 5.15: Negative Sequence Directional Element Operation During One Phase Breaker Open External To the Generator Terminal CTs, (a) Terminal Phase Currents; (b) Terminal Voltages; (c) Imaginary Component of Negative Sequence Impedance Measured at Terminal; (d) Real Component of Negative Sequence Impedance Measured at Terminal; (e) Magnitude of Negative Sequence Current Measured at Terminal; (f) Magnitude of Negative Sequence Voltage Measured at Terminal

current measured at terminal. Fig. 5.13 (f) shows the magnitude of negative sequence voltage measured at terminal.

Figures A.1 to A.5 in Appendix A show the negative sequence directional element operation for turn-to-to faults ranging from 10 to 2 turns. Section (h) in these figures also shows the sensitivity of zero sequence voltage elements for the turn-to-turn faults during different cases of loaded and loaded phase open conditions. But using zero sequence voltage alone cannot distinguish the difference between external faults and internal faults. So it cannot be used for turn-to-turn fault detection during loading conditions.

Negative sequence directional detection methods well for the cases shorting as few as 3 turns, but this directional element is not sensitive enough to provide supervision for faults shorting 1 or 2 turn on the laboratory generator (so not effective below 2% of the winding). Overall, the sensitive negative sequence directional element works for

detecting up to 2 turns short circuits, when measuring class CTs and PTs are used for measurements.

5.3.2 *Protection Elements Performance When Generator is Under No-load Condition*

When the generator is offline, the negative sequence differential protection and the proposed negative sequence directional element cannot detect turn-to-turn faults of stator winding since there won't be any stator currents at the terminals. In this case, the split phase element proves to be better at detecting the faults. As shown in Column 5 Table 5.6, there will be sufficient circulating current for the split phase element to detect the faults down to 2 turns. Fig. 5.16 (e) also shows the circulating current between branches with 10 turns shorted. But fault detection for generators that aren't under the split phase protection can be a big challenge under no-load conditions.

TABLE 5.6: Measurements During Testing when Generator Under no-load Condition

Test Case	**Fault current (A)**	**Pre-fault Voltage Across Turns (V)**	**Theoretical Pre-fault Voltage (V)**	**Circulating Current (A)**	**Impedance of Shorted Turns (ohm)**
10 Turns	230.8	15.02	14.11	14.98	0.0650
7 Turns	282.33	10.566	9.87	10.44	0.0374
5 Turns	324.58	7.538	7.05	8.544	0.0232
3 Turns	290.22	4.520	4.23	4.24	0.0155
2 Turns	237.08	3.0206	2.82	2.23	0.0127
1 Turn	138.43	1.496	1.41	0	0.0108

The method proposed in this thesis can also detect turn-to-turn faults that occur when the generator field is energized and the rotor at speed but the machine is disconnected from the grid. This technique uses a sensitive negative sequence voltage measurement at the terminals and combined with double frequency currents in the rotor field winding. This thesis strongly recommends the use of a measurement class PT to more accurately measure negative sequence voltages for improving the sensitivity of turn-to-turn fault detection under no-load conditions.

As mentioned earlier, turn-to-turn fault in a phase reduces the fundamental voltage of that phase causing the negative sequence voltage to rise. Fig. 5.16 shows the negative sequence overvoltage with 10 turns shorted when the generator is energized but disconnected from the grid. Fig. 5.16 (a) shows the terminal voltages. Fig. 5.16 (b)

shows the magnitude of negative sequence voltage measured at terminal. Fig. 5.16 (c) shows the magnitude of zero sequence voltage measured at terminal. It is to be noted that during turn-to-turn faults, the zero sequence voltage also increases but variation of zero sequence voltage measurement greatly depends on the grounding of the PT that is being used for the measurement. Fig. 5.16 (d) shows the turn-to-turn fault current. Fig. 5.16 (e) also shows the circulating current between branches.

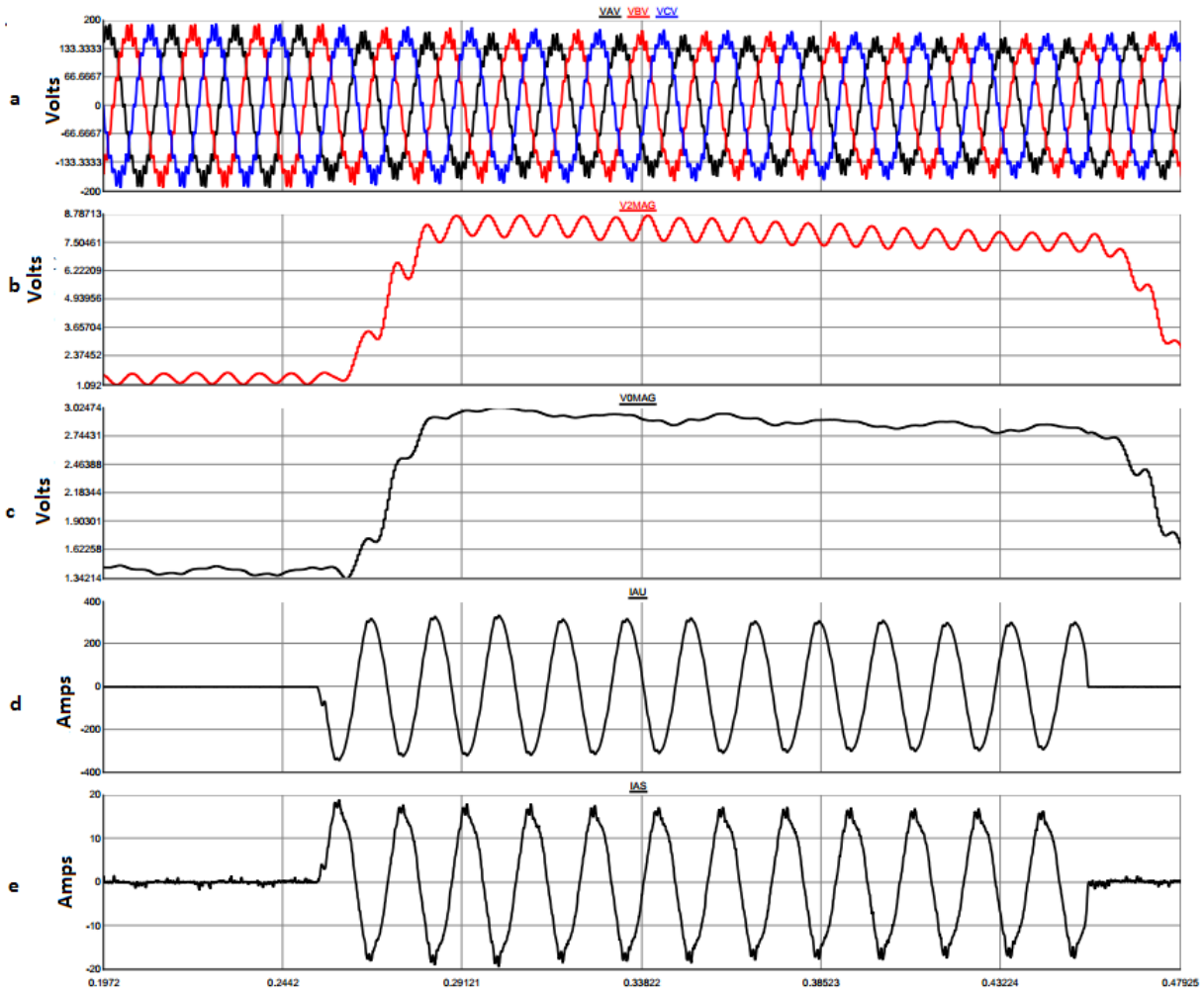

FIGURE 5.16: Negative Sequence Over Voltage with 10 Turns Shorted When the Generator Is Energized but Disconnected From the Grid (a) Terminal Voltages; (b) Magnitude of Negative Sequence Voltage Measured at Terminal; (c) Magnitude of Zero Sequence Voltage Measured at Terminal; (d) Turn-to-turn Fault Current; (e) Circulating Current Between Branches

Fig. 5.16 shows the negative sequence over voltage with 2 turns shorted when the generator is energized but disconnected from the grid. Fig. 5.17 (a) shows the terminal voltages. Fig. 5.17(b) shows the magnitude of negative sequence voltage

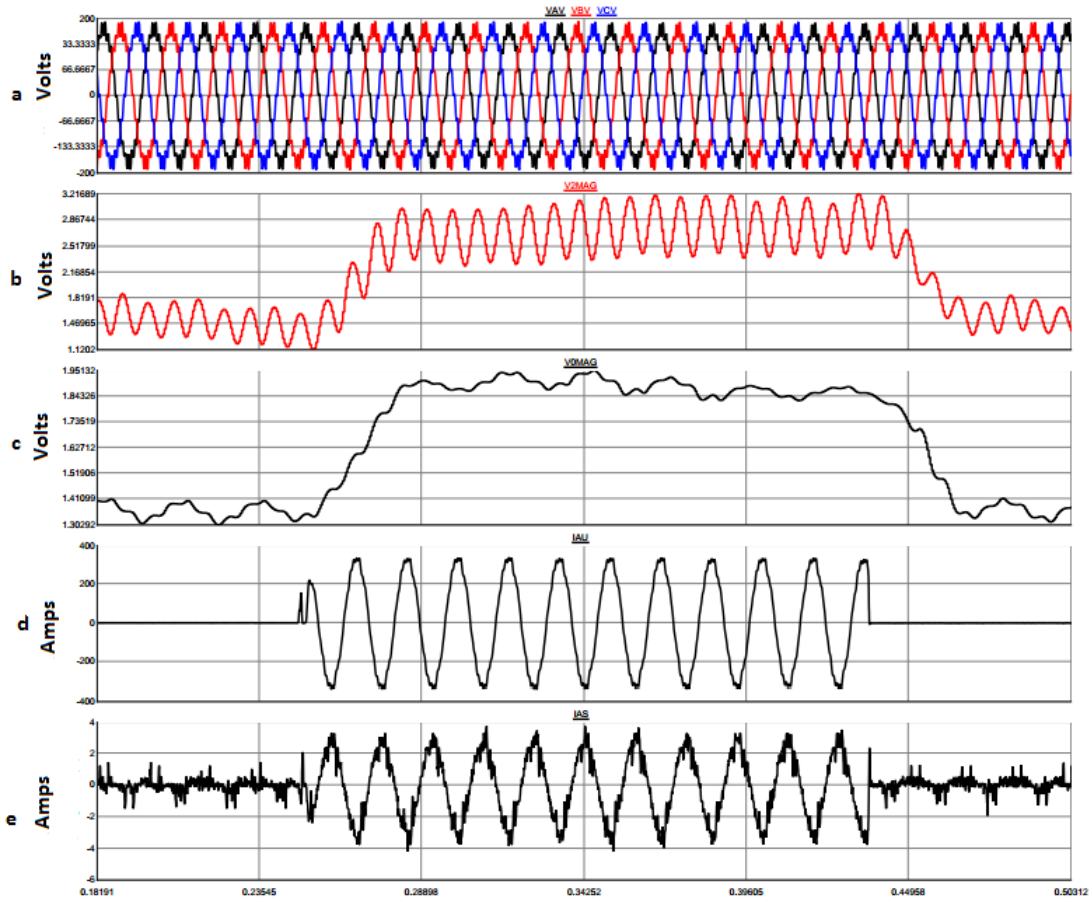

FIGURE 5.17: Negative Sequence Over Voltage with 2 Turns Shorted When the Generator Is Energized but Disconnected From the Grid (a) Terminal Voltages; (b) Magnitude of Negative Sequence Voltage Measured at Terminal; (c) Magnitude of Zero Sequence Voltage Measured at Terminal; (d) Turn-to-turn Fault Current; (e) Circulating Current Between Branches

measured at terminal. Fig. 5.17 (c) shows magnitude of zero sequence voltage measured at terminal. Fig. 5.17 (d) shows turn-to-turn fault current. Fig. 5.17 (e) shows the circulating current between branches. Again better accuracy PTs can sense the increase in negative sequence voltage for 2 turns shorted condition.

In addition to the stator quantities, the field current measurements with 10 turns shorted when the machine is energized but not connected to the grid are shown in Fig. 5.18. Fig. 5.18 (a) shows the magnitude of turn-to-turn fault current. Fig. 5.18 (b) shows the terminal voltages and Fig. 5.18 (c) shows the voltage across the shunt due to the double frequency currents induced in field winding by the negative rotating rmf produced by the turn-to-turn fault currents.

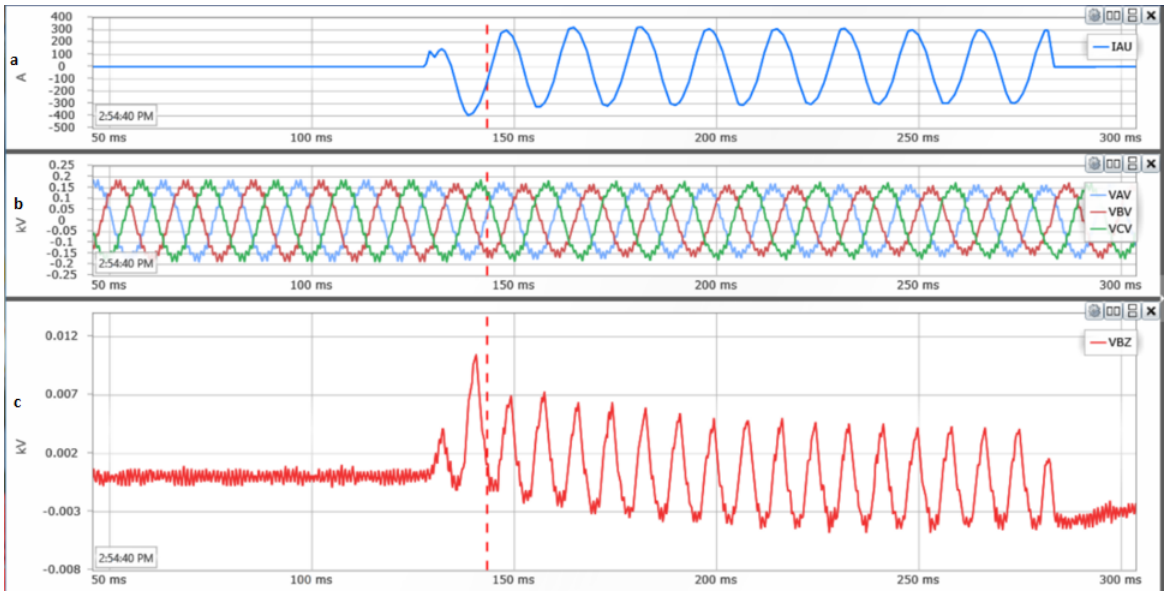

FIGURE 5.18: Measurements Including Rotor Field Current from Shunt for 10 turns Shorting Under No-load Condition, (a) Turn-to-Turn Fault Current; (b) Terminal Voltage; (c) Field Double Frequency Current Measured Across 1 Ohm Shunt

The rotor field current measurements with 2 turns shorted when the machine is energized but not connected to the grid are shown in Fig. 5.19. Fig. 5.19 (a) shows the magnitude of turn-to-turn fault current. Fig. 5.12 (b) shows the terminal voltages and Fig. 5.19 (c) shows the voltage across the shunt due to the double frequency currents induced in field winding by the negative rotating rmf produced by the turn-to-turn fault currents. It can be confirmed from this figure that double frequency currents can be seen for 2 turns shorted condition even when the generator terminals do not have any current.

Figs. A.7 to A.11 in Appendix A show the negative sequence voltage at the generator terminals for cases ranging from 7 turns to 1 turn short circuited under the unloaded conditions. Figs. A.15 to A.17 in Appendix show the voltage shunt measurement for the double frequency currents in the rotor field winding.

Overall, the results presented here and in Appendix A confirm that double frequency currents in the rotor combined with negative sequence voltage at the generator terminals can be used to detect the turn-to-turn faults involving as little as 2 turns of the winding under offline conditions. It is to be noted that these elements can also potentially detect branch faults although not shown here which sometimes may not even detected by split phase protection element.

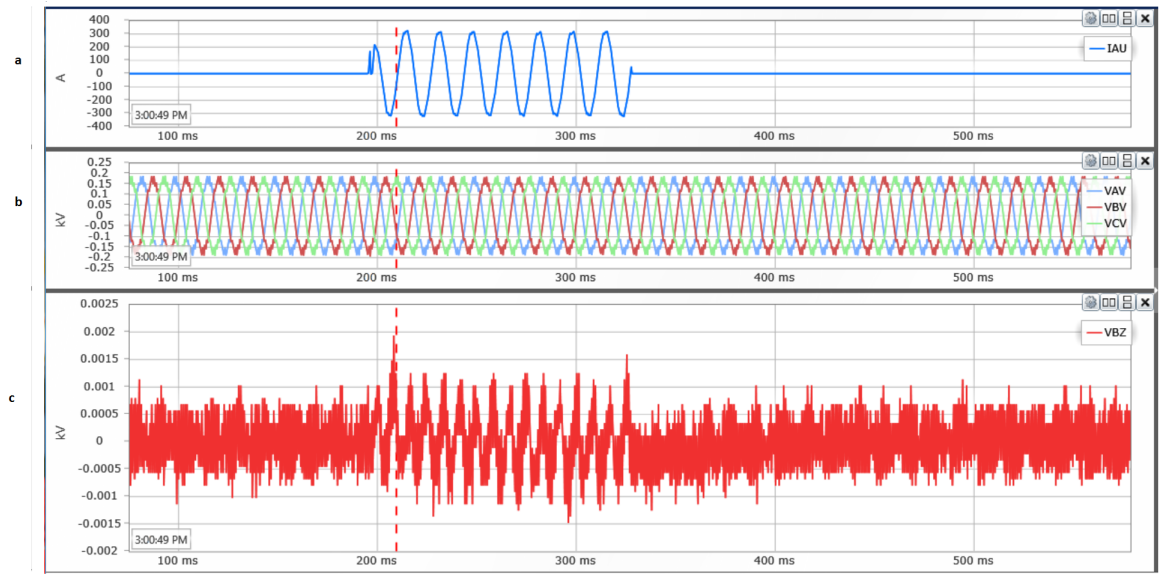

FIGURE 5.19: Measurements Including Rotor Field Current from Shunt for 2 turns Shorting Under No-loaded Condition, (a) Turn-to-Turn fault current; (b) Terminal voltage; (c) Field Double Frequency Current Measured Across 1 Ohm Shunt

5.4 SUMMARY

This chapter presented an analysis on the magnitude of turn-to-turn fault currents using rotor mmf and stator mmf relationships and concludes that the variation of magnitude of fault current from 1 to 10 turns shorting is due to the variation in saturation conditions of the machine.

This chapter also presented a summary on experimental results testing the split phase protection element and the negative sequence differential element; and concludes that split phase protection element offers a great deal of performance for detecting turn-to-turn faults under almost any condition provided the machine construction is suitable. Where as negative sequence differential element can only work if the generator is connected to the grid and it's sensitivity is also less than that of the split phase element.

This chapter also demonstrated two proposed detection techniques for detection of turn-to-turn faults. This chapter proves that negative sequence currents caused by turn-to-turn faults produce double frequency currents in the field winding and these double frequency currents can be used for the detection of faults shorting as few as 2 turns on the lab machine. If generator is loaded, these double frequency currents can be supervised by negative sequence directional element and if generator is energized

but unloaded then these double frequency currents can be supervised by negative sequence voltage measured at the terminal.

CHAPTER 6

Conclusions And Future Directions

6.1 CONCLUSIONS

1. This thesis has shown that approximate turn-to-turn fault currents can be calculated from the available machine parameters without needing to use complex models.

2. It was shown that the approximate turn-to-turn fault currents can also be calculated from the known zero sequence or leakage impedance of the machine. These approximate currents can be used to determine the approximate response of the field current for a fault detection scheme.

3. This work showed that negative sequence differential protection can be used to detect the turn-to-turn faults when the generator is loaded. But it has limited sensitivity.

4. This thesis proved that negative sequence directional elements can be used to detect the internal faults and they can also be used to discriminate between internal or external faults.

5. This thesis addressed the sensitivity issues of zero sequence overvoltage based elements, negative sequence directional elements and negative sequence differential elements.

6. This work proposed two methods for improved turn-to-turn fault detection: one method uses negative sequence directional element and double frequency currents in the field current to detect turn-to-turn faults under loaded condition.

7. This work concluded that negative sequence voltage along with the measured 2nd harmonic current in the field winding can be used to increase the sensitivity of the turn-to-tun fault when the generator is disconnected from the system or about to be connected to the system.

6.2 FUTURE WORK

1. More detailed modelling of the generator for internal fault analysis using the multi-loop method implemented in MATLAB and validating with experimental results. Doing this study will help characterize the accuracy of the approximate method.

2. Experimentally analyzing the field current and field voltage during internal faults using a high frequency sampling oscilloscope to see if there is observable travelling wave behavior for field winding ground faults.

3. Analyze short circuits faulting an entire branch in a generator with parallel branches per phase and develop a detection technique to identify a fault location.

4. Acquire data from a series of internal faults field tests on the 8.8MVA, 48 pole synchronous generator, and use the event records to effectively validate the proposed protection scheme that can detect faults up to 2% winding.

5. Analyze the performance of the negative sequence directional element when the generator is running asynchronous to the grid. This may cause incorrect operation of the turn-to-turn element.

6. Develop a technique to detect turn to turn or turn to ground faults in the rotor winding with greater sensitivity.

Bibliography

[1] N. Fischer, D. Finney, and D. Taylor, "How to determine the effectiveness of generator differential protection," in *Protective Relay Engineers, 2014 67th Annual Conference for*. IEEE, 2014, pp. 408–420.

[2] S. Kim, D. Finney, N. Fischer, and B. Kasztenny, "Ct requirements for generator split-phase protection," *38th Annual Western Protective Relay Conference*, 2011.

[3] "IEEE guide: Test procedures for synchronous machines part i–acceptance and performance testing part ii-test procedures and parameter determination for dynamic analysis," *IEEE Std 115-1995*, pp. 1–198, April 1996.

[4] *SIPROTEC Multifunctional Machine Protection 7UM62, Siemens Generator Protection Manual*. Siemens, 2013.

[5] C. J. Mozina and J. Gardell, "IEEE tutorial on the protection of synchronous generators," in *IEEE Power Engineering Society, IEEE*, vol. 95, 1995, pp. 1–78.

[6] *M-3425A Specification, Beckwith Generator Protection Manual*. Beckwith Electric, 2001.

[7] A. Fitzgerald, C. Kingsley Jr, and A. Kusko, *Electric Machinery: the Processes, Devices and Systems of Electromechanical Energy Conversion, 1971*. McGraw-Hill, New York.

[8] C.-M. Ong, *Dynamic Simulation of Electric Machinery: using MATLAB/SIMULINK*. Prentice Hall, 1998.

[9] R. Park, "Two-reaction theory of synchronous machines part ii," *Electrical Engineering*, vol. 52, no. 1, pp. 44–45, 1933.

[10] J. Marti and K. Louie, "A phase-domain synchronous generator model including saturation effects," *IEEE transactions on Power Systems*, vol. 12, no. 1, pp. 222–229, 1997.

[11] A. B. Dehkordi, "*Improved Models of Electric Machines for Real-Time Digital Simulation*," Ph.D. dissertation, University of Manitoba, 2010.

[12] Wikipedia, "Real time digital simulator — wikipedia, the free encyclopedia," 2016, [Online; accessed 1-May-2017].

[13] T. A. Lipo, *Analysis of Synchronous Machines*. CRC Press, 2012.

[14] J. Gao, X. Wang, and L. Zhang, "Circuit analysis of ac machines multi loop model and parameters," *AC Machine Systems: Mathematical Model and Parameters, Analysis, and System Performance*, pp. 1–57, 2009.

[15] J. Pyrhonen, T. Jokinen, and V. Hrabovcova, *Design of Rotating Electrical Machines*. John Wiley & Sons, 2009.

[16] A. Guzmán, N. Fischer, and C. Labuschagne, "Improvements in transformer protection and control," in *Protective Relay Engineers, 2009 62nd Annual Conference for*. IEEE, 2009, pp. 563–579.

[17] B. Kasztenny, N. Fischer, and H. J. Altuve, "Negative-sequence differential protection-principles, sensitivity, and security," in *Protective Relay Engineers, 2015 68th Annual Conference for*. IEEE, 2015, pp. 364–378.

[18] J. Roberts and A. Guzman, "Directional element design and evaluation," in *Proceedings of the 21st Annual Western Protective Relay Conference*, 1994.

[19] P. M. Anderson and P. Anderson, *Analysis of Faulted Power Systems*. IEEE press New York, 1995.

APPENDIX A

Turn-to-Turn Experimental Results

Figures A.1 to A.6 show the negative sequence directional element operation for turn-to-to faults ranging from 10 turns to 1 turn. In these figures, (a) shows the terminal phase currents; (b) shows the terminal voltages; (c) shows the imaginary component of negative sequence impedance measured at terminal; (d) shows the real component of negative sequence impedance measured at the terminals; (e) shows the magnitude of negative sequence current measured at the terminals; (f) shows the magnitude of negative sequence voltage measured at the terminals; (g) shows the magnitude of negative sequence impedance measured at the terminals; (h) shows the magnitude of zero sequence voltage measured at the terminals; and (i) shows the circulating current between branches.

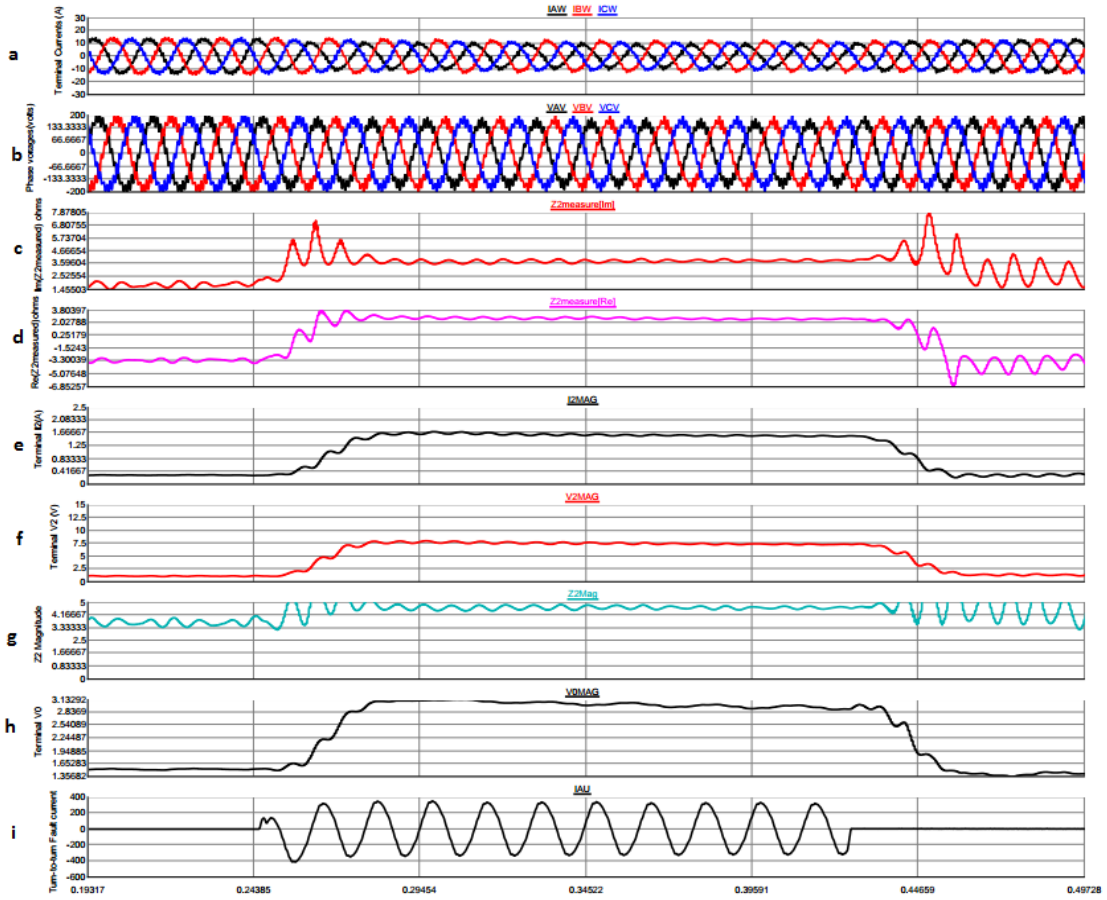

FIGURE A.1: 10 Turns Short Circuit Under Loaded Condition

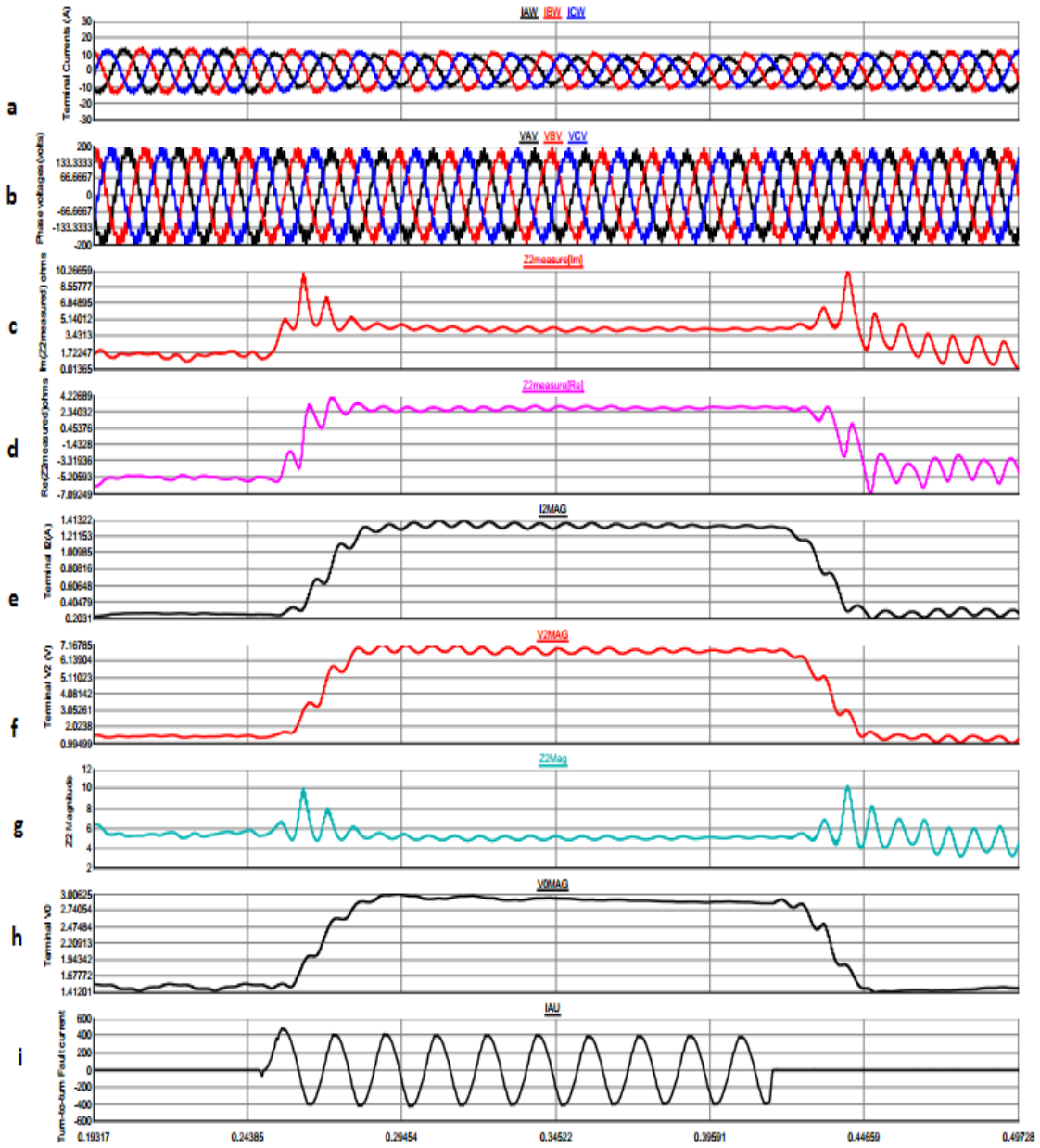

FIGURE A.2: 7 Turns Short Circuit Under Loaded Condition

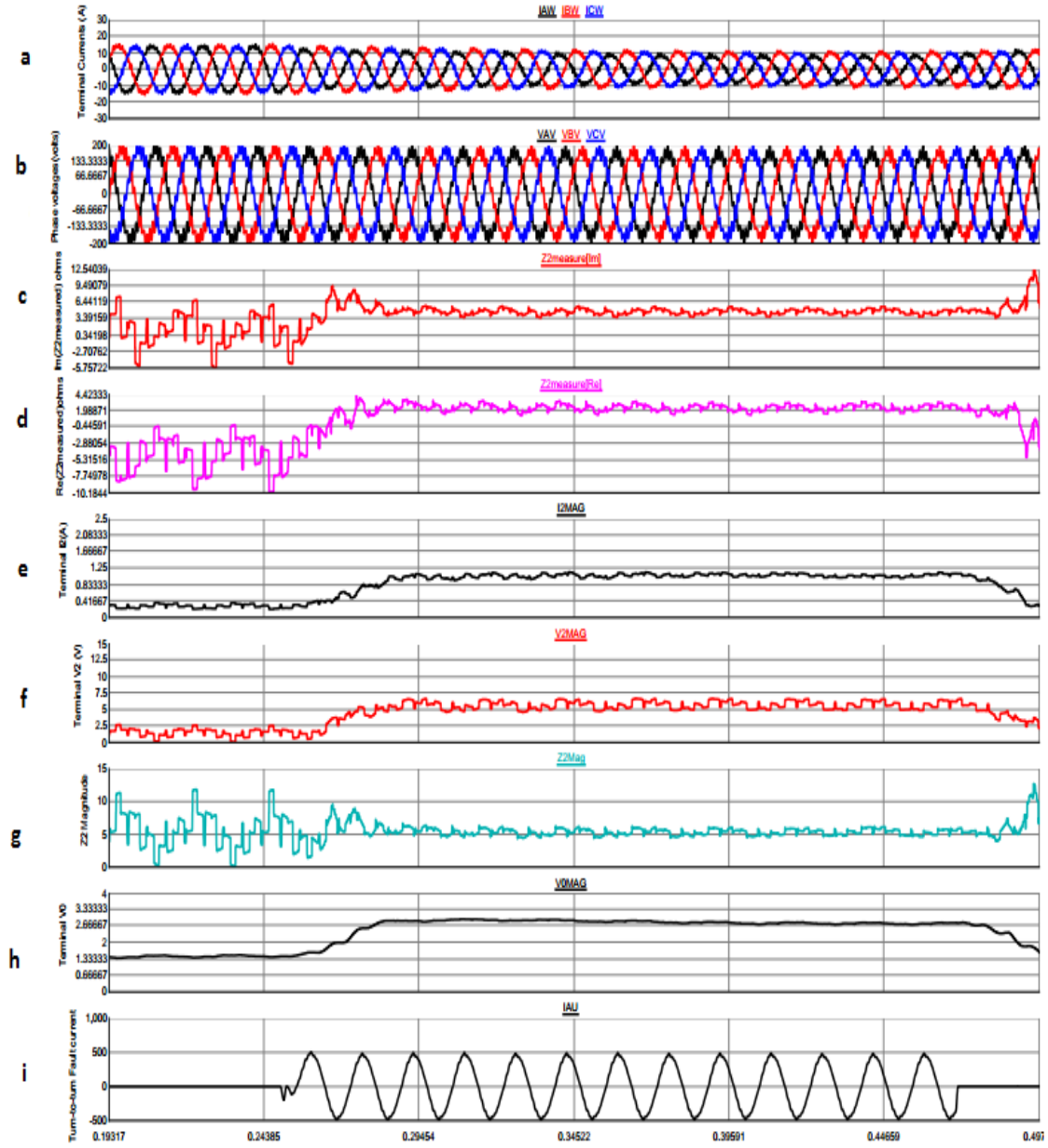

FIGURE A.3: 5 Turns Short Circuit Under Loaded Condition

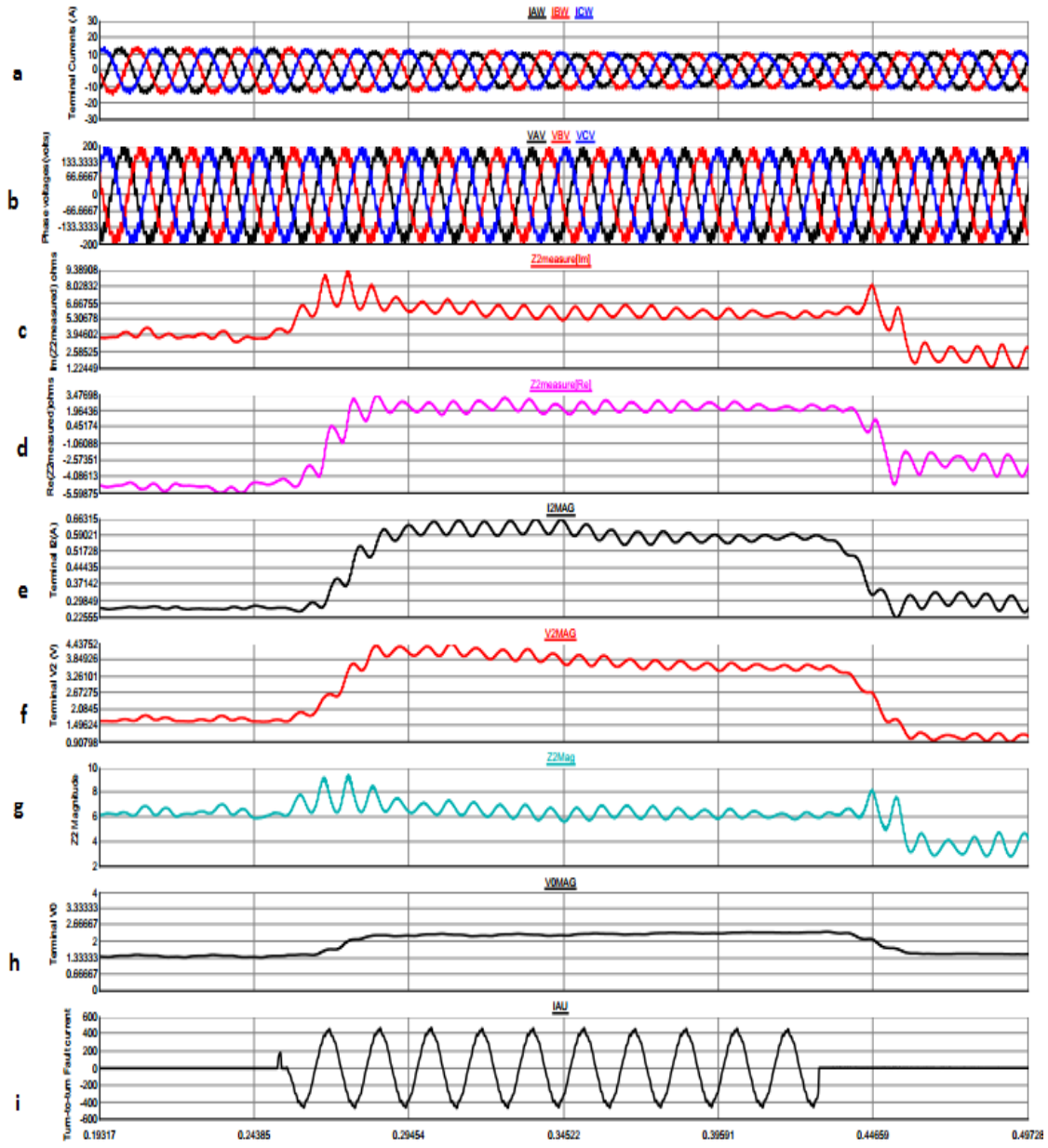

FIGURE A.4: 3 Turns Short Circuit Under Loaded Condition

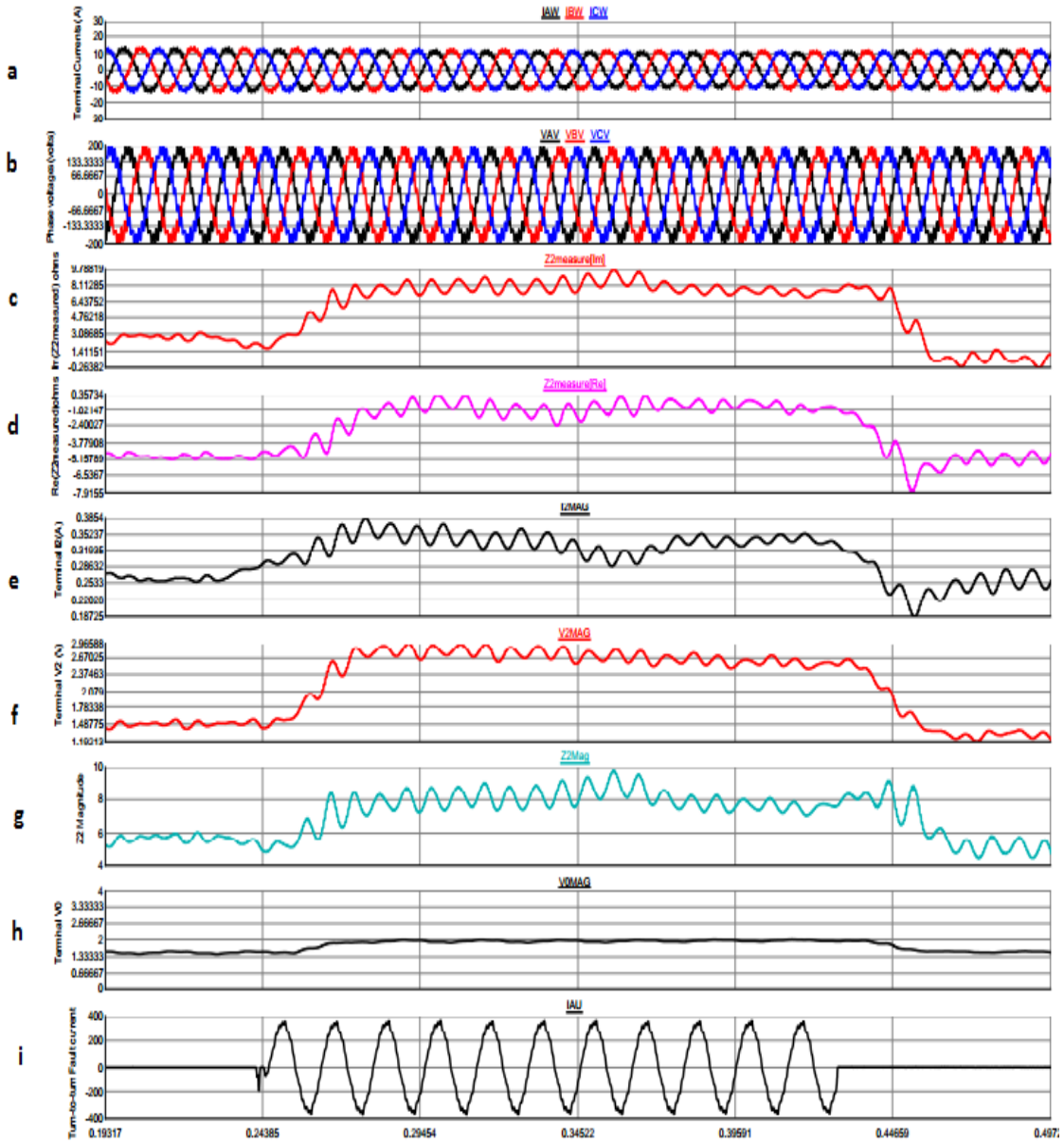

FIGURE A.5: 2 Turns Short Circuit Under Loaded Condition

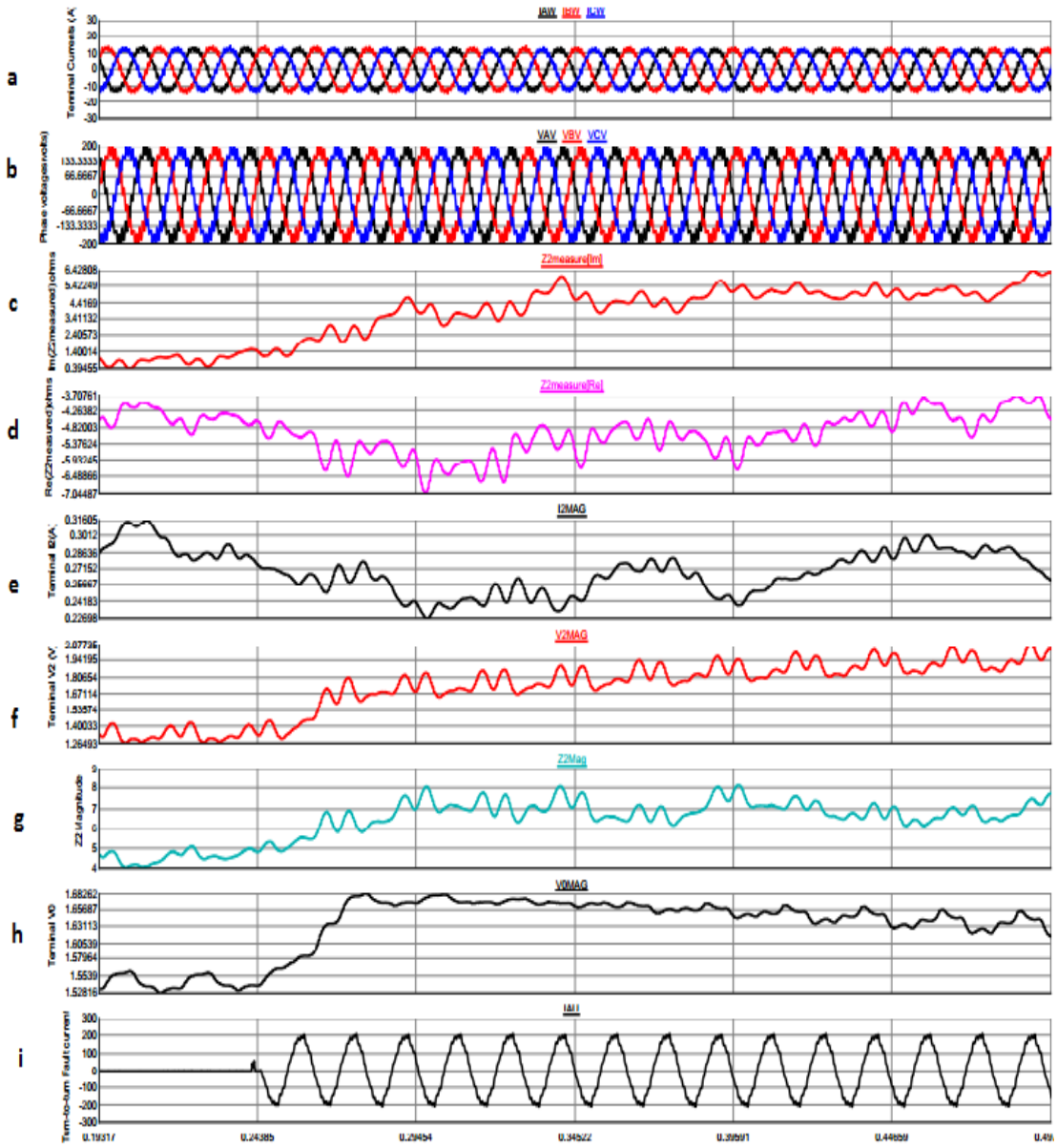

FIGURE A.6: 1 Turn Short Circuit Under Loaded Condition

Figures A.7 to A.11 show the negative sequence over voltages for the turns shorted from 7 turns to 1 turn when the generator is energized but disconnected from the grid. In these figures (a) shows the terminal voltages; shows the (b) magnitude of negative sequence voltage measured at terminal; shows the (c) magnitude of zero sequence voltage measured at terminal; (d) shows the circulating current between branches; (e) shows the turn-to-turn fault current.

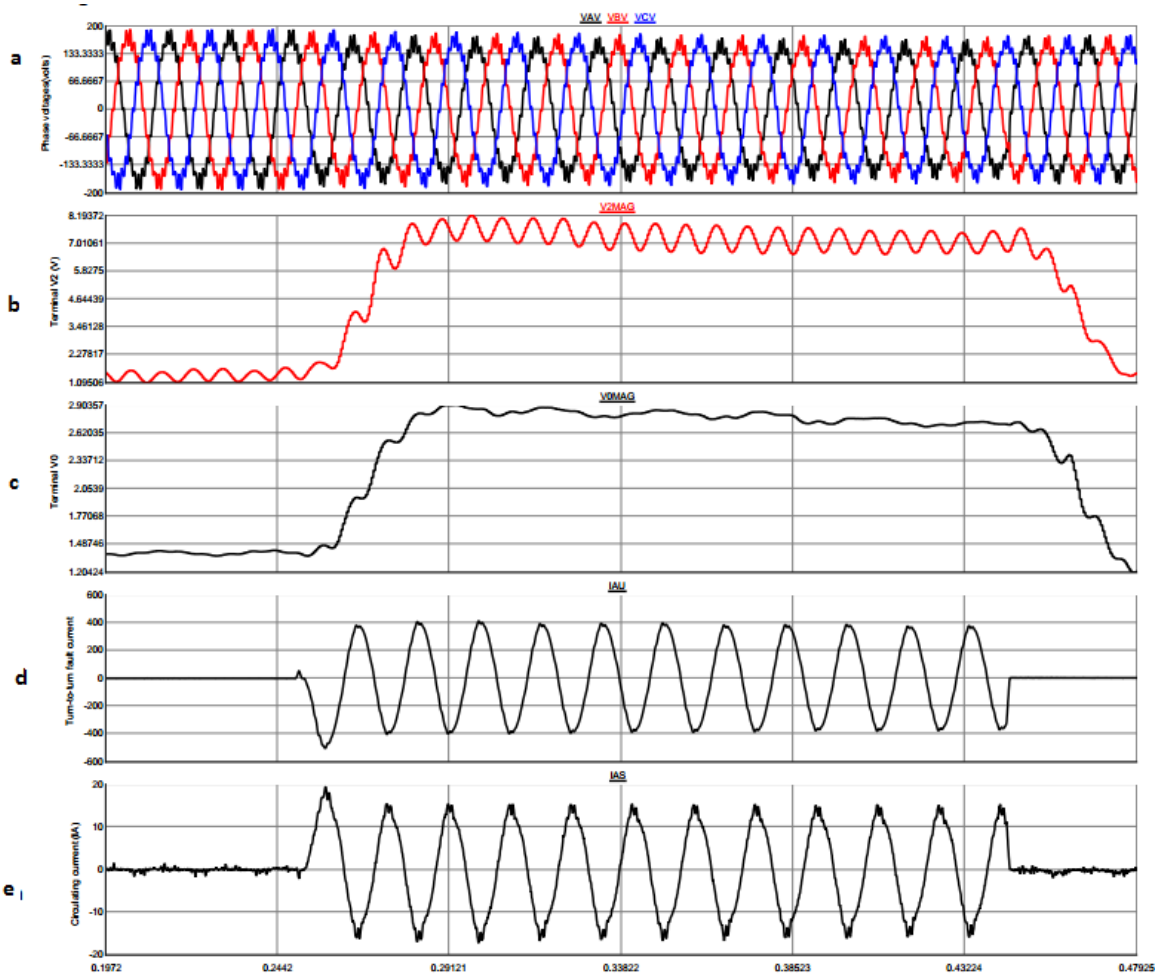

FIGURE A.7: 7 Turns Short Circuit Connected to Grid or Disconnected with P = 0, Q = 0

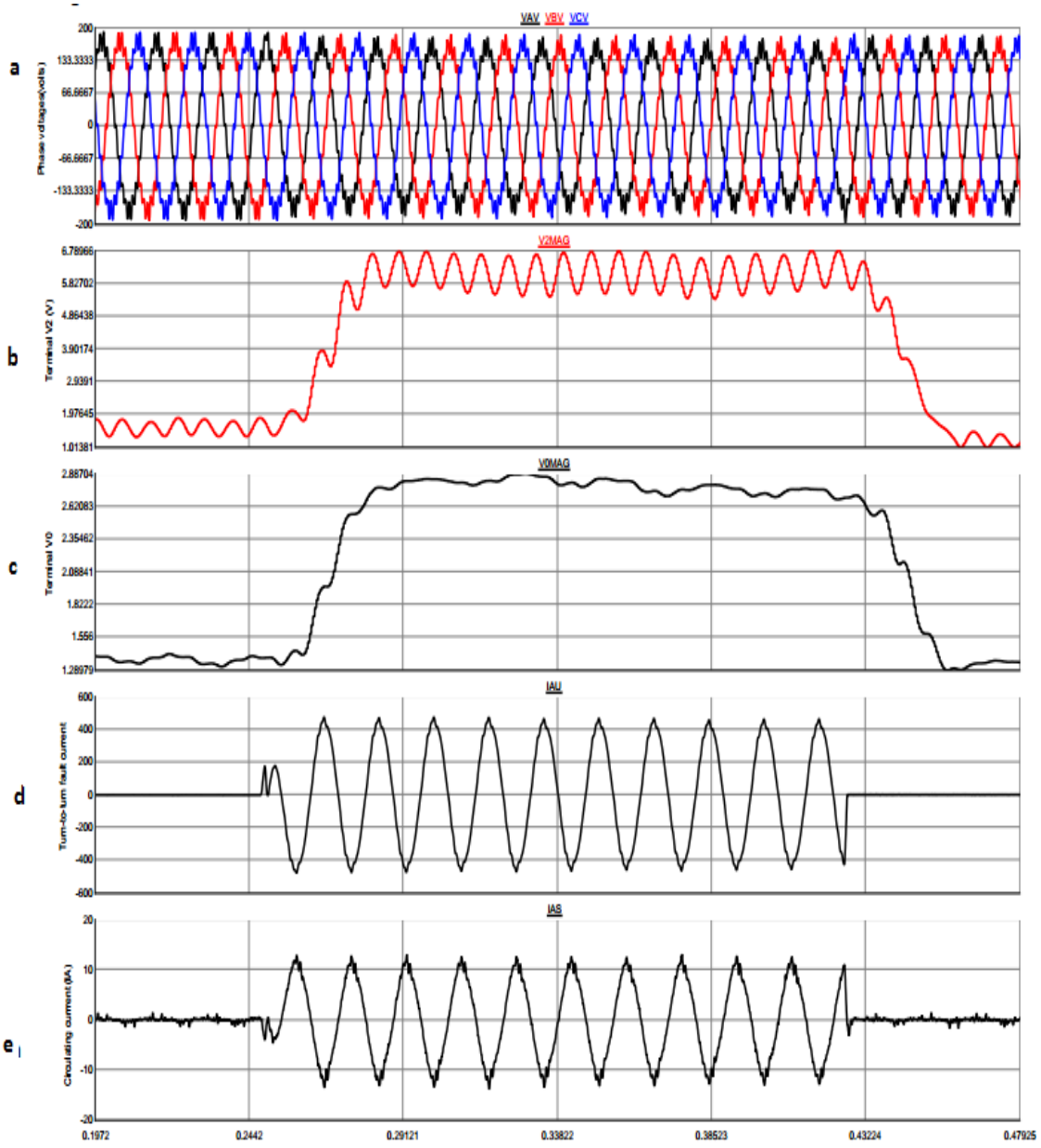

FIGURE A.8: 5 Turns Short Circuit Connected to Grid or Disconnected with P = 0, Q = 0

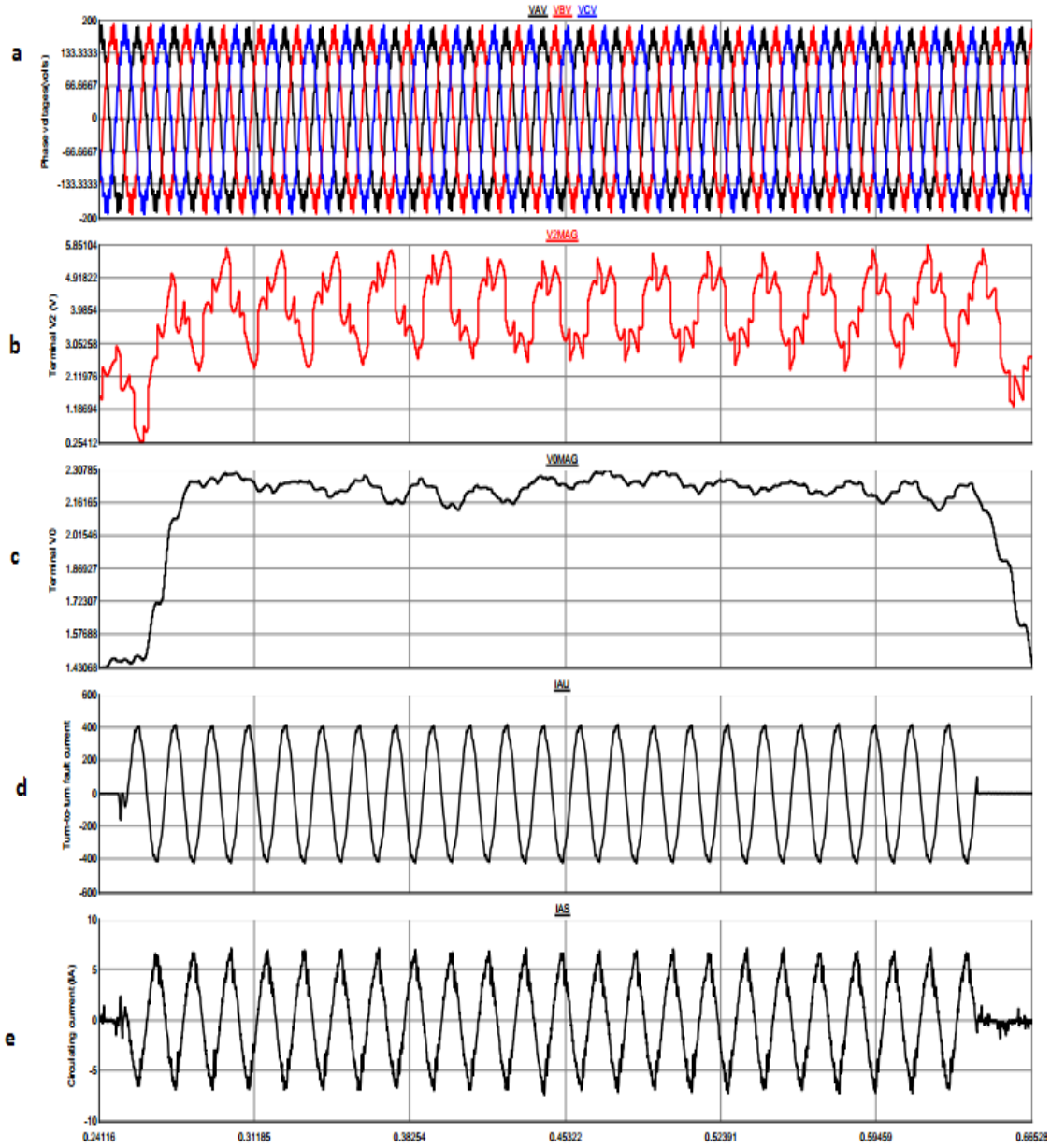

FIGURE A.9: 3 Turns Short Circuit Connected to Grid or Disconnected with P = 0, Q = 0

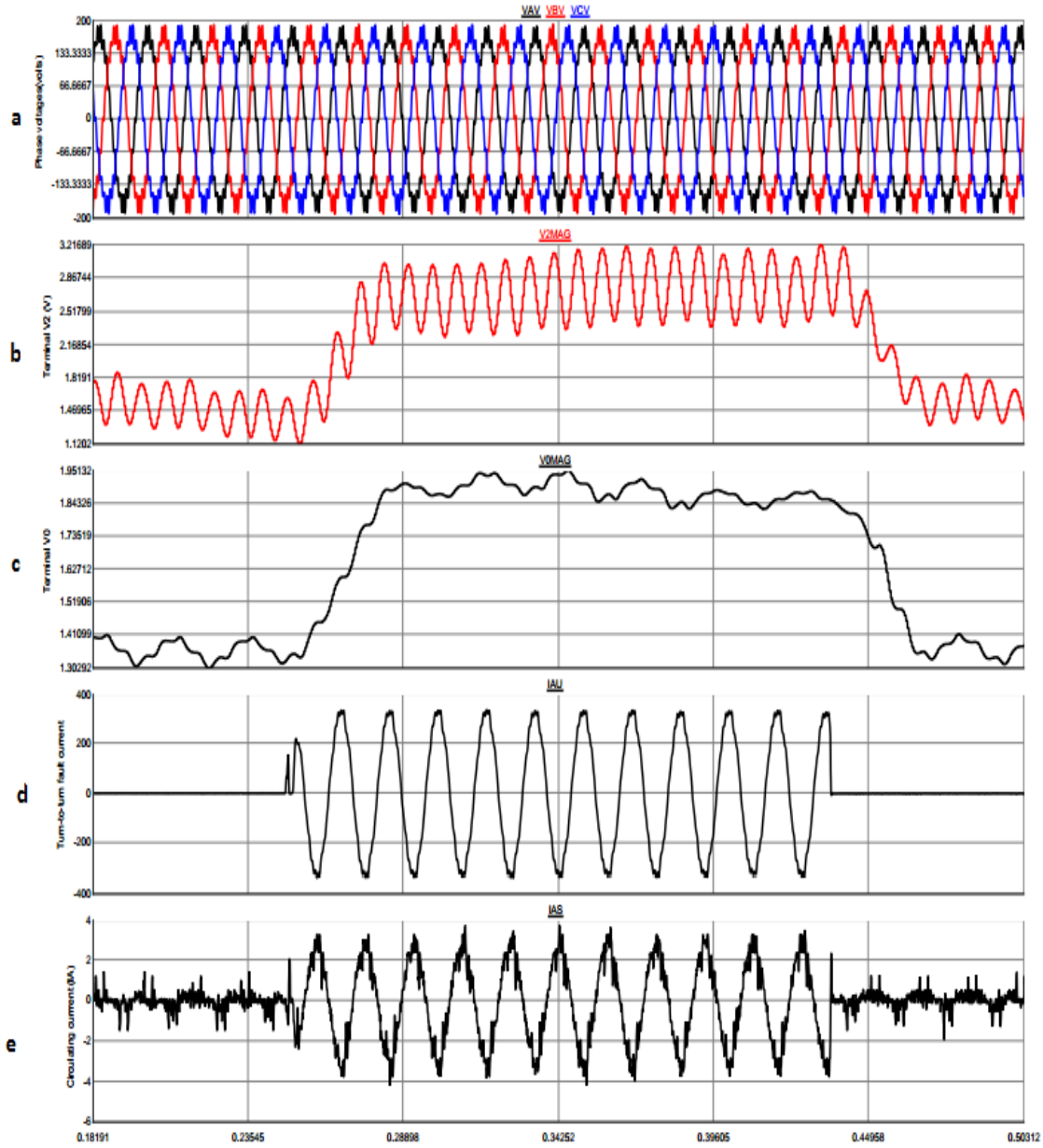

FIGURE A.10: 2 Turns Short Circuit Connected to Grid or Disconnected with P = 0, Q = 0

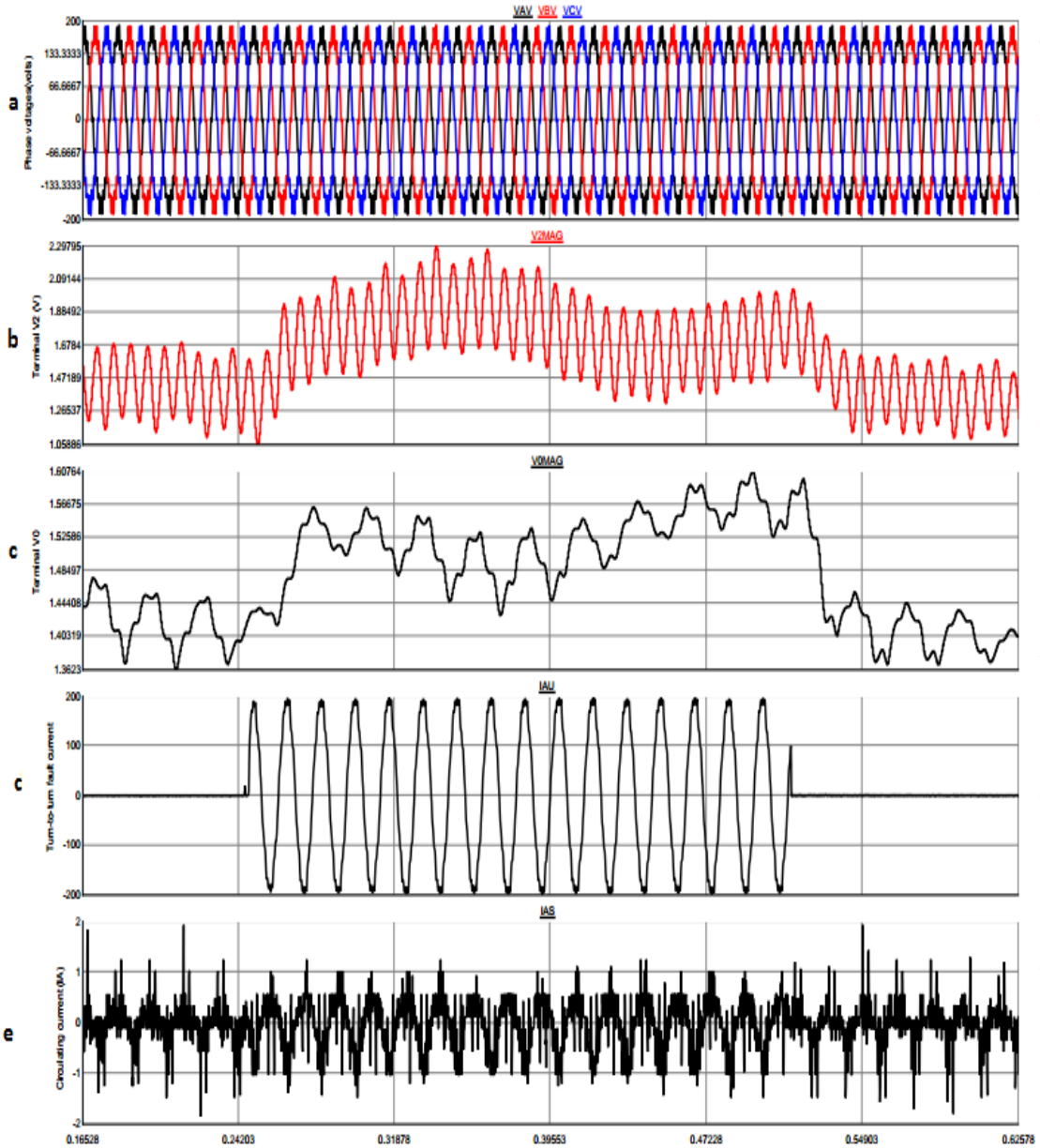

FIGURE A.11: 1 Turn Short Circuit Connected to Grid or Disconnected with P = 0, Q = 0

Figures A.12 to A.14 show the measurements including rotor field current from shunt, for turn-to-turn faults ranging from 5 turns to 2 turns. In these figures, (a) shows the increase in negative sequence currents measured at the terminal; (b) shows the terminal voltage; (c) shows the phase currents measured at the terminal; (d) shows the voltage across 1 ohm shunt in the field winding; (e) shows the negative sequence voltage calculated from the terminal measurements.

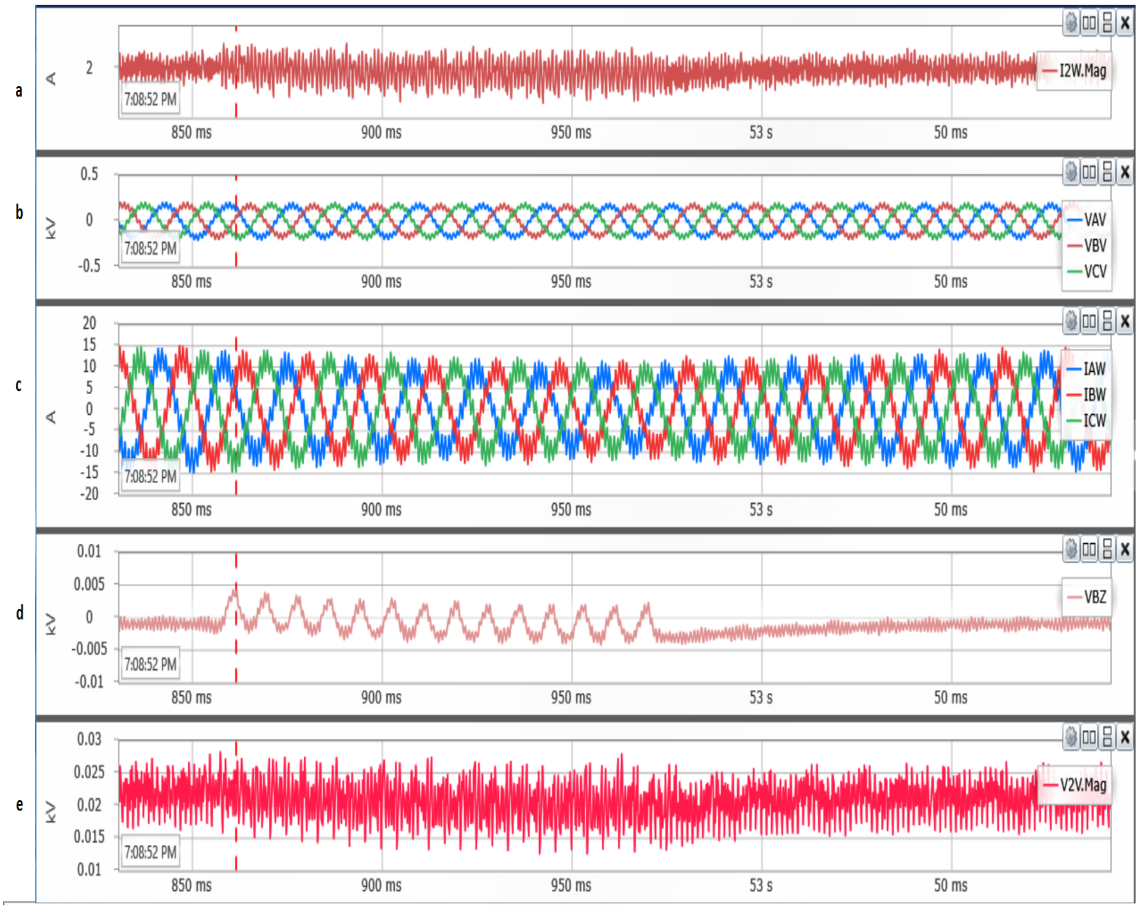

FIGURE A.12: Measurements Including Rotor Field Current from Shunt for 5 Turn Short Circuit in Loaded Condition

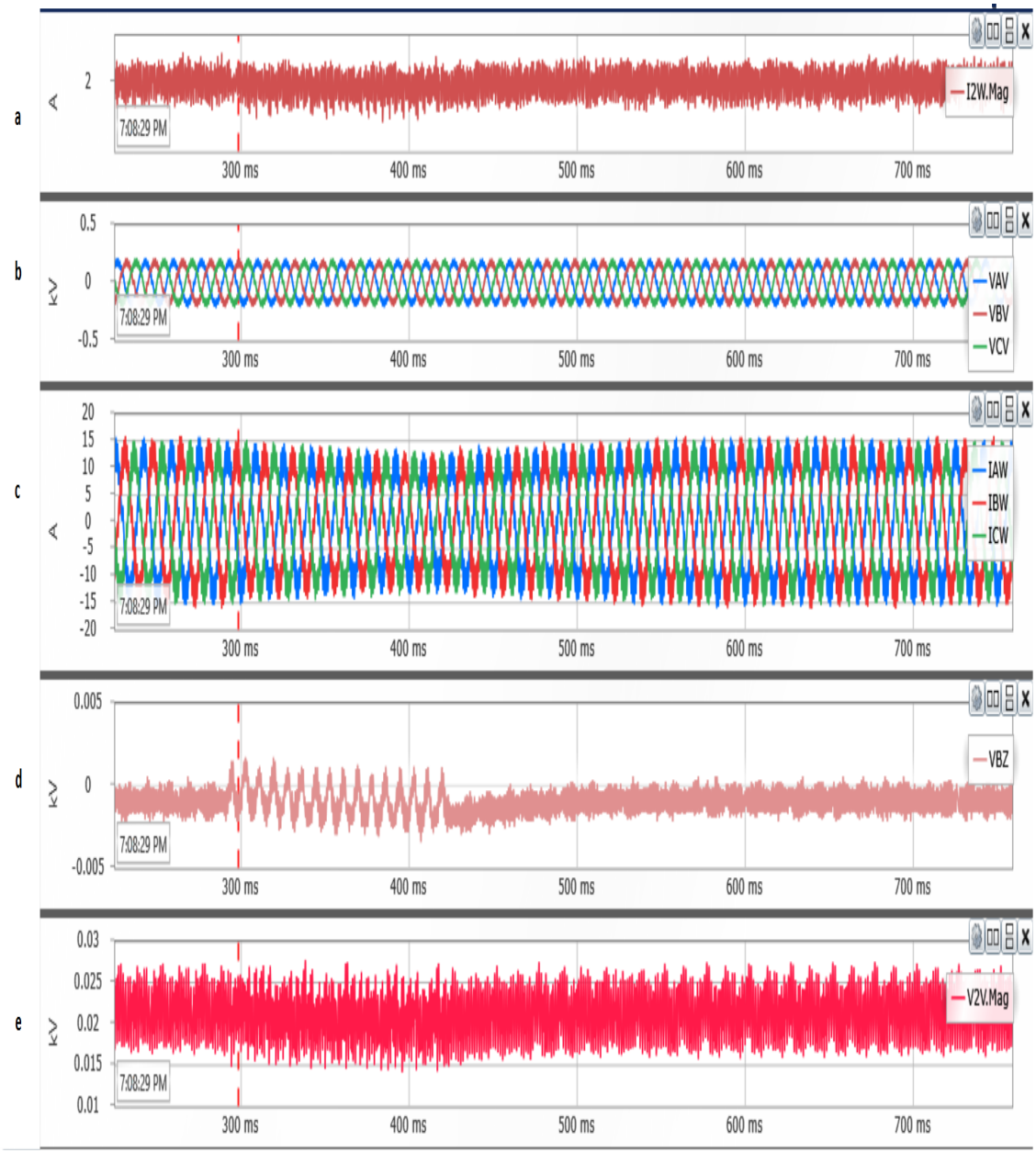

FIGURE A.13: Measurements Including Rotor Field Current from Shunt for 3 Turn Short Circuit in Loaded Condition

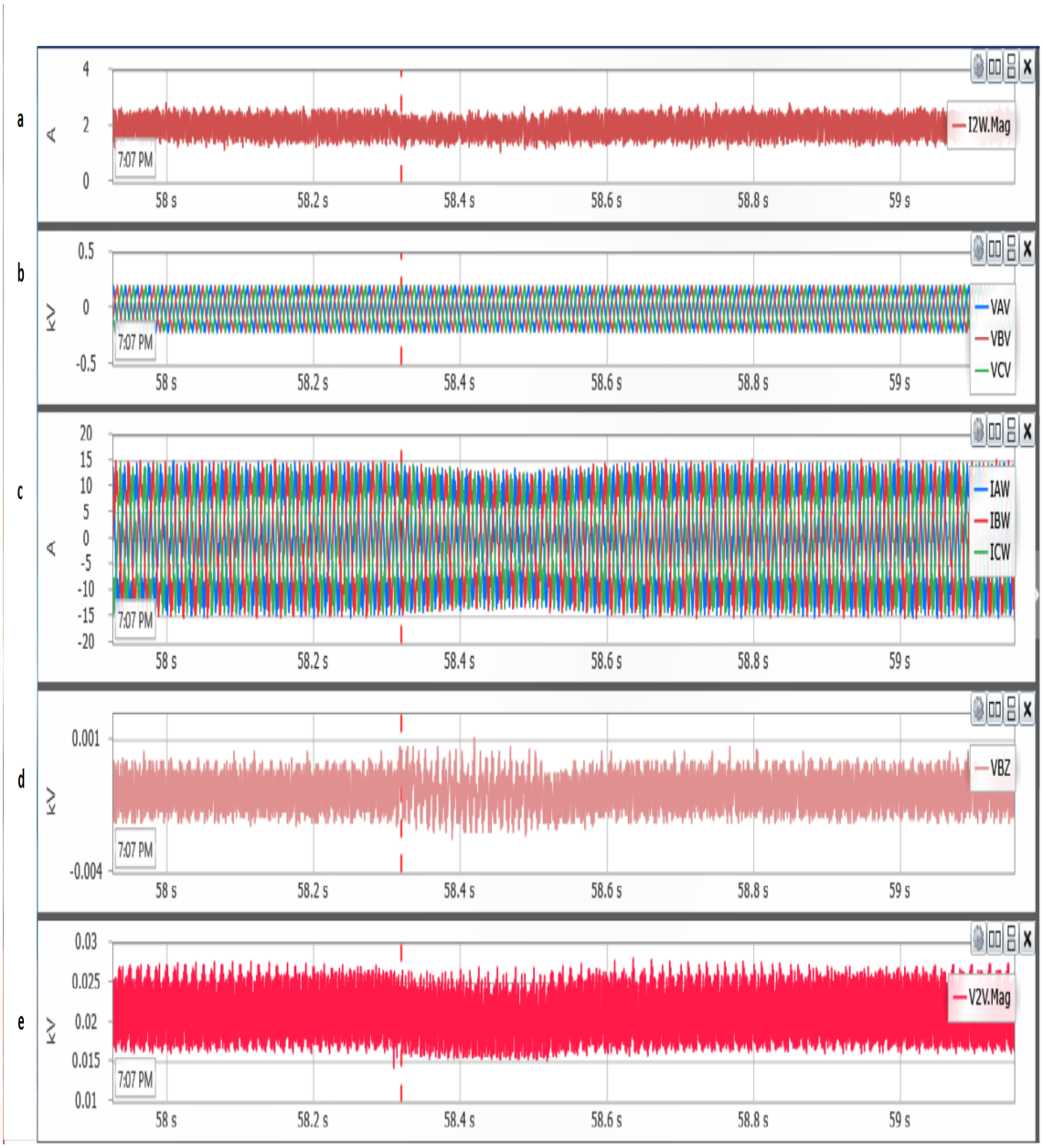

FIGURE A.14: Measurements Including Rotor Field Current from Shunt for 2 Turn Short Circuit in Loaded Condition

Figures A.15 to A.17 show the current shunt measurement for the double frequency currents in the rotor field winding for shorting of 2 turns to 5 turns. In these figures, (a) shows the magnitude of turn-to-turn fault current; (b) shows the terminal voltages and (c) shows the voltage across the shunt due to the double frequency currents induced in field winding.

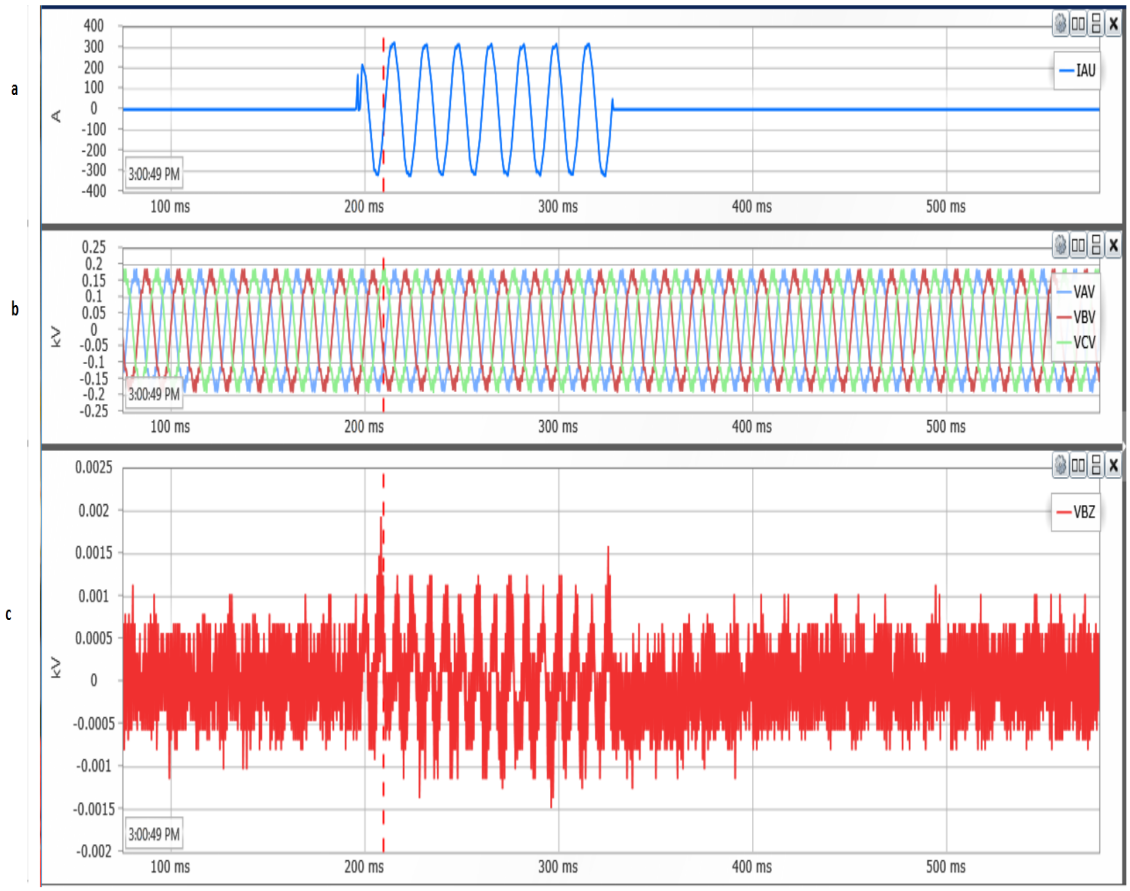

FIGURE A.15: Measurements Including Rotor Field Current from Shunt for 2 Turn Short Circuit Connected to Grid or Disconnected with P = 0, Q = 0

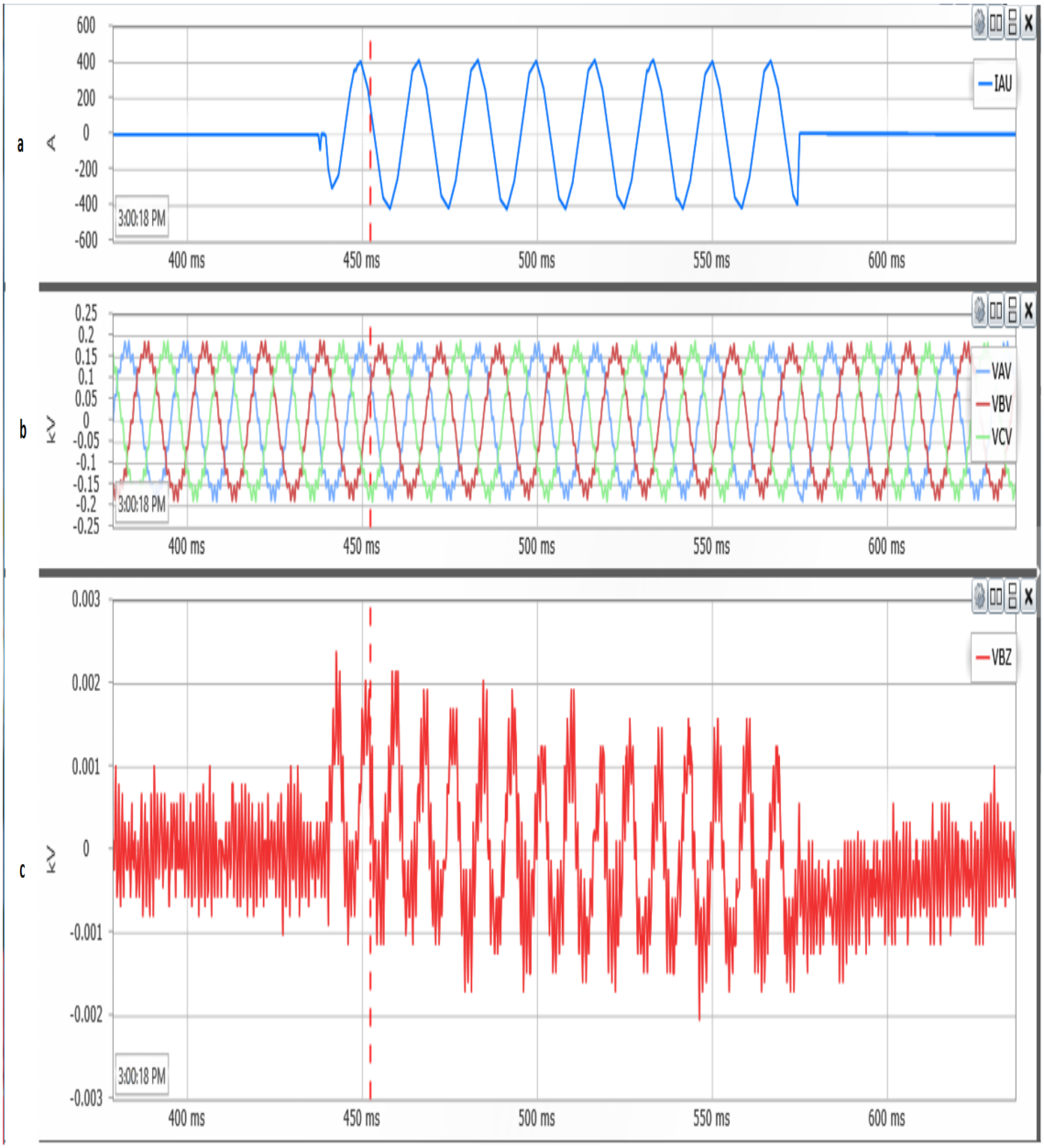

FIGURE A.16: Measurements Including Rotor Field Current from Shunt for 3 Turn Short Circuit Connected to Grid or Disconnected with P = 0, Q = 0

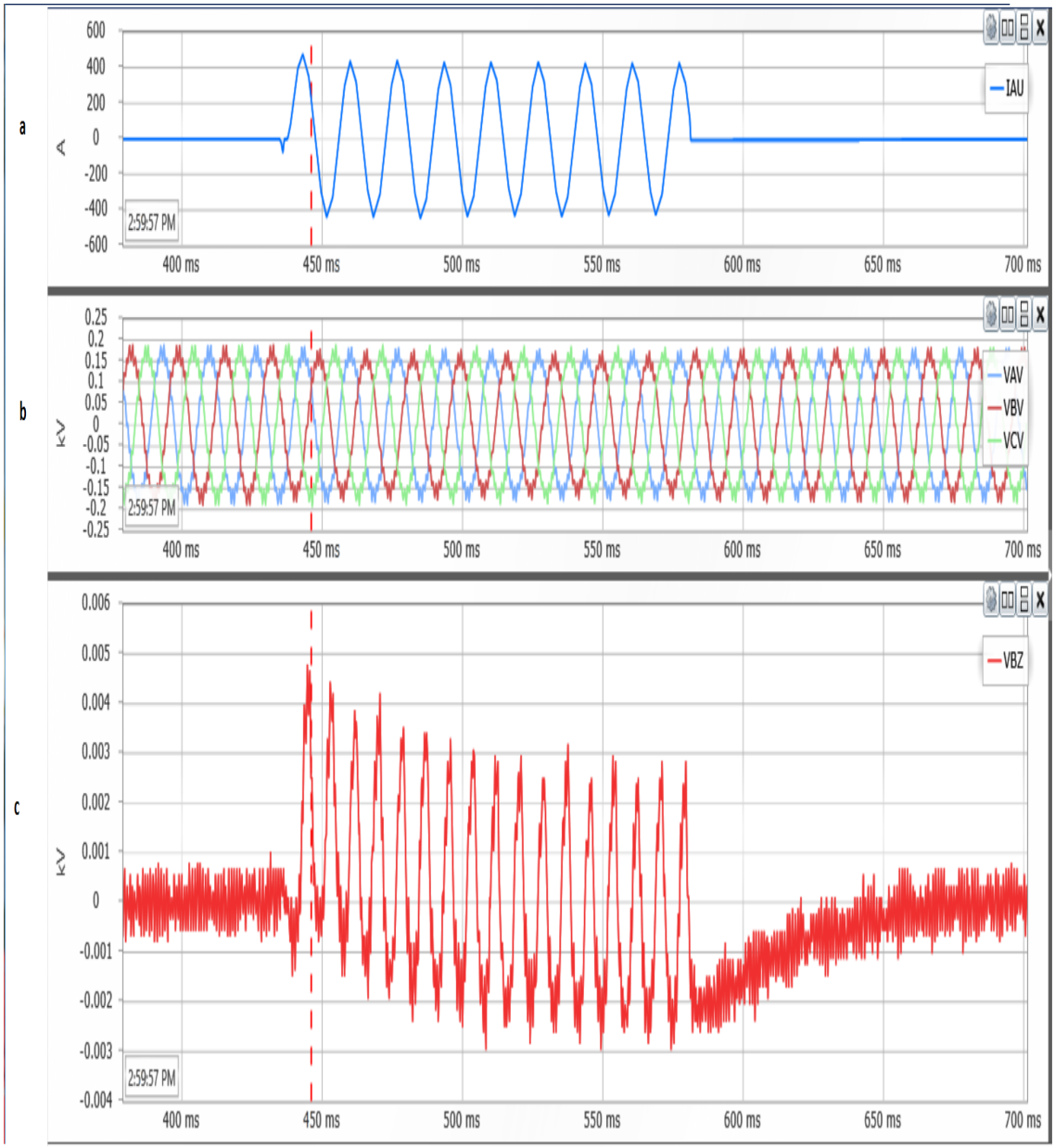

FIGURE A.17: Measurements Including Rotor Field Current from Shunt for 5 Turn Short Circuit Connected to Grid or Disconnected with P = 0, Q = 0

APPENDIX B

Power Lab Machine Analysis

Machine Inductance Approximate Calculations

Airgap_g := 0.138in V_{rated} := 220V I_{rated} := 46A

Pole := 6 f := 60Hz I_{frated} := 6A

Pole_length:= 4.5in Pole_width:= 4.6in

Nf_pole := 536 Number of field turns per pole

N_s := 90 Number of stator turns per branch

R_{IR} := 2.5495in Inner Radius of the rotor

R_{OR} := 6.375in Outer Radius of the rotor

Core_length:= 7.5in $\mu_o := 4\cdot\pi\cdot 10^{-7}\cdot\frac{H}{m}$

No_of_slots:= 54

$Slots\_per\_pole := \frac{No\_of\_slots}{Pole}$ Slots_per_pole= 9

$\gamma := \frac{180deg}{Slots\_per\_pole}$ $\gamma = 20\cdot deg$ Slot angle

$k_P := \cos\left(\frac{2\gamma}{2}\right)$ $k_P = 0.9397$ Pitch Factor

$K_d := \frac{\sin\left(\frac{3\cdot\gamma}{2}\right)}{3\sin\left(\frac{\gamma}{2}\right)}$ $K_d = 0.9598$ Distribution Factor

$K_w := K_d\cdot k_P$ $K_w = 0.9019$ Winding factor

Short_pitch= 2slots

Winding skewing and slot harmonic factors are neglected.

$$E_{rms} := \frac{220V}{\sqrt{3}} = 127.0171\,V$$

$$Airgap\_radius := \left[\frac{\left(R_{OR} + Airgap\_g\right)\cdot 2\cdot\pi}{Pole}\right]$$

$$Airgap\_radius = 0.1732\,m$$

$$Flux\_per\_pole := \frac{E_{rms}}{\left(4.44\cdot f\cdot N_s\cdot K_w\right)}$$

$$Flux\_per\_pole = 0.0059\,Wb$$

$$Area\_effective := \left[\left(\pi\cdot R_{OR}\cdot 2\right)\cdot Pole\_length\frac{2}{\pi\cdot Pole}\right]$$

$$Area\_effective = 0.0123\,m^2$$

$$B_{rms} := \frac{(Flux\_per\_pole)}{Area\_effective} \qquad B_{rms} = 0.476\,T$$

From the no load characteristic

$$I_{fld\_noload} := 3.13A \qquad N_{rotor\_per\_pole} := 536$$

$$MMF_{rotor} := I_{fld\_noload}\cdot N_{rotor\_per\_pole} \qquad MMF_{rotor} = 1677.68\,A$$

MMF spent in the air gap

$$B_{max} := \frac{MMF_{rotor}\cdot\mu_o}{Airgap\_g} \qquad B_{max} = 0.6015\,T$$

Maximum magnetic flux density

$$B_{rms} := \frac{B_{max}}{\sqrt{2}} \qquad B_{rms} = 0.4253\,T$$

Assuming the permeability of the iron is infinite

$$Mean\_length\_path := 2\cdot(Pole\_width + Airgap\_g) + \frac{2\cdot\pi\cdot Airgap\_radius}{9}$$

$$54$$

Mean_length_path= 0.4221 m

$$\text{Area\_of\_coil} := 0.9 \cdot \text{Core\_length}\left(\frac{2 \cdot \pi \cdot \text{Airgap\_radius7}}{54}\right)$$

$\mu_r := 7000, 8000 .. 10000$ N=1

$$\text{Emf\_turn:=} \frac{E_{rms}}{90} = 1.4113\,\text{V} \qquad \text{Area\_of\_coil} = 0.0242\,\text{m}^2$$

$$L_{turn}(\mu_r) := \frac{\mu_o \cdot \mu_r \cdot N^2 \cdot \text{Area\_effective10\%}}{\text{Mean\_length\_path}}$$

This assumes that10% of the inductance is leakage inductance and that is going to oppose the current flow during turn-to-turns

$$X_{1turn}(\mu_r) := 2 \cdot \pi \cdot 60\text{Hz} \cdot L_{turn}(\mu_r) \qquad I_{short}(\mu_r) := \frac{\text{Emf\_turn}}{X_{1turn}(\mu_r)}$$

$X_{1turn}(\mu_r)$ =

0.0097	Ω
0.0111	
0.0125	
0.0138	

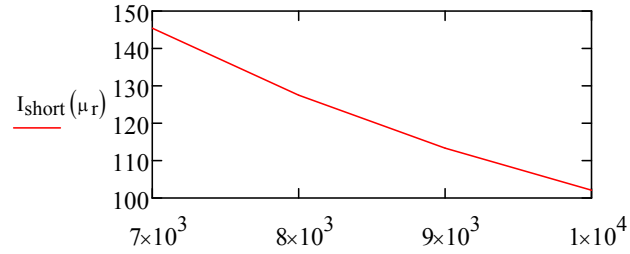

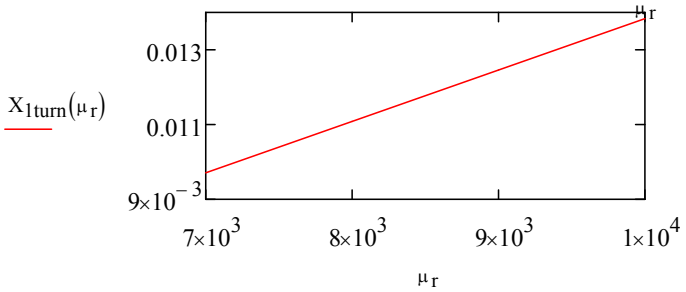

From Table 2.1 and Table 2.2, impedances summary

S.No	Field winding open and B& C phases are open			Field winding open and B& C phases are short			Field winding close and B& C phases are open	Field winding close and B& C phases are short	leakage impedance when field winding is short
	Min	Max	Avg	Min	Max	Avg	Avg	Avg	Avg
Impedance per branch (ohms)	0.9779	1.761	1.361	0.7234	0.9916	0.8334	1.019	0.7291	0.1456
Impedance per 10 turn (ohms)	0.1117	0.2034	0.1575	0.0859	0.1136	0.09969	0.1139	0.08598	0.02008
Impedance per 5 turn (ohms)	0.05665	0.1025	0.07783	0.04379	0.0536	0.05043	0.05925	0.4436	0.01309
Impedance per 1 turn (ohms)	0.01505	0.0252	0.02011	0.01165	0.01413	0.01271	0.012	0.0116	0.006855

From Table 5.5, the measured impedances during no load condition

S.No	Test Case	Impedance of shorted turns(ohm)
1	10 Turns short	0.065
2	7 Turns short	0.0374
3	5 Turns short	0.02322
4	3 Turns short	0.0155
5	2 Turns short	0.0127
6	1 Turn short	0.0108

When zero sequence leakage reactance of the generator is given

$X_d := 3.6\text{ohm}$

$X_{zero} := 2 \cdot 3.6 \cdot \text{ohm} \cdot 10\% = 0.72\,\Omega$

Impedance for 10 turns

$$X_{10\_leakage} := \frac{X_{zero}}{9}$$

$X_{10\_leakage} = 0.08\,\Omega$

$Turn := 1$

$$I_{10turns} := 10 \cdot \frac{Emf\_turn}{X_{10\_leakage}}$$

$$I_{10turns} = 176.4126\,A$$

This is somewhat closer.

Fundamental components of airgap mmf

From the Table 5.6

$$MMF_{Speak\_10turns} := \frac{4}{\pi} \cdot K_w \cdot (218 \cdot 10\sqrt{2} \cdot A)$$

$$MMF_{Speak\_10turns} = 3540.3479\,A \cdot Turn$$

$$MMF_{Speak\_7turns} := \frac{4}{\pi} \cdot K_w \cdot (7 \cdot 277 \cdot \sqrt{2} A)$$

$$MMF_{Speak\_7turns} = 3148.9609\,A \cdot Turn$$

$$MMF_{Speak\_5turns} := \frac{4}{\pi} \cdot K_w \cdot (5 \cdot 313 \cdot \sqrt{2} A)$$

$$MMF_{Speak\_5turns} = 2541.5801\,A \cdot Turn$$

$$MMF_{Speak\_3turns} := \frac{4}{\pi} \cdot K_w \cdot (3 \cdot 289 \cdot \sqrt{2} A)$$

$$MMF_{Speak\_3turns} = 1408.0191\,A \cdot Turn$$

$$MMF_{Speak\_2turns} := \frac{4}{\pi} \cdot K_w \cdot (2 \cdot 233 \cdot \sqrt{2} A)$$

$$MMF_{Speak\_2turns} = 756.79\,A \cdot Turn$$

$$MMF_{Speak\_1turns} := \frac{4}{\pi} \cdot K_w \cdot (141 \cdot 1 \cdot \sqrt{2} A)$$

$$MMF_{Speak\_1turns} = 228.9858\,A \cdot Turn$$

APPENDIX C

MATLAB MODEL

```
%Butterworth filter

function [ Output ] = AAFilter(Input,Wn,n)
[b,a]=butter(n,Wn);
out=zeros(length(Input),1);
k=1;
for j=3:length(Input);
if k>2
out(k)= (b(1)*Input(j)+b(2)*Input(j-1)+b(3)*Input(j-2)-a(2)*out(k-1)-a(3)*out(k-
2))/a(1);
else
out(k)=0;
end
k=k+1;
end
Output=out;
end

% Zero sequence impedance calculation
Location='U:\Matlab_comtrade\Raju';
Filename='10225.csv';

data=readtable(fullfile(Location,Filename));

I=data.x1_IAW;
V=data.x1_VAY*1000/100; % scaling factor
TOT=6*(data.x1_ZTOT);
Tenturn=3*(data.x1_Z10);
Fiveturn=3*(data.x1_Z5);
Oneturn=3*(data.x1_Z1);

TOT(isnan(TOT))=0
Tenturn(isnan(Tenturn))=0
Fiveturn(isnan(Fiveturn))=0
```

```
Oneturn(isnan(Oneturn))=0
srate=ceil(8000/60);
 wn=(10)/(8000/2);
%in Butterworth filter, Wn is fc/(fs/2) where c is cutoff and s is sampling
 %In spec fc is mentioned to be 40Hz*spc/2
n=2;       %order of butterworth filter
Zaabranch=AAFilter(TOT,wn,n);
 % Measured Zero sequence impedance calculation of branch
Zaa10turn=AAFilter(Tenturn,wn,n);
%Zero sequence impedance calculation of ten turn
Zaa5turn=AAFilter(Fiveturn,wn,n);
%Zero sequence impedance calculation of five turn
Zaaoneturn=AAFilter(Oneturn,wn,n);
%Zero sequence impedance calculation of one turn
plot(ZONEBWF);

%Impedance of winding
Location='U:\Matlab_comtrade\Raju';
Filename='1022.csv';

data=readtable(fullfile(Location,Filename));

I=data.x1_IAW;
V=data.x1_VAY*1000/100;
TOT=2*(data.x1_ZTOT);
Tenturn=(data.x1_Z10);
Fiveturn=(data.x1_Z5);
Oneturn=(data.x1_Z1);

TOT(isnan(TOT))=0
Tenturn(isnan(Tenturn))=0
Fiveturn(isnan(Fiveturn))=0
Oneturn(isnan(Oneturn))=0
```

```
srate=ceil(8000/60);
[FreqZ,MagZ]=fftfunc(TOT);
 wn=(10)/(8000/2);
%in Butterworth filter, Wn is fc/(fs/2) where c is cutoff and s is sampling
 %In spec fc is mentioned to be 40Hz*spc/2
n=2;   %order of butterworth filter
Zaabranch=AAFilter(TOT,wn,n);
%  Measured Impedance calculation of branch
Zaa10turn=AAFilter(Tenturn,wn,n);
%  Measured Impedance calculation of ten turn
Zaa5turn=AAFilter(Fiveturn,wn,n);
%  Measured Impedance calculation of five turn
Zaaoneturn=AAFilter(Oneturn,wn,n);
%  Measured Impedance calculation of one turn
```